Technische Universität München

Institut für Nanoelectronik

Modeling and Design of
Single-Molecule Devices

Ahmed Hanafy Ramadan Mahmoud

Vollständiger Abdruck der von der Fakultät für Elektrotechnik und Informationstechnik der Technischen Universität München zur Erlangung des akademischen Grades eins

Doktor - Ingenieurs

genehmigten Dissertation.

Vorsitzender: Univ.-Prof. Dr. rer. nat. Thomas Hamacher

Prüfer der Dissertation: 1. Univ.-Prof. Paolo Lugli, Ph.D.

2. Prof. Aldo Di Carlo, Ph.D.
Universitá degli Studi di Roma "Tor Vergata", Italien

To my parents and my wife

Abstract

Molecular electronics, in which a single molecule is employed for building a functional electronic device, has become a promising technology since it provides an ultimate reduction in device dimensions. Several research groups are able to realize single-molecule devices and observe interesting transport characteristics. Such achievements increase the demand for understanding the quantum physics that dominates the transport at such nanoscale devices. Theoretical studies are based on methods of computational chemistry as well as non-equilibrium transport calculations.

We have performed theoretical research on various molecular devices in order to explain the observed behavior in their transport. We are able to link the different outputs from atomistic analysis and correlate them to the final device performance. This allows us further to have a control on the transport behavior, whence designing new molecular devices with interesting features (e.g. high rectification ratio, negative differential resistance and standalone logic gates). We focus not only on two terminal molecular devices which are intensively investigated in literature, but also on three terminal devices since molecular transistors are key components for functional electronic systems. Moreover, in order to provide a technique that allows fast assessment to the response of single-molecule devices, we propose a novel circuit modeling methodology. The method is found applicable to different molecular devices from literature, and it is successfully utilized in reproducing measurement and atomistic simulation results of the testbed devices.

Contents

Contents

1 Introduction

Thanks to electronic devices, applications that provide welfare to humanity are made possible. The current dominating technology in the fabrication of electronic devices is the silicon semiconductor technology. In 1965, Moore's law predicted that the density of transistors (number per square centimeter) doubles every 18 months [1]. This implies a reduction in the transistor size at the same rate. Up till now, this was achieved by refining the photolithographic technology which is one of the key enabler for the semiconductor industry.

There are two major obstacles facing the current device fabrication process. First, the photolithographic technology is approaching its limit soon with transistor size of few nanometers. Second, doping semiconductors, which is required to control the conductivity to pure silicon by adding impurities, faces limitation of solid solubility. In other words, with the reduction of the device size, only few doping atoms would exist in device areas leading to random behavior whence unreliable performance [2]. Furthermore, there are limitations on device operation like the speed saturation, current leakage, parasitic capacitance, etc [3].

Due to increasing demand for advances in miniaturization, power consumption and speed of electronic devices, new technologies are emerging in order to replace/ support the current semiconductor technology. Molecular electronics[1] is one of the promising technologies that can offer extremely high integration densities since single molecules, intrinsically in nanometer dimension, could be employed as active electronic devices. Molecular devices are capable of providing features like rectification, negative differential resistance (NDR) and

---

[1]The term molecular electronics used in this entire thesis is referred to a branch of applied physics in which single molecules are employed to build electronic devices.
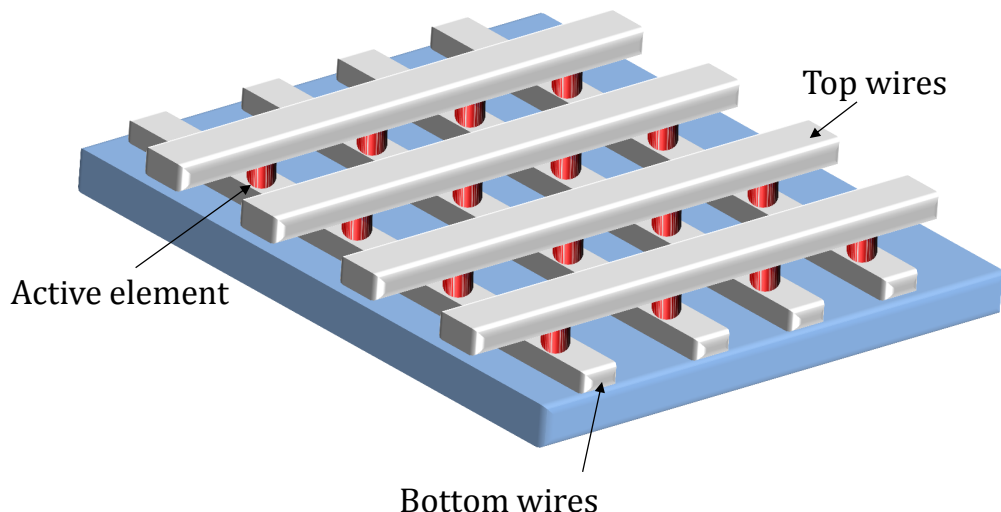
Figure 1.1: A typical schematic of a crossbar array.

conductance switching [4–6], which open the way for a variety of electronic applications.

The attractive properties of molecular devices have triggered the attention of researchers like Mark Ratner, Ari Aviram, James Tour, Mark Reed and many others. Moreover, research on single molecular electronics was conducted at international information-technology play-makers like HP [7,8], IBM [9,10] and Sony [11,12].

Application like memories with huge size and programmable logic gates can be realized in a simple implementation namely, crossbar arrays [7,13–15]. In a nutshell, a crossbar array consists of sets of horizontal and vertical parallel metal wires (Figure 1.1). In most cases, the layer between the crossing wires is composed of nonlinear resistors, whose electric characteristics determine the performance of the crossbar and its electronic functionality. Thanks to the behavior provided by molecular devices, they are expected to be good candidates for active cells in crossbar arrays [16–19]. It is worth mentioning that the highest dense memory circuit up till now was achieved with a molecular crossbar array ($10^{11} \, bit/cm^2$) [13].

Beside the importance of realizing different molecular devices, theoretical studies are necessary for understanding the physics behind the observed performance. Theoretical analyses of molecular devices can help in the design and

development of molecular species that provide improved performance and unique functionalities. For analyzing molecules and evaluating the transport behavior within devices, methods of computational chemistry like ab-initio first-principles methods or semi-empirical methods are coupled to transport calculation methods like non-equilibrium Greens function formalism.

We hereby theoretically develop and study several devices with interesting transport characteristics. We design a molecular current rectifier with rectification ratio more than three orders of magnitude while preserving high on-current [20]. In addition, we propose a molecular device that exhibits a distinguishable NDR behavior in which the behavior is preserved over a wide bias range with a negative slope around -1 MΩ and a peak to valley ratio greater than 10 [21]. Furthermore, we study other various two/three terminal molecular devices and try to provide an argument for the transport characteristics of such devices by building relationships among the different atomistic analyses [22, 23]. One of the main targets of this thesis is to provide a complete picture of the quantum transport through molecular devices and the factors that control this transport behavior.

Historically, modeling tools play a vital role in the rapid development of technologies since it saves time and money required for a prototype production. We hereby try to provide a circuit modeling for molecules by substituting atoms or molecular segments by circuit elements. This circuit modeling could provide a fast qualitative evaluation for the behavior of many molecular devices [24]. We validate the method on some molecular devices versus real measurement and first-principles calculations of the same devices.

This dissertation is organized in six chapters, in addition to, this introduction. The first two chapters formulate state of the art and background for the thesis . Chapter 2 provides the necessary information about the transport mechanism in such nanoscale devices as well as the theory of methodologies employed in this thesis . Chapter 3 discusses different molecular devices in literature and the device realization techniques. The background part of the dissertation is self-contained so that a reader with little basic knowledge can follow and understand. Moreover, the background should pave the way for the understanding of the main contributions and findings discussed in the later parts of the dissertation.

Chapter 4 focuses on different molecular rectifiers that we studied. We illustrate important factors that can control the rectification behavior of molecular devices using a dipyrimidinyl-diphenyl molecule as an example. We also propose a novel molecular rectifier employing simple oligo-phenylene vinylene (OPV) molecule that shows a strong rectification behavior. In addition, we examine the influence of doping on transport behavior of the well-known donor-sigma-acceptor molecular devices. The last section finally discusses a molecular device with an interesting NDR behavior.

Chapter 5 focuses on three terminal molecular devices. We first study two different derivatives of OPV molecular transistors with electrostatic gates. One of them already realized, thus simulation results are compared to measurement data. Secondly, we provide a study on three-leg molecular devices which are used for building molecular logic gates and molecular transistors. Chapter 6 illustrates a newly proposed circuit modeling technique that can be generally applied to different molecular devices. Finally, chapter 7 concludes the thesis and states an outlook for possible extensions to our work.

2 Atomistic Simulation Methodologies

Supriyo Datta once wrote in his book "Quantum transport: Atom to Transistor" that

> Regardless of what form future electronic devices take, we will have to learn how to model and describe the electronic properties of the device structures that are engineered on an atomic scale.

In this chapter, we shall illustrate the basis for understanding the methodologies employed for studying/designing molecular and nanoscale devices. We shall first discuss a simplified calculation process that explains the charge transport through nanoscale devices. After that, we shall briefly refer to actual methodologies applied in the calculation. We shall finally discuss the main atomistic analyses which we usually conduct in our studies on molecular devices. We shall refer to the derivation of these atomistic analyses and their interpretation. In some cases we will refer to the clues these analyses provide for understanding device behavior.

2.1 Simplified Explanation for Charge Transport in Molecular Devices

Molecular orbital (MO) theory suggested that a molecule can be treated as a collection of nuclei in which electrons are described by wave-functions called molecular orbitals [25]. For an isolated molecule, MOs are discrete. According to Pauli exclusion principle orbitals with lower energy are filled first with electrons (Figure 2.1a). When a molecule is brought between two metallic electrodes and coupled to them, the Fermi-level of the whole system must align. Consequently,
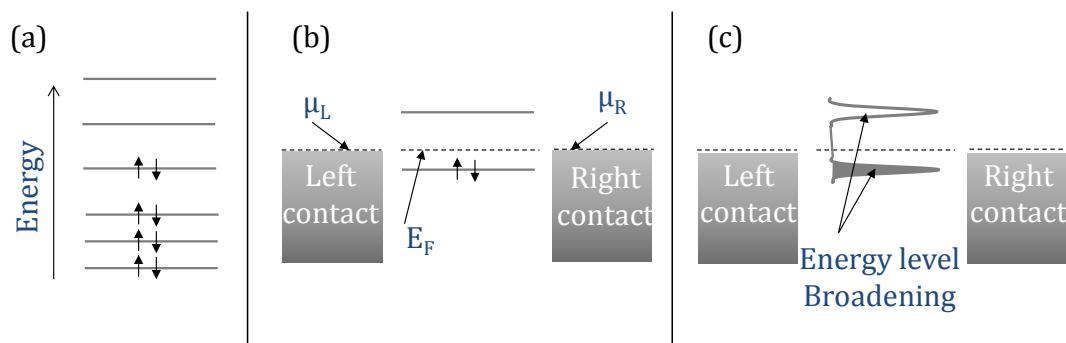
Figure 2.1: (a) MO filling configuration based on Pauli Exclusion Principle for a molecule in free space. (b) MO filling configuration after contacting with the electrodes, $\mu_{L,R}$ are the chemical potential of the left and right electrodes. (c) illustration for the broadening induced in the MO.

MOs below the Fermi-level will be filled with electrons, but MO above will be empty (Figure 2.1b). When electrodes are connected to the molecule, they cause a broadening in the MO energy level (Figure 2.1c). This is because the electrodes have energy bands. This broadening effect is due to the presence of electrons in the electrodes having the same energy of MO, whence electrons can be exchanged between the molecule and electrodes [26]. The broadening in the energy level is described by Heisenberg's uncertainty principle for energy

$$\Delta t \gamma = \hbar, \tag{2.1.1}$$

where γ is the broadening in the energy-level and Δt is the time in which electron escape from one electrode to another electrode through the MO [27]. Thus, electron will stay forever ($\Delta t = \infty$) in the MO for a sharp energy level ($\gamma = 0$), yet the broadening $\gamma = \hbar / \Delta t$ for finite escape time.

Assume a certain bias is applied on the two electrodes such that a MO (regardless whether it is filled or not) becomes between the chemical potentials (Fermi-levels) of the two electrodes, see Figure 2.2. Each electrode has a different agenda; the left electrode would like this MO to be filled because it is below its chemical potential. On the other hand, the right electrode would like it to be empty because it is above its chemical potential. Hence, such non-equilibrium condition results in charges flow through the molecule.
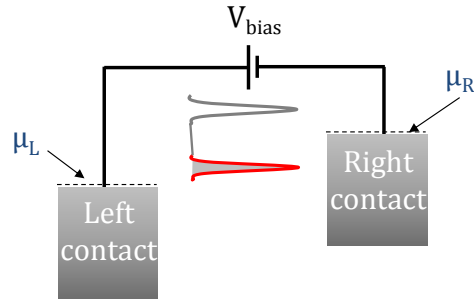
Figure 2.2: The configuration of the chemical potential of electrodes and MOs under bias.

How do the current equation for such system look like? First, we know that each orbital can be filled with 2 electrons. The number of electrons that the left and the right electrodes want the MO to be filled with are

$$N_L = 2f(E_{MO} - \mu_L) \tag{2.1.2}$$

$$N_R = 2f(E_{MO} - \mu_R) \tag{2.1.3}$$

where $f(E - E_F) = \frac{1}{1 + e^{\frac{E}{KT}}}$ is the Fermi-function. The current is defined as the rate of flow of charge. The current from the left electrode is

$$I_L = e\frac{N_L - N}{\Delta t} = e\frac{\gamma_L}{\hbar}(N_L - N), \tag{2.1.4}$$

where N is the actual number of electrons in the MO and γ_L is the broadening due to coupling with the left electrode. The same equation applies to the current from the right electrode

$$I_R = e\frac{\gamma_R}{\hbar}(N_R - N) \tag{2.1.5}$$

According to Kirchoff current law, the current form the left electrode is equal to negative the current from the right electrode $I_L = -I_R$, thus we can deduce the actual number of electrons

$$N = \frac{\gamma_L N_L + \gamma_R N_R}{\gamma_L + \gamma_R} \tag{2.1.6}$$

Substituting in equation 2.1.5, one can find out that the magnitude of current

$$I = \frac{2e}{\hbar}\frac{\gamma_L \gamma_R}{\gamma_L + \gamma_R}|f(\mu_L, E_{MO}) - f(\mu_R, E_{MO})| \tag{2.1.7}$$

We have assumed that the whole MO contributes in conduction. However, the broadening makes the energy level form a density of states D(E), where

$\int_{-\infty}^{\infty} D(E) = 1$. This changes equation 2.1.7 such that only the states located between the chemical potentials of the two electrodes will contribute in the current. Thus, the equation becomes

$$I = \frac{2e}{\hbar} \frac{\gamma_L \gamma_R}{\gamma_L + \gamma_R} \int_{\mu_L}^{\mu_R} D(E)|f(E - \mu_L) - f(E - \mu_R)|dE \qquad (2.1.8)$$

There are some important points that we did not cover in the previous discussion. First of all, we assumed that the energy level of each MO contributing in the conduction is fixed before and after bias. This is not correct for such a small device. The initial number of electrons occupying this MO differs from the actual number which is derived from equation 2.1.6. Any induced charge to the molecule will result in interactions with the molecular nuclei, in addition to, interactions with the charges in the molecule. Accordingly, the position of MOs will shift. This new state of the MO needs to be incorporated in the calculation of the new actual number of charges in the MO. The process needs to be repeated till the difference in charge in two successive iterations is less than a predefined accuracy value. This reclusive process is known as self-consistence field (SCF) solution.

It is worth noticing that the impact of induced charges is reduced with the increase in molecules' size (approaching macroscopic system). This behavior is notable in large simulated molecules in which the position of MOs barely shifts under the various applied biases.

Another very important aspect that should be highlighted is the potential drop along the device. Figure 2.3 illustrates the energy diagram of a simple device under the same bias but with different drop along the device. A completely different current will flow through the device due to the different positions of the potential drop. This emphasizes that the potential drop profile plays a vital role in transport performance of devices. It is worth mentioning that different calculation methods might determine different energies for MOs. This would lead to a significant variation in the transport results of the whole device.

2.2 Brief Background on Employed Methodologies

The calculation of the charge transport through atomic-scale devices is implemented typically using nonequilibrium Green's function (NEGF) formalism.
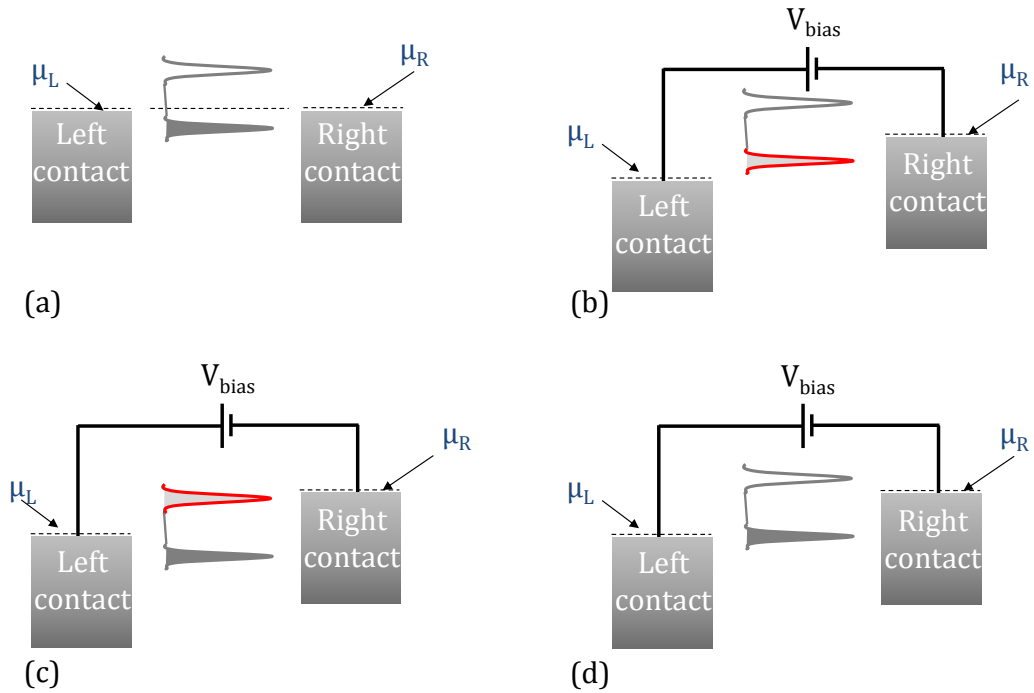
Figure 2.3: (a) The configuration of the chemical potential of electrodes and MOs at equilibrium. (b,c,d) are different possible configuration for the chemical potential of electrodes and MOs under the same bias.

NEGF needs to be coupled to either ab-initio first-principles approaches or semiempirical approaches. These approaches allow the evaluation of the electronic structure of the device. In this section, we shall provide a brief introduction to these approaches.

2.2.1 Molecule's Schrödinger equation

According to quantum mechanics, any system can be described by a wave-function Ψ. In addition, if an operator function acts on a system, an observable property can be noticed. A chemical system (e.g. a molecule) can be described as a wave-function employing Schrödinger equation. Schrödinger equation assumes that energy (E) of the system is the observable property and introduces an operator ($\hat{H}$) called Hamiltonian which is responsible for characterizing the total energy of the system. Thus, Schrödinger equation that describes a molecular system can be written as

$$\hat{H}\Psi = E\Psi \tag{2.2.1}$$

In the absence of any electric or magnetic effects, there are five components that define the energy of the system: inter-electron interaction, inter-nuclei repulsion, kinetic energies of both electrons and nuclei, and the nuclei-electron interaction. Since nuclei movement can be neglected compared to electron movement, the kinetic energy of nuclei can be discarded in calculation. Moreover, inter-nuclei repulsion is constant for fixed nuclei coordinates, and wave-functions are invariant to constant terms. Hence, Schrödinger equation can be solved without including these terms. Such approximation is known as Born-Oppenheimer approximation, which is a very important tool in quantum chemistry since it gives the opportunity for computing wave-functions for larger molecules [28]. The Hamiltonian can, therefore, be written as

$$\hat{H} = -\sum_i \frac{\hbar^2}{2m_e} \nabla_i^2 - \sum_{i<j} \frac{e^2}{r_{ij}} + \sum_i \sum_k \frac{e^2 Z_k}{r_{ik}}, \quad (2.2.2)$$

where the indexes i and j run over electrons, k runs over nuclei, m_e is electron mass, ∇^2 is Laplacian operator, Z is the atomic number, r_{ij} is the distance between electrons i and j, and r_{ik} is the distance between electron i and nucleus k.

2.2.2 Variational Principle and Derivation of Secular Equation

Referring back to equation 2.2.1, it is worth noticing that there exists various (or infinite) wave-functions that can be substituted in the equation and each would result in different corresponding energy eigenvalue. A real system tends to have the lowest possible ground state energy. Thus, we assume Ψ_o to be the optimum wave-function that describes the system having the lowest possible energy (E_o). Any guessed wave-function Ψ_G would result in eigenvalue E_G greater than or equal E_o. Hence we can reformulate equation 2.2.1 to be

$$\hat{H}\Psi_G \geq E_o\Psi_G \quad (2.2.3)$$

On multiplying both sides with Ψ_G and integrating over space, one can deduce

$$\int \Psi_G \hat{H} \Psi_G dr \geq \int \Psi_G E_o \Psi_G dr$$
$$\frac{\int \Psi_G \hat{H} \Psi_G dr}{\int \Psi_G \Psi_G dr} \geq E_o \quad (2.2.4)$$

This is what is known as the **variational principle**. It is a very important principle since one can estimate the quality of any guessed wave-function based on the calculated value from the left hand side of the last equation (the lower the closer to optimum).

Another important point in the calculation is that one may assume that Ψ_o is a linear combination of an infinite number of wave-functions. This leads to a very important rule of thumb in computational chemistry, known as the linear combination of atomic orbitals (LCAO) approximation for molecular orbitals [29]. This rule indicates that a linear combination of atomic orbitals (Φ_i) can give a good guess for molecular wave-function.

$$\Psi_G = \sum_{i=1}^{N} c_i \Phi_i \tag{2.2.5}$$

where c_i are the coefficient of each corresponding atomic orbital Φ_i. One concludes that increasing the number (N) of atomic orbitals results in better estimation. By substituting equation 2.2.5 into equation 2.2.4, one can deduce

$$
\begin{aligned}
E_G &= \frac{\int \sum_{i=1}^{N} c_i \Phi_i \hat{H} \sum_{j=1}^{N} c_j \Phi_j dr}{\int \sum_{i=1}^{N} c_i \Phi_i \sum_{j=1}^{N} c_j \Phi_j dr} \\[2ex]
&= \frac{\sum_{i=1,j=1}^{N} c_i c_j \int \Phi_i \hat{H} \Phi_j dr}{\sum_{i=1,j=1}^{N} c_i c_j \int \Phi_i \Phi_j dr} \\[2ex]
&= \frac{\sum_{i=1,j=1}^{N} c_i c_j \omega_{ij}}{\sum_{i=1,j=1}^{N} c_i c_j \chi_{ij}}
\end{aligned}
\tag{2.2.6}
$$

where ω and χ are abstract notation for the resonance integral and overlap integral, respectively. The overlap integral emphasizes that it is proportional to the overlap between two atomic orbitals in space. The resonance integral cannot be interpreted generally, however, ω_{ii} can be physically understood as the ionization potential of the orbital [30].

Minimizing E_G in variational equation 2.2.6 would help us to achieve the optimum wave-function that describes the molecular system [30]. Thus, we may

use rules of calculus which state that a necessary condition for a function's minimum is that the derivative of function is equal to zero for all free variables c_i. Performing such partial differentiation on equation 2.2.6 for all N variables would lead us to N equations that need to be satisfied, explicitly.

$$\sum_{i=1}^{N} c_i(\omega_{ji} - E_G\chi_{ji}) = 0 \quad \forall j \tag{2.2.7}$$

Using linear algebra, we can obtain a non-trivial solution for these N-equations by equating a determinant composed of the coefficients of each variable to zero (e.g. for c_m the coefficient is $(\omega_{jm} - \chi_{jm}E_G)$). This determinant is known as the Secular determinant.

In order to solve such problem, we need to calculate first the N^2 values of ω_{ij} and χ_{ij} explicitly, then solve out the determinate to get N valid solution for E_G. Finally, for each E_G solve out the atomic orbitals' coefficient (c_i) to get the corresponding molecular orbital. The most complicated part in this process is the computation of the $\omega_{ij} = \int \Phi_i H \Phi_j dr$ values because the Hamiltonian operator in equation 2.2.2 needs to be applied on each atomic orbital wave function.

2.2.3 Density Functional Theory

One of the most famous first-principles ab-initio approaches is the Hartree-Fock method. It assumes independent electrons to overcome the complexity discussed in the previous subsection [31]. This assumption allows one to write the Hamiltonian operator on the wave-functions in an easier formula. The method then introduces a new term that handles the electron-electron interaction. Finally, a recursive self-consistence field is applied such that solving the secular determinate allows the evaluation of the orbital energy while the orbital coefficients are used to build up the density matrix and the secular determinate.

The typically used ab-initio method in many studies is density functional theory (DFT). DFT suggests using the electron density as the observable of the system since this allows easier calculation process with the help of some simplifications [32–35]. The electron density is used to compute the external potential which allows the evaluation of the Hamiltonian, whence the wave-functions [30]. After that, the most difficult part comes which is solving the Schrödinger equation to evaluate the energy in the presence of the electron-electron interaction term in the Hamiltonian.

DFT starts the calculation assuming an imaginary non-interacting system of electrons with the same electron density of the real device. After that, Kohn-Sham self-consistent field is applied such that electron density is used to determine the secular matrix. At the same time, the electron density itself needs to be computed from the derived orbitals which are determined from solving the secular equations [30, 36].

Standard DFT calculations, as discussed above, do not properly treat the exchange interaction. Thus exchange-correlation functionals (e.g. local density approximation and density gradient corrections) are used to mitigate this limitation [37]. Moreover, the DFT used in this thesis provides solutions for ground state systems. Time-dependent DFT is an extended method that allow the treatment of a system in an exited state or a system exhibiting a time-dependent characteristics [38, 39].

DFT with Tight binding approximation (DFTB) is considered as a semi first-principles methodology [40]. The main idea of DFTB is that it ignores the core electron of the molecule (tightly bounded electrons) in calculation. Accordingly, the secular determinant size is reduced. The calculation of the integrals is then performed explicitly like in case of DFT. The reduction of the size of secular determinant leads to a drastic reduction in computation costs [41, 42]. Despite the approximation, DFTB method showed successful and reliable results on many molecules. This makes the method a good candidate calculation approach used by many research groups and outstanding publications [43–46]. DFTB is used, in combination with NEGF formalism from DFTB+NEGF code [42, 47–49], for studying some of the molecules presented in this thesis.

2.2.4 Standard and Extended Hückel Theories

Due to the fact that the ab-initio solution for systems with large molecules requires extremely high computational resources, semiempirical computation methods that perform reasonable approximations have received wide acceptance in investigations of such systems. The common approximation adopted by the different semiempirical methods is employing parametric models in calculation such that parameters are selected to allow best fitting to available experimental data [50–53]. There are several factors that helped in the development of semiempirical methods mainly the availability of experimental data, in addition

to the strong need of such methods in facilitating the geometric optimization[1] of large molecules [30, 53].

Standard Hückel theory suggests the usage of approximate and empirical parameters. These parameters can solve easily and successfully the secular determinant for planner aromatic and unsaturated hydrocarbons. The theory assumes that the basis set is formed only from the $2p_Z$ orbital of each carbon atom which is responsible for the pi-bond. Thus, the overlap integrals (χ_{ij}) between different atomic orbital is zero, and the overlap integrals for equal atomic orbital (χ_{ii}) is one (Kronecker delta function). The method uses constant empirical values for the resonance integrals (ω_{ij}) such that

$$\omega_{ij} = \begin{cases} \alpha & \text{when } i = j, \\ \beta & \text{when atom "i" is bonded to atom "j".} \\ 0 & otherwise \end{cases} \tag{2.2.8}$$

where α and β are constant values equal to negative the ionization energy of methyl radical and negative energy related to pi-bond stability, respectively. Thus, the secular determinant can be easily solved to calculate the energies of the molecule.

Extended Hückel theory (EHT) developed by Roald Hofmann 1963 is considered one of the most famous semiempirical methods [54–57]. EHT assumes that only valence electrons need to be considered while ignoring core electrons. Hence, the size of secular determinate is reduced to the number of valence orbitals. The electronic structure of the system is expressed in a basis set of LCAOs. Each valence orbital is described by a so-called Slater-type orbital (STO) which is driven by the following equation

$$STO = \Phi_{nlm}(\mathbf{r}, \varsigma) = \frac{(2\varsigma)^{n+1/2}}{\sqrt{(2n)!}} r^{n-1} e^{-\varsigma} Y_l^m(\theta, \varphi), \tag{2.2.9}$$

where spherical coordinates $\mathbf{r}$, θ and φ are used. n,l and m are principal, angular momentum and magnetic quantum numbers, respectively. $Y_l^m(\theta, \varphi)$ is the real-valued spherical harmonics. ς is called the orbital exponent which is evaluated according to set of predefined rules [58].

---

[1]Geometric optimization is to find the geometry of a specific molecular structure that guaranties the lowest ground state energy.

Similar to standard Hückel theory, the diagonal elements of the Hamiltonian matrix are equal to the ionization potential of the corresponding orbital. On the other hand, off-diagonal elements of the Hamiltonian matrix are given by Wolfsberg and Helmholz approximation which relates an off-diagonal element (H_{ij}) to the average ionization potential of orbitals i and j

$$\omega_{ij} = K \, \chi_{ij} \frac{\omega_{ii} + \omega_{jj}}{2}, \qquad (2.2.10)$$

where K is the Wolfsberg-Helmholtz constant. It is worth noting that, unlike standard Hückel theory in which the overlap matrix elements are equal to kronecker delta, the overlap integrals between STOs are computed explicitly as a function of interatomic distance [59].

After evaluating the diagonal and non-diagonal elements of the matrix, energies and wave-functions of valence orbitals are computed by solving a standard eigenvalue-problem. It is worth noticing that, although electron-electron interaction is not calculated in EHT, it is not ignored. This is because electron-electron interaction is incorporated in a sort of average way, while driving the Hamiltonian matrix from the experimental data [30].

EHT, recently developed by Quantumwise Atomistic toolkit (ATK) [60], is the mostly employed calculation methodology in this thesis. The provided EHT has additional extensions that account for self-consistent Hartree potentials. This allows the involvement of external bias and its consequent charge reconfiguration within the device [61, 62]. Hence, it provides a comprehensive picture for the electrostatic interactions in the device. The EHT method within the ATK tool is used by different research groups and shows successful results [44, 63–65].

EHT performs approximations that imply lower prediction accuracy. However, it was shown that EHT provides more accurate results than DFT-based methods for systems in which experimental data are available [61]. This is the case for all molecular devices studied in this thesis. This comes besides the main advantage of semiempirical methods in general, which is the high reduction in computational costs.

2.2.5 Non Equilibrium Green's Functions

The previously discussed ab-initio and semiempirical approaches allow the calculation of the electronic structure of a system and provide the Hamiltonian
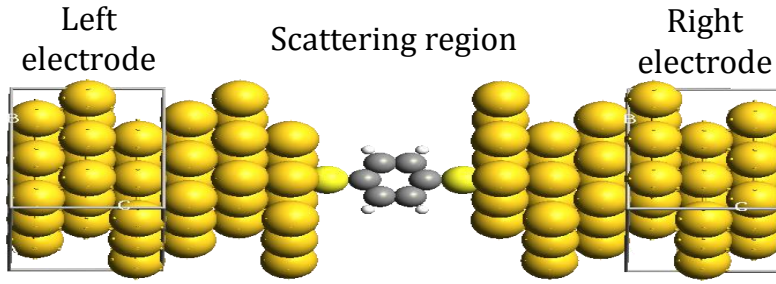
Figure 2.4: Typical structure of a molecular device. The molecule is bounded to gold electrodes through thiol-gold bond. A (111) gold with 3×3 surface is employed. The scattering region here includes the molecule and the first 3 layers of the gold contact. The electrodes regions are illustrated with wire boxes.

matrix which is required for all system's analyses. Nevertheless, induced charges in the device under bias conditions, should be considered while calculating the Hamiltonian. NEGF is typically coupled to these approaches to account for such non-equilibrium conditions [42,47,61]. Besides, NEGF provides the calculation of current and charge density of the device under bias.

Molecular/nano devices with leads are considered as an infinite system; thus a device is divided into scattering and electrode regions (Figure 2.4). The electrode regions are assumed to be semi-infinite by imposing periodic boundary conditions to allow retrieving the bulk behavior of the electrode material. The scattering region includes the main part of the device (molecule) and usually a part of the contact to allow consistent charge density with the electrode and guarantee the electrodes' bulk property [42]. In what follows, we shall assume devices with two terminal electrodes, for simplicity, but the methodology applies to general multi-terminal devices.

The subdivision of the system is translated into a subdivided Hamiltonian and wave-function of the Schrödinger equation:

$$
\begin{pmatrix} \hat{H}_1 & \tau_1 & 0 \\ \tau_1^\dagger & \hat{H}_S & \tau_2^\dagger \\ 0 & \tau_2 & \hat{H}_2 \end{pmatrix} \begin{pmatrix} \Psi_1 \\ \Psi_S \\ \Psi_2 \end{pmatrix} = E \begin{pmatrix} \Psi_1 \\ \Psi_S \\ \Psi_2 \end{pmatrix}, \tag{2.2.11}
$$

where $\hat{H}_1$, $\hat{H}_2$ and $\hat{H}_S$ are the Hamiltonian of the left electrode, right electrode and scattering region, respectively. τ_1 and τ_2 represent the interaction between

the electrodes and the scattering region [66]. Since it is considered dealing with an infinite system, two solutions corresponding to outgoing (retarded) and incoming (advanced) waves can be driven. The superscripts (R and A) will denote the case for retarded and advanced solutions, respectively. The Green's function of the system ($G(E)$) is defined as

$$(E - \hat{H})G(E) = I \tag{2.2.12}$$

Similar to the Hamiltonian matrix, G(E) is also subdivided into sub-matrices due to the different electrodes and scattering regions:

$$G(E) = \begin{pmatrix} G_1 & G_{1s} & G_{12} \\ G_{s1} & G_s & G_{s2} \\ G_{21} & G_{2s} & G_2 \end{pmatrix} \tag{2.2.13}$$

Assuming a constant perturbation η is induced to the Schrödinger equation

$$H\Psi = E\Psi + \eta \tag{2.2.14}$$

The Green's function can be considered as the function that provides the system response to such perturbation, where

$$(E - H)\Psi = -\eta \Rightarrow \Psi = -G(E)\eta \tag{2.2.15}$$

Evaluating the Green's function is usually simple, in addition it allows the evaluation of many device behavior as shall be elaborated in section 2.3. Given the wave-function of the system, the wave-function of isolated electrodes (e.g. the first electrode) can be driven from the first row of equation 2.2.11:

$$\begin{aligned} \hat{H}_1\Psi_1 + \tau_1\Psi_s &= E\Psi_1 \\ (E - \hat{H}_1)\Psi_1 &= \tau_1\Psi_s \\ \Psi_1 &= g_1\tau_1\Psi_s \end{aligned} \tag{2.2.16}$$

where g_1 is the Green's function of the first isolated electrode ($(E - H_1)g_1 = I$). This Green's functions of isolated electrodes can be driven in a simple mathematical way exploiting the periodicity property of the electrode material [67]. The isolated Green's functions are used in the calculation of the so called self-energy ($\sum$), where

$$\sum_1 = \tau_1^\dagger g_1 \tau_1 \tag{2.2.17}$$
$$\sum_2 = \tau_2^\dagger g_2 \tau_2 \tag{2.2.18}$$

These self-energies measure the impact of contacts on the device [67]. They are incorporated in the evaluation of different analytical behavior of the device. With a simple substitutions and calculations in equations 2.2.11 to 2.2.13, one can evaluate the sub-matrix Green's function of the scattering region:

$$G_s(E) = (E - \hat{H}_S - \sum_1 - \sum_2)^{-1} \qquad (2.2.19)$$

Furthermore, Green's function G(E) is used to compute density of state (D(E)) of the device by first evaluating the so-called spectral function (A(E)) where

$$A(E) = i(G(E) - G^\dagger(E)), \qquad (2.2.20)$$

$$D(E) = Tr(A(E))/2\pi \qquad (2.2.21)$$

Finally and most importantly, Green's function allows the calculation of the density matrix [ρ] of the device

$$\rho = \frac{1}{2\pi} \int_{-\infty}^{\infty} [f(E, \mu_1) G_s \Gamma_1 G_s^\dagger + f(E, \mu_2) G_s \Gamma_2 G_s^\dagger] dE \qquad (2.2.22)$$

This density matrix needs to be supplied back to the ab-initio or the semiempirical calculation methods. This is in order to recalculate the Hamiltonian matrix self-consistently while considering the induced charges due to the non-equilibrium condition.

2.3 Atomistic Analyses Derivation and Interpretation

2.3.1 Charge Density Distribution

Atoms of a molecule accumulate charges due to bonding with other atoms of different electronegativity or attracting some charges from the semi-infinite contact electrodes. The charge density of the molecular is driven from the density matrix. The intended charge density distribution in the analysis is calculated as the difference between the actual self-consistent total charge density of the molecular device and the density one would obtain by adding up the densities of neutral atoms [42, 60].

In order to identify the change in charge density under different biasing condition (e.g. excess charge due to applying a gate bias compared to equilibrium), one simply needs to subtract the charge densities of the two biasing conditions. It is worth mentioning that, the NEGF formalism is involved in the evaluation of the density matrix under bias conditions.
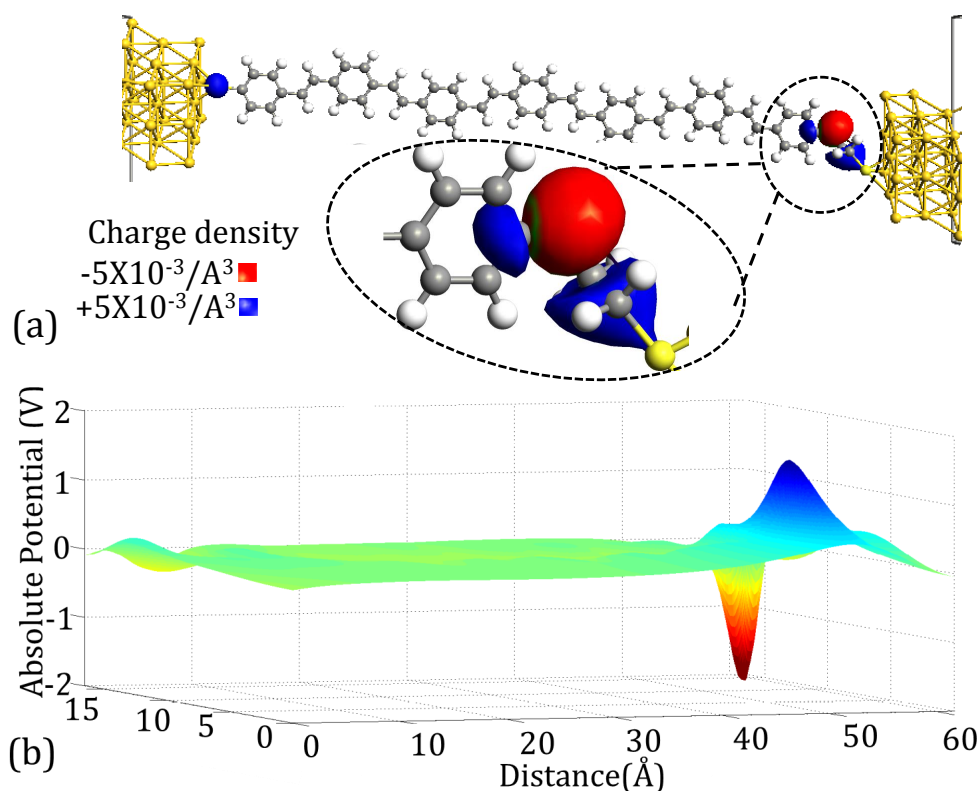
Figure 2.5: The distributions of charge density and electrostatic potential of a sample molecular device at equilibrium.

2.3.2 Electrostatic Potential Distribution

The Hartree potential of the device is simply driven by solving the three-dimensional Poisson equations on the charge density distribution. A negligible charge exchange at equilibrium (e.g. graphene sheet) is interpreted as a planer potential profile without any barriers, vice versa for a strong charge exchange within the device (e.g. boron-nitrogen sheet). Both charge density and electrostatic potential are outputted from the atomistic simulation tools as discrete points in three dimensions mesh.

Figure 2.5 illustrates the distribution of charge density and electrostatic potential of a sample molecular device at equilibrium. Oxygen atom have higher electronegativity than carbon, thus shared electrons with neighbor carbon atoms are attracted to oxygen. This results in the observed negative charge accumulation over oxygen. Solving Poisson equations shows a potential profile with potential energy barrier near oxygen.

The potential drop profile along the device under specific bias is the difference between the electrostatic potential of the device under bias and the equilibrium electrostatic potential. The potential drop profile along the molecule usually plays a key role in understanding the device functionality, as explained in section 2.1.

2.3.3 Molecular Orbital Distribution

After solving the Schrödinger equation, the eigenvalues of the system are the energy values of molecular orbitals, while the eigen functions represent the molecular orbitals. In a nutshell, molecular orbitals are the functions that describe the wave-behavior of electrons within the molecule. The probability of finding electrons within different regions of the molecule at a certain energy level (eigenvalue) is what we call here as the molecular orbital distribution.

Usually the interesting molecular orbitals for transport analysis are the frontier ones whose energy values are near the Fermi-energy of the device namely, highest occupied molecular orbital (HOMO) and lowest unoccupied molecular orbital (LUMO). If the distribution of the conducting molecular orbital is delocalized along the molecule (see the example of a molecular wire in Figure 2.6right), these MOs afford channels for electron transport along the molecule. Hence, this molecule will allow high conductance, which is favorable for molecular wires. If the molecular orbitals, responsible for conduction, are localized on particular regions of the device (see the example of a molecular rectifier in Figure 2.6left), this molecule will generally have low conductance. Such localization of molecular orbital is favorable sometimes depending on the device functionality (e.g. in molecular rectifiers).

Let us join this information with the previous discussion regarding the conduction through single level system. For a device to conduct perfectly: a molecular orbital should exist between the chemical potentials of the contact electrodes, and the distribution of this molecular orbital should be delocalized along the molecule.

2.3.4 Density of States

Density of States (DOS) stands for the number of states available at each energy level that can be occupied with electrons. DOS of isolated molecules are dis-
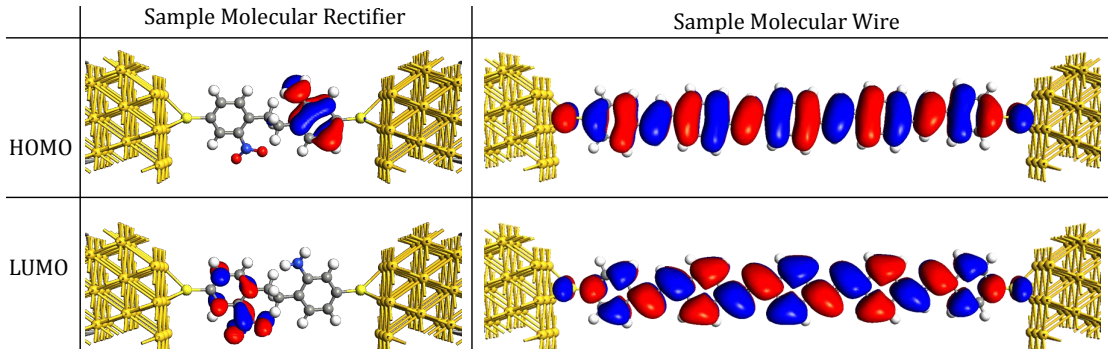
Sample Molecular Rectifier	Sample Molecular Wire
HOMO	
LUMO	

Figure 2.6: The HOMO/LUMO distribution of a molecular rectifier (left) and a molecular wire (right).

cretized, but DOS of semi-infinite electrodes are continuous (forms a kind of bands). For a molecular device, discrete states are broadened by the influence of the electrodes. The position of peaks in the DOS over the molecular device corresponds to molecular orbital energy levels which are the eigenvalues solution of the Schrödinger equations. High DOS at a given energy level mean that there are many states available for occupation while zero DOS indicates that no states exist at that energy level.

In many cases in molecular devices, some states are localized only on a specific region within the device which is usually due to inhomogeneity that can be generated by doping for instance. In these cases, it is recommended to analyze the so called local density of states (LDOS) over the different regions of the device to gain a better understanding. LDOS is related to the localization of molecular orbital distribution discussed above.

2.3.5 Transmission Function

Transmission function is calculated self-consistently using the NEGF model taking into consideration the non-equilibrium and open boundary conditions within the device. It is evaluated by the following equation

$$T(E, V_b) = Tr[\Gamma_1(E)G^R(E)\Gamma_2(E)G^A(E)], \qquad (2.3.1)$$

where "Tr" is the trace of the matrix, Γ_1 and Γ_2 are the coupling coefficient (broadening) at the first and second electrodes, respectively. $G^R(E)$ and $G^A(E)$
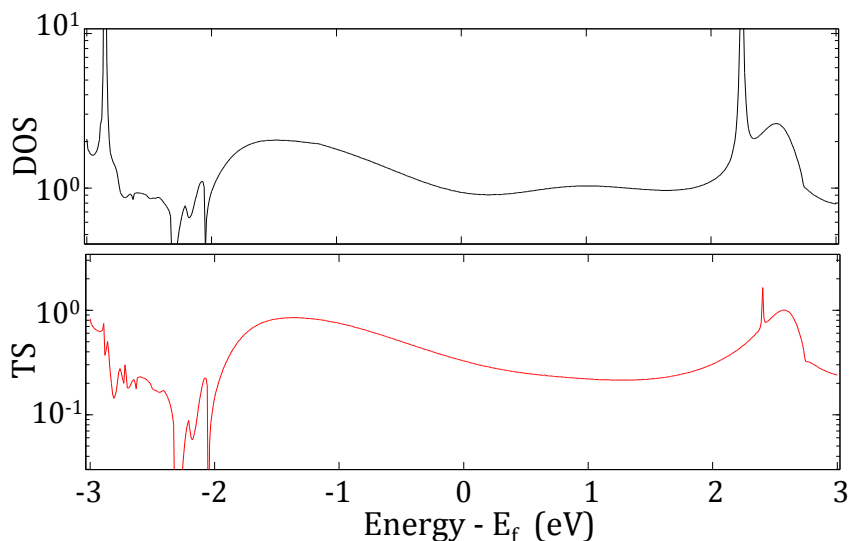
Figure 2.7: An illustration for density of state and transmission function of a sample di-thiol benzene molecular device. Both curves have similar behavior in terms of peak positions.

are the retarded and advanced Green's functions of the device, respectively. The coupling coefficient (e.g. Γ_1) is evaluated using the equation:

$$\Gamma_1 = i\left(\sum_1^R - \sum_1^A\right), \tag{2.3.2}$$

where $\sum_1^{R(A)}$ are the retarded and advanced self-energies of the first electrode. Transmission function represents the probability for an electron at specific energy to flow through the device from one electrode to another. The Green's functions parameters, as well as, the transmission probability strongly depend on the DOS within the device. This is because an electron with a particular energy can flow through the device if there exists an energy state delocalized along the device.

Figure 2.7 illustrates the density of state and transmission function of a sample dithiol benzene molecular device. It can be noticed that most of the peaks are at the same energy positions in both curves, except for some peaks in the density of states that do not exist in the transmission function. Those exceptional peaks correspond to states which are localized on some parts of the molecule only. This can be verified by other analysis (molecular orbital distribution or LDOS).

Another parameter that affects the transmission probability is the length of the molecule. Even if the HOMO/LUMO is far from the Fermi-level, electrons can tunnel through the HOMO-LUMO gap of a short molecule. This kind

of tunneling, in the absence of energy states, is reduced with the increase of molecule's length.

2.3.6 Conduction Current

The current is computed from the transmission probability function using the well-known Landauer formula [68]

$$I = \frac{2e}{h} \int_{\mu_1}^{\mu_2} T(E, V_b)[f(E - \mu_1) - f(E - \mu_2)]dE, \qquad (2.3.3)$$

where $T(E, V_b)$ is the transmission probability through the device for an electron at energy E and an applied bias equals V_b; f is the Fermi function. The chemical potential of the first and second electrodes are $\mu_1 = E_F - V_b/2$ and $\mu_2 = E_F + V_b/2$, respectively. E_F is the Fermi energy of the device. Therefore, the current can be interpreted as the area under the transmission curve within the bias window $[\mu_1, \mu_2]$. For multi-terminal devices, the current between each two terminals is calculated using the same equation. However, the transmission function is changed to include the impact of the bias of the other terminals.

Although standard NEGF provides a good description of coherent tunneling, it does not involve dissipation (e.g. electron/phonon interactions) [69]. There are currently many attempts to include dissipation effects in the transport calculation in order to render the analysis closer to real devices [70].

3 Basics of Molecular Electronics

3.1 The Rise of Molecular Electronics

Molecular electronics is considered one of the promising technologies which are based on bottom-up approach, in which microscopic components are assembled together to build complex macroscopic systems. This is opposite to the current semiconductor technology which is based on top-down approach aiming at reducing the dimension of components that build the systems.

In fact, molecular electronics contains several advantages that qualify it to be a promising technology. Molecular electronics provides an ultimate increase in integration density since single molecules intrinsically in nanometer dimension could be employed as active electronic devices. Most importantly, molecular devices are capable of providing features like rectification [4,71–73], negative differential resistance [64,74–76], conductance switching [9,77,78], magnetoresistance [79–81], coulomb blockade [82,83] and Kondo effect[1] [83,84], which open the way for a variety of novel electronic applications. In addition, molecular devices are expected to provide a high operating speed which will be further emphasized in Appendix A.

Despite the promising advantages offered by molecular electronics, it is hard to claim that it can replace the current semiconductor technology since the performance of the main electronic components like transistors and rectifiers are still far below that offered by semiconductor devices. Nevertheless, it seems reasonable that molecular devices can support the current semiconductor technology in some applications that can exploit its size, speed and distinguishable device functionalities.

---

[1]Kondo effect is an unusual scattering mechanism in which the conductivity of a device is varied with temperature change due to the presence of spin impurities.

3.2 Molecular Devices Realization

Understanding the quantum transport behavior of molecular devices is of a great importance, however reader with limited background on single-molecule devices should also have an idea regarding the realization and measurement of such tiny devices. The preparation of molecules is done through chemical synthesis and this is out of the scope of the thesis. In terms of electronic devices, everything other than the active region (the molecule) is desired to be ideal in the sense that any observed behavior is only dependent on the molecule. This condition is rather difficult when it comes to atomic scale devices. In this subsection we discuss how molecules are linked to contacts, some realization techniques of atomic contacts, and the required measurement cautions for such molecular devices.

Molecules are connected to electrodes via linkers which are known as anchor groups. The anchor groups should provide a reliable and mechanically stable connection between molecules and electrodes. The anchor is not supposed to generate any potential barriers so that any observed behavior can be directly attributed to the molecule itself. The commonly used anchor groups are the thiols because typically metallic electrodes (specifically gold) are used and thiol form a strong covalent bond with gold and other metals [85, 86]. Other anchor groups like amines, nitro, carboxylic-acid and cyano are also used in literature, yet they show weaker electronic coupling to metals than thiols [87–92].

The common method of preparation is by dropping the solution containing molecules over the surface containing the metallic electrodes with the atomic-gap. The molecules are chemisorbed by electrodes via anchor groups [89, 92]. After that, the device is dried leaving the molecule only contacted to the electrodes. Another popular assembling technique is the self-assembled mono-layer (SAM) in which the substrate is immersed into the solution containing the molecules [93–95]. The anchor groups of the molecules are spontaneously chemisorbed on the substrate in a self organized domain. This technique is typically used for rod-like molecules [95].

In fact, there are many techniques that were developed to provide atomic-scale contacts, a review of these techniques can be found in [2]. The main goal of all these techniques is to create a nanometer-wide insulating gap between
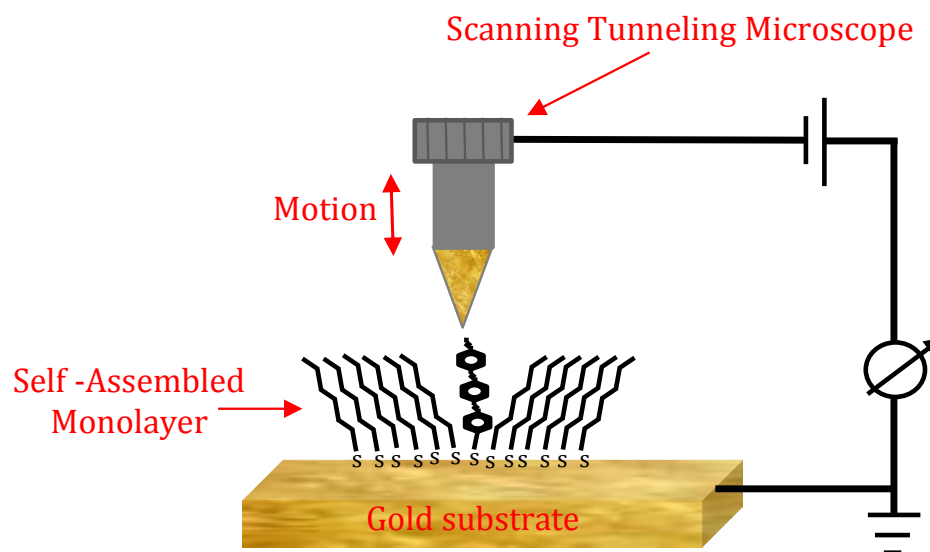
Figure 3.1: A simple schematic for a scanning tunneling microscope measurement setup of a self-assembled monolayers molecules grown on a gold substrate.

conductive terminals. These conductive terminals should act as the contact electrodes of the device so that ideally current cannot flow in the absence of the molecule (active device element).

Scanning tunneling microscope (STM) is among the commonly used techniques for contacting molecules and measuring the currents flowing through them [94, 96]. Figure 3.1 illustrates a schematic the STM. In this technique, a thin metallic tip electrode is kept at a distance from the other metallic electrode. STM measures the tunneling current which is reduced exponentially by increasing the distance, till the atomic gap is created. Atomic force microscope (AFM) is also used in a very similar way, but the gap is detected from measurement of forces between the tip and the surface [97, 98]. SAM method is employed for assembling molecules on the surface.

Another widely used technique for realization of atomic-scale contacts is mechanically controllable break-junction (MCBJ). MCBJ is implemented by suspending a metallic wire that bridges a nanogap on a flexible substrate (Figure 3.2). The substrate is positioned within a three-point configuration composed of two counter supports and a pushing rod which is controlled by a motor or a piezo-driver [99–101]. Pushing the rod causes an increase in the bending curvature of the substrate, which elongate the wire until it is broken. The breaking of the
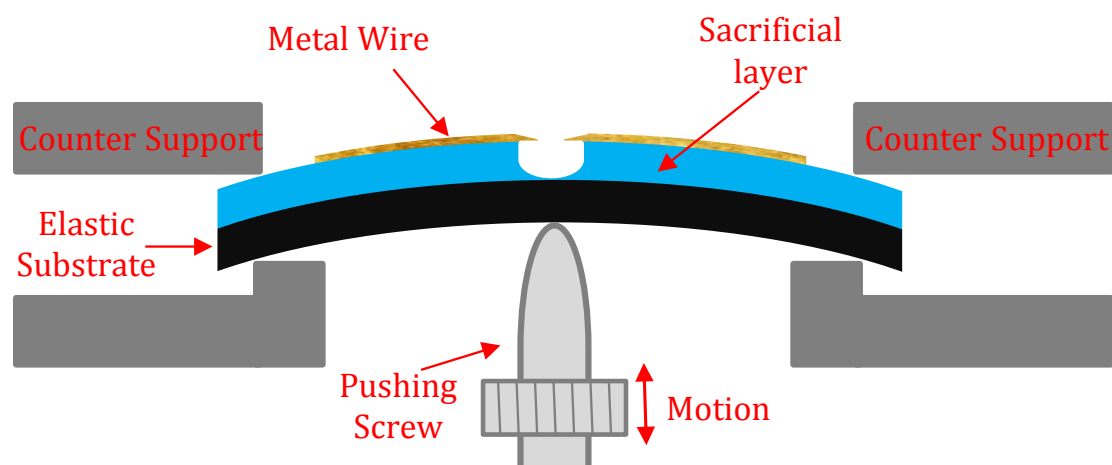
Figure 3.2: A simple schematic for the working setup of a mechanically control-
lable break-junction.

wire is detected at the instance when no current flow through the wire under
bias. Similar to MCBJ, electromigration technique aims at breaking a metallic
wire, but by applying an electrical process. The basic idea of electromigration is
that thin metallic wire has a threshold current density. Beyond this threshold,
ions of the metallic wire start to move, and this causes the wire to break. In
fact, the process is not so simple as might be seen because many parameters
has to be carefully considered for managing the final size and structure of the
induced gap [83,84]. Unlike MCBJ, any insulating substrate can be used, and the
produced gab has an ultimate stability [2]. One disadvantage of electromigration
method is that once the gap is produced there is no way to tune it [84].

Other electrochemical techniques can be found in literature [102–104]. Nan-
otransfer printing is currently rising as a promising technique for creating
nanogaps since it would afford a reliable and fast fabrication process [105]. In
Chapter 5, we shall discuss another method based on growing a hetero-structure
nanowire which was employed by a collaborate group to build a molecular
device with a back-gate.

There are some points that should be carefully considered when discussing
molecular device measurement and characterization [2,69]. It is important to
decide on the measurement circuitry: which is to be supplied and which is to
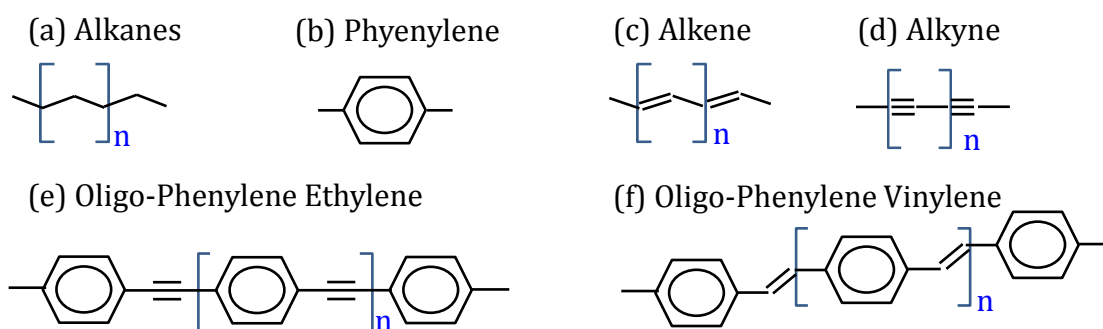be measured, current or voltage? Commonly, voltage supply is preferred if

(a) Alkanes
(b) Phyenylene
(c) Alkene
(d) Alkyne

(e) Oligo-Phenylene Ethylene
(f) Oligo-Phenylene Vinylene

Figure 3.3: Various important molecules commonly used as a building block for the molecular devices.

the molecule has low conductance. However, it is worth noting that an abrupt high applied bias may destroy the sample thus it is recommended to use a ramp bias to define the boundaries of biases in the first measurement cycle. One should also notice that some junctions have a limited lifetime. In addition, self-heating/electromigration generated in molecular junctions needs to be carefully monitored to prevent device mal-functionality or at least incorrect measurement [2]. Finally, it is recommended to conduct repeated measurement on different samples in order to identify the average behavior of the molecular device. This can be referred to the non-symmetric coupling between the molecules and the electrodes.

3.3 Reviewing Important Molecular Devices

Figure 3.3 sheds light on some of the main molecules which are frequently used as a building block in various molecular devices. The first is the phenylene ring which is a benzene ring connected from both sides to other molecules. Due the presence of exchanging single/double bonds where electrons can move easily, phenylene has a high conductivity. Similarly, chains of carbon with exchanging single and double/triple bond allow high charge conductance. Combinations of such molecules like in case of Oligo-Phenylene Ethylene (OPE) and Oligo-Phenylene Vinylene (OPV) are considered among the most famous species employed in molecular wires, since their delocalized pi-bonds facilitate the charge's transport along them [106–110]. Moreover, OPEs and OPVs are mechanically very stable and rigid which are favorable properties for contacting molecular devices [111].

On the other hand, alkane chains consisting of carbon with only saturated sigma bonds are known to possess good insulating properties [111–113]. This is because sigma bonds force electrons to be localized. Alkane chains enjoy excellence self-assembly property which let it a good candidate for many research studies [114, 115]. Unfortunately, alkanes are not rigid, thus only short chains are used in molecular devices.

3.3.1 Molecular Rectifier

Rectifiers represent the simplest and most fundamental components used for logic circuits and memory cells. Aviram and Ratner proposed the first single molecular device working as a molecular rectifier in 1974 [4]. Since then, other promising molecular devices exhibiting rectification have been proposed. In 1997, Metzger et al. were able to realize a molecular rectifier, based on similar mechanism from the proposed Aviram-Ratener rectifier. They employed Hexadecylquinolinium Tricyanoquinodimethanide molecules and achieved a rectification ratio[2] up to 13 [71, 116].

Rectification is usually due to two main factors: inherited asymmetry within the molecule and/or asymmetric linkage between the molecules' terminals and the electrodes. There are several ways available in literature to realize the asymmetric linkage between the molecule and the electrode, for instance, by using asymmetric linker groups [8, 117, 118] or by letting the molecule with no covalent bond to one electrode [72, 119]. In addition, it was reported that using two different electrode materials provide current rectification due to the formation of asymmetric molecule/electrode barriers [73, 120]. On the other hand, inherited asymmetry within molecules can arise from a structural asymmetry [121, 122] or it can be forced by adding dopants at specific parts of molecules [123, 124]. There are many devices in literature where two or more of the asymmetry factors are merged aiming at enhancing the rectification performance [125, 126].

Employing a prototype molecule from the family molecular rectifier that possesses asymmetric linkers, Kornilovitch et al. at Hewlett-Packard Laboratories

---

[2]The rectification ratio is defined as the ratio of positive bias current to negative bias current $RR = I(V)/I(-V)$.
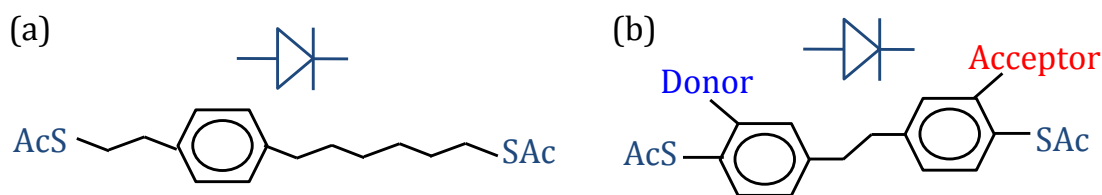
(a)

(b)

Figure 3.4: (a) A molecular rectifier with asymmetric tunneling barriers at the two terminals. (b) A prototype D-sigma-A molecular rectifier.

are able to achieve a rectification ratio up to 500 [8] (Figure 3.4a). This family of molecular rectifiers with asymmetric linkers to electrodes is characterized by creation of asymmetric tunneling barriers at the two terminals. This in turns leads to asymmetric variation in the electrodes chemical potential under positive and negative bias. Consequently, current flows under forward bias earlier than under reverse bias. Unfortunately, using long chains of tunneling barriers in their proposed device led to a strong reduction in the on-current [8].

The donor-sigma-acceptor (D-σ-A) molecules are the most popular molecules in the family of molecules exhibiting inherited asymmetry. Figure 3.4b illustrate a simple prototype D-σ-A molecule. The name D-σ-A of the molecules comes from the fact that they are composed of two electroactive regions, donor (D) and acceptor (A). The two regions are linked by a σ covalent bond which has some sort of insulation since it forms a potential barrier.

Examples for substitutes used as electron acceptors are NO_2, CN, CHO. The commonly used substitutes for electron donors are NH_2, OH, CH_3. The acceptor region is electrostatically negatively charged while the donor region is electrostatically positively charged; thus an electric dipole moment is created in the direction of transport. This forces the charge transport to be favorable when the bias is in the same direction of the dipole than the other bias direction. Hence, current rectification occurs.

The alignment of molecular orbitals with the chemical potential of the electrodes under high bias causes the molecule to heat, and this may change the device response. Hence, the measurement may become irreproducible. In fact, this problem was observed in Metzger's experiment in which the current is reduced after each measurement of the IV curves [123].

3.3.2 Molecular Tunnel Diode

Tunnel diode (or Esaki diode) is a device characterized by negative differential resistance (NDR) behavior such that there is a bias interval in which the current decreases with increasing voltage [127]. This NDR behavior has many applications in low power memories as well as high speed circuits and systems like oscillators and microwave amplifiers [128,129]. Many researches were conducted on molecular devices that were found to exhibit NDR behavior [64,74–76].

John Le et al. examined bilayer molecular junction composed of two SAMs with a structure Hg-alkanethiol//arenethiol-Au [76]. They reported the observation of a reproducible NDR behavior and a peak-to-valley ratio up to 4.5. They suggested that the NDR behavior could be related to a reduction in the effective number of contacted molecules. This might return to a loss of contact with electrodes or a loss of contact in-between the SAM layers [76]. Yongqiang Xue et al. investigated SAM 4-p-terpheylthiol molecules and observed a NDR in the measured IV curves [64]. They utilized extended Hückel theory to theoretically study the molecule. They claimed that the potential drop profile along the molecular devices, especially near the contact electrodes, is responsible for the observed NDR behavior.

Moreover, many recent theoretical studies on molecular devices that exhibit NDR behavior were conducted [130–133]. According to the equations used for current calculation in subsection 2.3.6, the NDR behavior corresponds to a reduction in the area under the transmission spectrum curve within the bias window. In most cases, the origin of this reduction is a broadening of the molecular energy level due to the influence of the applied bias on coupled electrodes (Figure 3.5).

3.3.3 Molecular Switch

Molecules that exhibit conductance switching have gained a lot of research interest in the recent years since they can be used as memory elements. There are some debates regarding physics behind the conductance switching in some molecules. The conductance switching occurs usually for one or a combination of the following reasons:

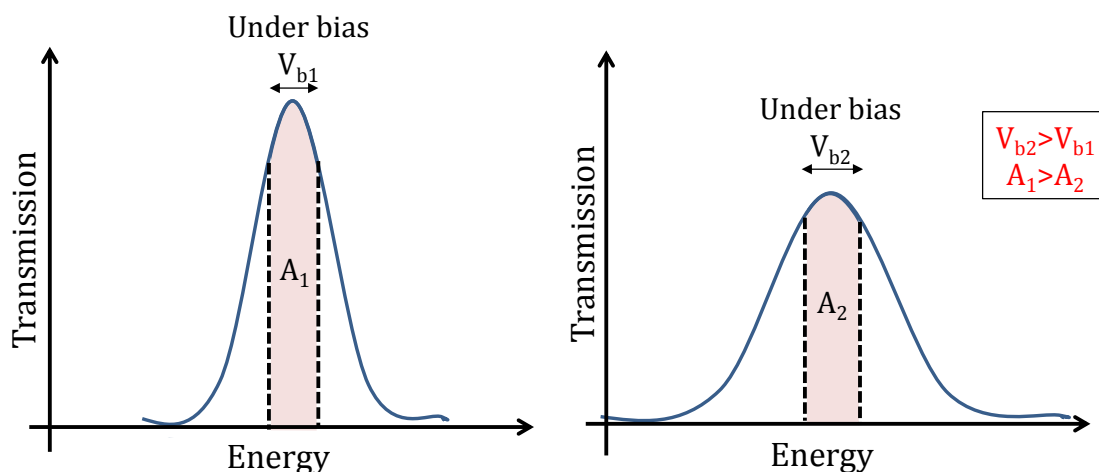- Changing the angle between the molecule and the contact electrodes

Figure 3.5: The TS of a device under two different bias $V_{b2} > V_{b}1$. Although the bias window increases, the current which is proportional to the area under the TS curve within the bias window is reduced leading to the NDR behavior.

- The molecule exhibit new stable charging state due to an oxidation or reduction process

- The molecule exhibit a new stable isomeric state (change in the organization of the atoms in the molecule)

Peter Liljeroth et al. employed naphthalocyanine molecule that has advantages of being planer, symmetric and self-assembled [77]. The switching occurs under high bias (1.8 V to 2.0 V) by the action of induced tunneling electrons to the molecule. The origin of bistability was claimed to be due to a change in the positions of two hydrogen atoms within the molecule (hydrogen tautomerization). This hydrogen tautomerization causes a significant change in the molecule's conductivity.

Another prototype molecular switch that gained the interest of many research groups is the bipyridyl-dinitro oligophenylene-ethynelene dithiol (BPDN-DT) molecule (Figure 3.6a). Lörtscher et al. at IBM were able to realize this molecular device and demonstrate the conductance switching behavior [9]. They verified that the switching is not spontaneously stochastic by building a similar molecular device without the nitro-groups namely bipyridyl oligophenylene-ethynelene dithiol (BP-DT) molecule (Figure 3.6b). Unlike BPDN-DT molecule, BP-DT molecule does not show any switching behavior. The BPDN-DT shows bi-stable
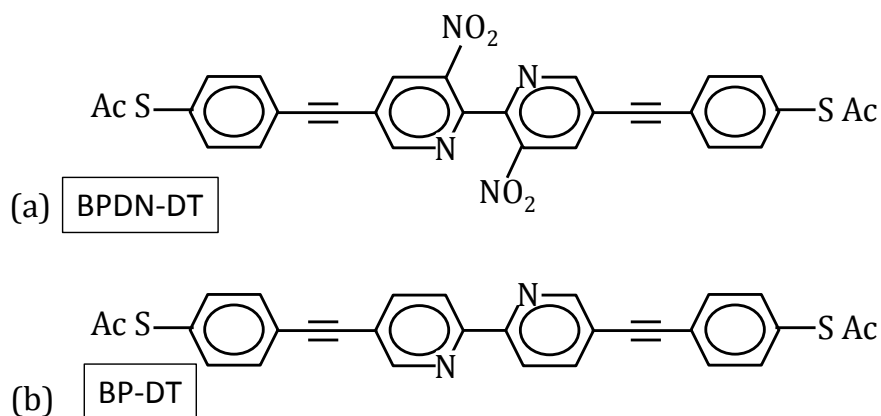
Figure 3.6: Molecular structures A) Bipyridyl-dinitro oligophenylene-ethynylene dithiol and (b) bipyridyl oligophenylene-ethynylene dithiol.
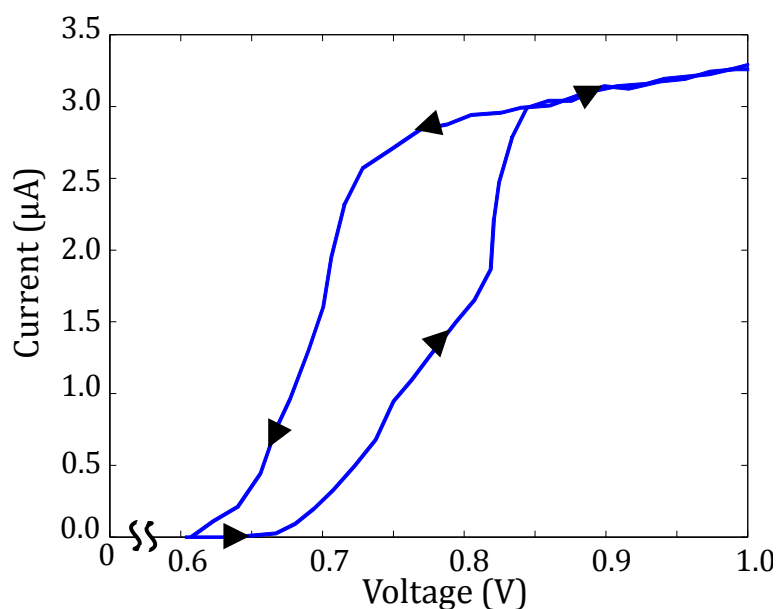

Figure 3.7: The IV curve of the BPDN-DT molecule illustrating the conductance switching behavior, adopted from [9].

IV curves in the bias window 0.6 V to 0.9 V (Figure 3.7). Both molecules show non-linear current curves where they start conducting at a threshold bias around 0.6 V. However, BP-DT shows conductance value of 4-6 times that of the BPDN-DT after threshold.

Various arguments were proposed for explaining the reason of switching behavior of BPDN-DT molecule. Tour et al. conducted the measurement of the

BPDN molecule in air and within electrolyte to allow electrochemical potential controlling of the molecule [78]. They found out a strong correlation between the electrochemical potential of BPDN molecules on one hand, and the value of bias that causes switching and current peaks, on the other hand. This suggests that a redox process is responsible for the switching. In addition, Nitzan et al. analysis based on Marcus theorem came to the same conclusion, namely that the redox process is the source of the switching behavior [134].

On the other hand, Evers et al. illustrated that the energy required to insert/remove an electron is much higher than the observed switching bias in the experiment [135]. Moreover, they showed through first-principles simulation that a reorientation in the angle between the molecule and the gold electrode could be the reason for the switching. This reorientation originates from the impact of the electric field on a dipole created by the nitro-groups [135]. Based on few atomistic analysis from our side, we believe that relating the switching to redox process is the most appropriate for this particular molecule. Noting that, there is no complete loss/gain of single electrons in the redox process; instead only variation in a fraction of charges causes the switching (see Appendix B).

3.3.4 Three Terminal Molecular Devices (Molecular Transistors)

Up to now, molecules are used almost exclusively in two terminal devices. Nevertheless, gated molecular devices were realized, and the gate influence was experimentally investigated by many research groups [83, 136–139]. Hyunwook Song et al. reported the ability to achieve direct molecular orbital modulation using a gate bias, which allows a direct control on the transport current through the molecular device [138].

Jiwoong Park et al. were able to realize a molecular transistor employing single cobalt ion linked to gold electrode via an organic barrier [83]. Coupling strength between the cobalt ion and the electrodes is controlled by varying the length of the barrier. The device behaves as a single-electron transistor in case of a weak coupling, yet a Kondo-assisted tunneling is detected in case of a strong coupling.

Moreover, some outstanding theoretical work was recently conducted to investigate feasible molecular device application that can employ such molecule. N. Lang and P. Solomon at IBM studied the gate effect on a three-leg
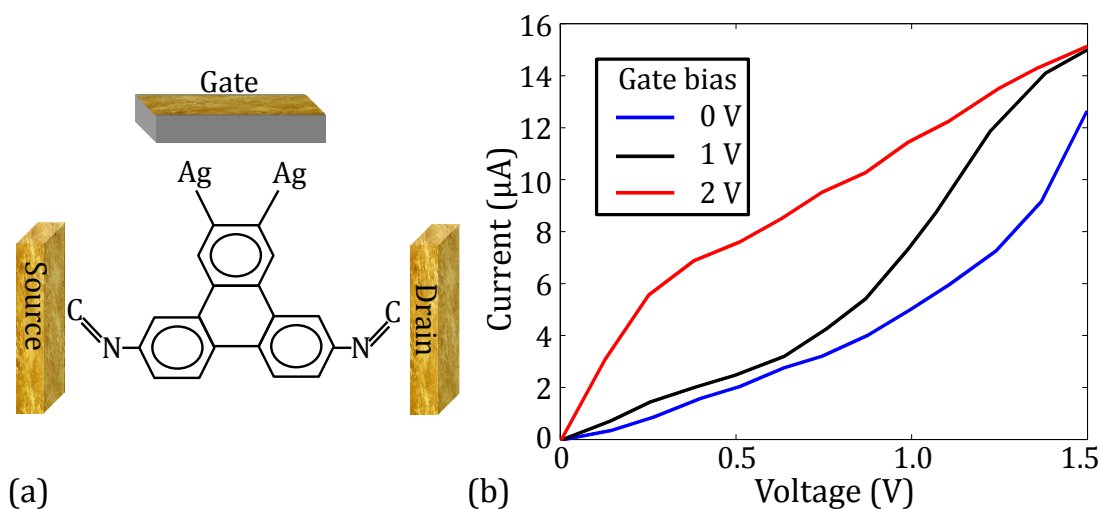
Figure 3.8: (a)Structure of a three-leg molecular transistor and (b) its output characteristic curves, adopted from [140].

molecule [140, 141]. They applied an electrostatic gate to one leg having silver atoms attached to it, in order to allow a good coupling with the gate, see Figure 3.8a. The device shows very interesting transmission spectra modulation with the gate bias. Figure 3.8b illustrates the output current characteristic of the device under different gate biases.

M. Hliwa et al. proposed different three-leg molecules which can be employed for building standalone logic gates [142–144]. Figure 3.9a illustrates a three-leg molecular device which acts as a standalone logic OR [142]. In this implementation, they interpret the input logic as high voltage (0.4 V) for logic '1' and low voltage (0 V) for logic '0'. On the other hand, they interpret the output logic as high current for logic '1' and low current for logic '0'. Figure 3.9b shows an approximate contour view of the result which demonstrates a correct functionality of the molecule.

3.4 Challenges Facing Single-Molecule Devices Technology

This section illustrates the main challenges facing single-molecule devices technology. It is worth mentioning that, the previously described advantages of molecular electronic devices are sufficient to motivate several research groups to currently work on resolving these challenges. The fast development in the-
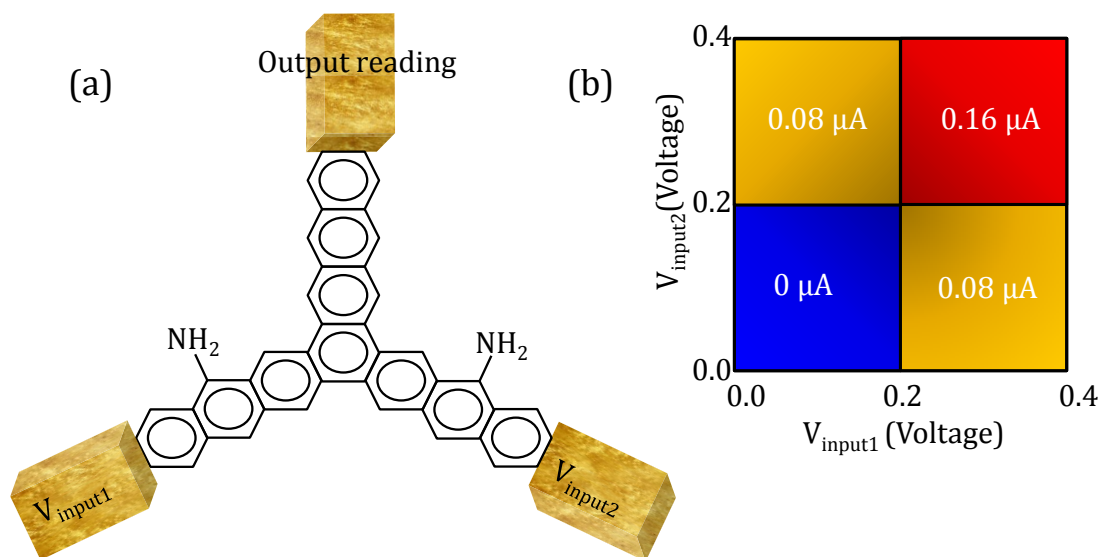
Figure 3.9: (a) Structure of a three-leg molecular device working as a standalone logic OR. (b) An approximate contour view of the output current reading under various biases at the inputs.

oretical methods for modeling and simulation of transport through molecular devices like Non-equilibrium Greens' functions [145–147] and density functional theory [40, 47] approaches and semi-empirical methods [42, 148] shows a great success in reducing the gap between theory and experimental results. These approaches provide perfect involvement of coherent tunneling; however, they usually do not involve electron/phonon interactions and electron coupling to the solvent where the molecule exist [69]. Such involvements could further enhance the accuracy of theoretical methods in mimicking the experimental results.

Despite the outstanding attempts to model molecular transport [8,149,150], there is still some lack in understanding the fundamentals of quantum transport properties within molecules. Consequently, the ability to design/improve molecules for a specific device functionality is still a difficult task. This constitutes one of the major challenges before the fast development of molecular devices.

Moreover, there are challenges encountered in realization such as molecules' synthesis, fabrication of the nano-contacts and device robustness. Last but not least, the ultimately difficult realization challenge is integrating sets of single-molecule devices together in one system and letting molecules electronically coupled in a guided way.

4 Two Terminal Molecular Devices

4.1 Introduction

Thanks to major advances in chemical and fabrication processes, various electronic devices based on single molecules have been developed. On the theoretical level, many attempts have been made to provide a clear view of the charge transport mechanism through molecules. Nevertheless, the overall picture is not yet complete. For instance, despite the success of the first single molecular diode prototype by Aviram and Ratner [4], the factors that control the transport behavior still need more investigation.

In this chapter we focus on two terminal molecular devices, mainly molecular rectifiers. These devices deserve all attention because they represent the simplest and most fundamental components used in logic circuits and memory cells. After Aviram and Ratner diode proposal, other promising molecular devices exhibiting rectification have been developed [72, 122, 151–153]. In 1997, Metzger et al. were able to realize a molecular rectifier employing Hexadecylquinolinium Tricyanoquinodimethanide molecules [123]. They achieved a rectification ratio[1] up to 13. Recently, Díez-Pérez et al. employed a simple diblock dipyrimidinyl-diphenyl molecule as a molecular rectifier with rectification ratio around 2.5 [154]. Kushmerick et al. managed to achieve a rectification ratio that reaches up to 4 by using a simple OPE molecules with asymmetric linkers between the terminals of the molecule and the contact electrodes [72]. Interestingly, Kornilovitch et al. at HP-Labs were able to achieve a rectification ratio up to 500 for molecules with asymmetric linkers that create asymmetric tunneling barriers at the two

---

[1]The rectification ratio is defined as the ratio of positive bias current to negative bias current $RR = I(V)/I(-V)$.

terminals [8]. Using long chains of tunneling barriers in their proposed device led to a strong reduction in the on-current [8].

This chapter is organized as follows: we first illustrate the general methodology used for studying the different molecular devices in this chapter. After that, we discuss an important design concept that can be used to control the rectification direction and strength of a molecular device. We then verify this concept via controlling the rectification behavior of a dipyrimidinyl-diphenyl molecule. Moreover, we propose a novel molecular rectifier employing simple OPV molecules and demonstrate that we can achieve a rectification ratio of more than three orders of magnitude. Subsequently, we provide a study for the influence of doping on the rectification performance of molecular devices.

The last section illustrates a study on a two-terminal molecular device that shows an interesting NDR behavior. All the studies on the molecular devices are based on atomistic analyses, which help in understanding the devices behavior and build relations among the different properties of molecules.

4.2 Methodology

Molecules are built and geometrically relaxed, using either Broyden-Fletcher-Goldfarb-Shanno (BFGS) method [60] or Conjugate gradient algorithm [155], until all residual forces in each atom are less than $0.05\,\text{eV}/\text{Å}$. Afterwards, each molecule is attached to a semi-infinite ($3{\times}3$) (111) gold electrodes through thiol-gold bonds (Figure 4.1). The sulfur atoms are located 1.71Å from the gold surface which corresponds to S-Au bond length 2.38Å. This is similar to values validated in [156]. We have verified that the small variations in angles or distances between the molecule and the electrodes, as well as, the size of the electrodes do not change the qualitative behavior of the device, except for some small variations occur.

In order to describe the charge transport under an applied bias, the NEGF formalism is coupled to either extended Hückel theory by Atomistix ToolKit [60, 61] or to Density Functional Theory and its tight-binding approximation from DFTB+NEGF code [47, 147, 157].

Results from the EHT or DFTB are fed into the NEGF model to calculate the drain current self-consistently while considering the non-equilibrium and open
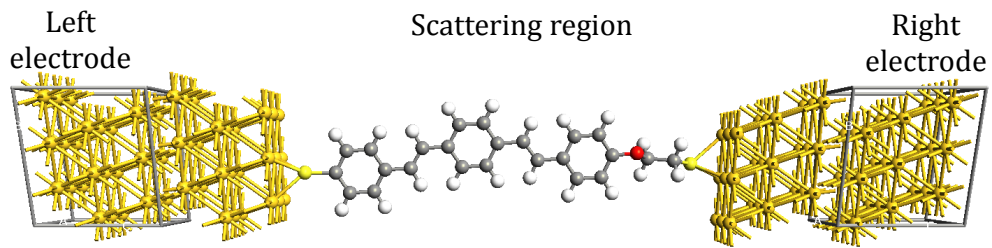
Figure 4.1: Typical structure of a molecular device. The molecule is bounded to gold electrodes through thiol-gold bond. A (111) gold with 3×3 surface is employed. The electrodes regions are illustrated with wire boxes.

boundary conditions. According to [34, 158], these are typical for the quantum transport in devices. The self-consistence solution also considers the electrode screening effect and molecule-electrode coupling. The current is calculated using the Landauer formula [68]

$$I = \frac{2e}{h} \int_{\mu_L}^{\mu_R} T(E, V_{ds})[f(E - \mu_L) - f(E - \mu_R)]dE, \qquad (4.2.1)$$

where $T(E, V_{ds})$ is the transmission function of the device at energy E and an applied drain-source bias V_{ds}, f is the Fermi function and μ_L/μ_R are the chemical potential of the left/right electrodes, respectively. Thus, the current is determined by calculating the area under the transmission curve within the bias window ($\mu_L - \mu_R$). For all devices, the employed boundary conditions in the Multi-grid Poisson solver are Dirichlet along the transport direction and Neumann in the directions perpendicular to the transport.

4.3 Important Design Concept

An important design concept is schematically presented in Figure 4.2. It shows a molecular device whose conduction is dominated by transmission through its Lowest Unoccupied Molecular Orbital (LUMO). The molecule has a highly resistive region near the right electrode where the whole applied potential drop occurs.

In general, current can flow through a molecular device if a molecular orbital lies in between the chemical potential of the left and right electrodes [27]. As a result, the molecule in Figure 4.2 shall conduct current only when the negative potential
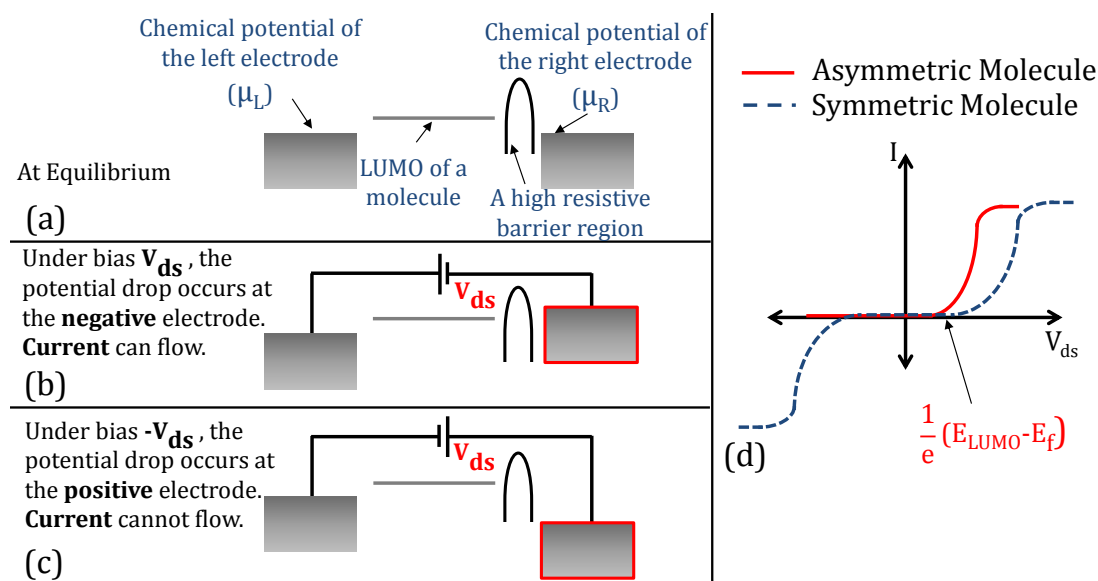
Figure 4.2: A simplified energy diagram of an asymmetric device that conducts through LUMO and has a high resistive barrier at the right electrode (a) at equilibrium, (b) under bias V_{ds} where the potential drop occurs only at the negative electrode, and (c) under bias $-V_{ds}$ where the potential drop occurs only at the positive electrode. (d) A comparison between the IV-curves of this asymmetric device and another symmetric one. The asymmetric device resembles a rectifier with an on-threshold bias equal to the difference between the LUMO energy level and the device Fermi-level at equilibrium.

is applied on the right electrode relative to the left electrode. In other words, the magnitude of current is only dependent on the amount of the applied potential that drops at the negative electrode. If this molecular device is symmetric (either no barrier or a barrier at both electrodes), the same potential drop would occur at the negative electrode for both positive and negative biases. Thus, an anti-symmetric IV-curve will be obtained (dashed curve in Figure 4.2d). Note that, the on-threshold bias would be higher for the symmetric device since not the whole potential drop occurs at the negative electrode.

As a consequence, we can conclude that any asymmetric molecular device that conducts through a single molecular orbital (LUMO or HOMO) shows rectification. *We claim that the strength of the rectification depends on the difference in*

resistance of the terminal portions of the molecule near the contacts[2]. In case that the molecule has a LUMO (HOMO) dominating conduction, the side of the molecule with higher resistivity, that absorbs most of the potential drop, acts as the cathode (anode).

4.4 Results and Discussion

4.4.1 Dipyrimidinyl-Diphenyl Molecular Rectifiers

Recently, a lot of attention has been devoted to a diblock dipyrimidinyl-diphenyl molecule, because of its simple molecular structure and rectification response [10, 122, 159–161]. In this subsection, we show that the rectification of a molecular device can be controlled by enforcing the potential drop profile along molecules. The insertion of a resistive molecular path near the metallic electrode(s) can drastically alter the rectification performance.

As a testbed for the analysis, we employ the diblock dipyrimidinyl-diphenyl molecule shown in Figure 4.3a. Since alkanes are known for their high insulating property [8, 115], they can be used to modify the resistivity of the molecule region in touch with the electrodes, . We use a dimethyl group attached to the last phenyl group of the molecule on the right side (Figure 4.3b) and attached to the last pyrimidinyl group on the left side (Figure 4.3c), respectively. This ensures higher resistivity, and consequently higher potential drop, at the side where it is added. Therefore, the insertion of the resistive element allows us to control the transport behavior of the molecular device. As we will demonstrate below, we can improve the molecule rectification and even invert it.

Figure 4.4 shows the transmission spectra (TS) of the dipyrimidinyl-diphenyl (Mol1) molecule at different positive and negative drain biases. The current is directly proportional to the integral of the transmission curve between the limits set by the applied potentials (diagonal dashed lines indicating the position of the two chemical potentials of left and right electrodes). As can be noted, the current is dominated by LUMO transmission. The contribution of LUMO within the bias window is larger for the positive bias than for the negative one. This leads to the rectification response in the IV-curve, see Figure 4.5.

---

[2]For multi-ring molecules, the terminal portion can be considered as the last ring near the contacts.

(a) Mol1: Dipyrimidinyle-diphenyle rectifier

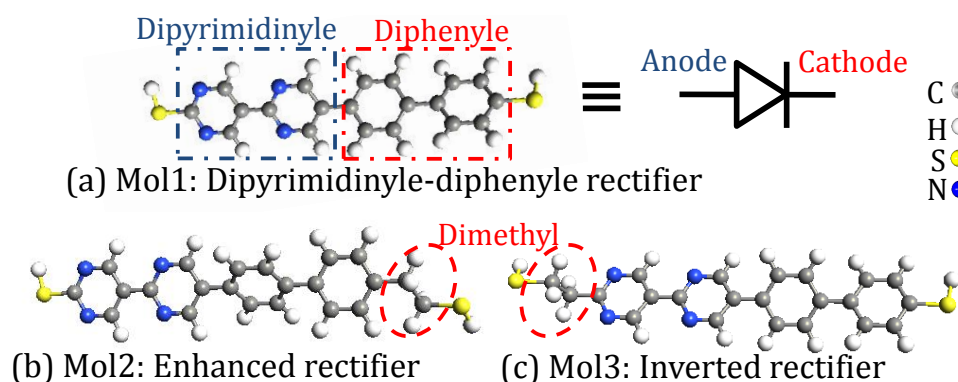(b) Mol2: Enhanced rectifier   (c) Mol3: Inverted rectifier

Figure 4.3: The structure of diblock dipyrimidinyl-diphenyl based molecules under investigation. Mol1 is the molecule studied in [10, 122, 159, 160]. Mol2 and Mol3 are modified version of the molecule after adding a dimethyl group at the cathode and anode terminal of the molecule, respectively.
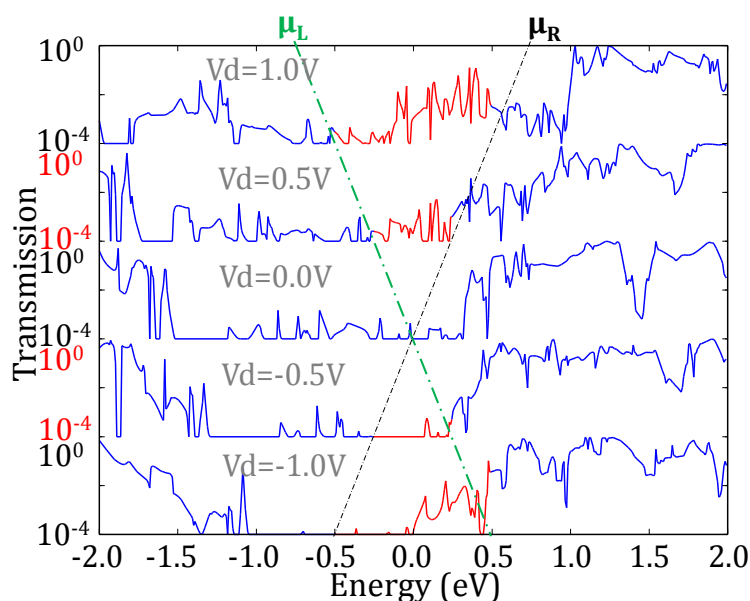

Figure 4.4: Semi-log plot of the TS at various positive/negative biases applied on the left electrode of a device with Mol1. The device E_F is set to be zero. The transmission window over which the current is calculated is in red color and surrounded by the dashed lines.

Figure 4.6a shows the potential profile along Mol1. At forward bias (1 V), one can notices that the potential drops smoothly over the whole molecule. At reverse bias (-1 V), the potential drop over the dipyrmidinyl is smaller than the diphenyl one. Correspondingly, the resistance near the dipyrmidinyl side is
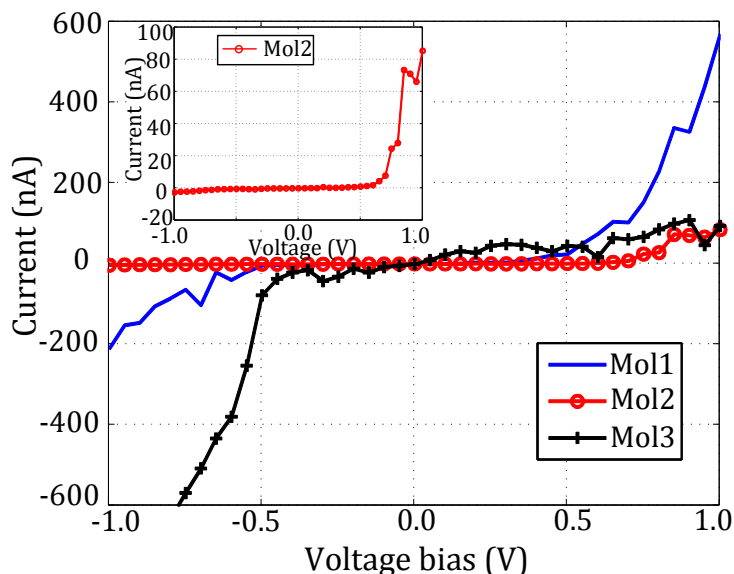
Figure 4.5: The simulated IV-curves of the three molecular devices. All IV-curves show clear asymmetries. The inset is the IV-curve of Mol2 alone since it has a rather lower current values compared to Mol1 and Mol3.

almost half of the resistance near the diphenyl side. The difference in resistivity can be justified from the length of the corresponding bonds; the C-N bond in the dipyrmidinyl side is around 1.35 Å, which is shorter than the C-C bond in the diphenyl[3] (around 1.4 Å). Since both bonds are aromatic, the shorter bond implies a relative higher mobility.

The small current at reverse bias is related to the fact that the dipyrmidinyl, with small resistivity, is connected to the negative electrode. In general, the LUMO-supported current through the molecule is directly proportional to the potential drop near the negative electrode.

In order to verify the discussed design concept, we enhance the rectification of Mol1 by adding a dimethyl group at the cathode terminal to increase the resistance near the negative contact (Figure 4.3b). Figure 4.6b shows the potential profile along Mol2 at positive/negative bias and the approximate resistance of each segment of the molecule. Now, the resistance of the dimethyl group, connected at the cathode, dominates. Consequently, the potential drop increases near the cathode. At positive bias, the cathode is connected to the negative

---

[3]The mentioned bond lengths are based on our geometry relaxed structures, and they are in the expected range from experimental measurement in [162, 163].
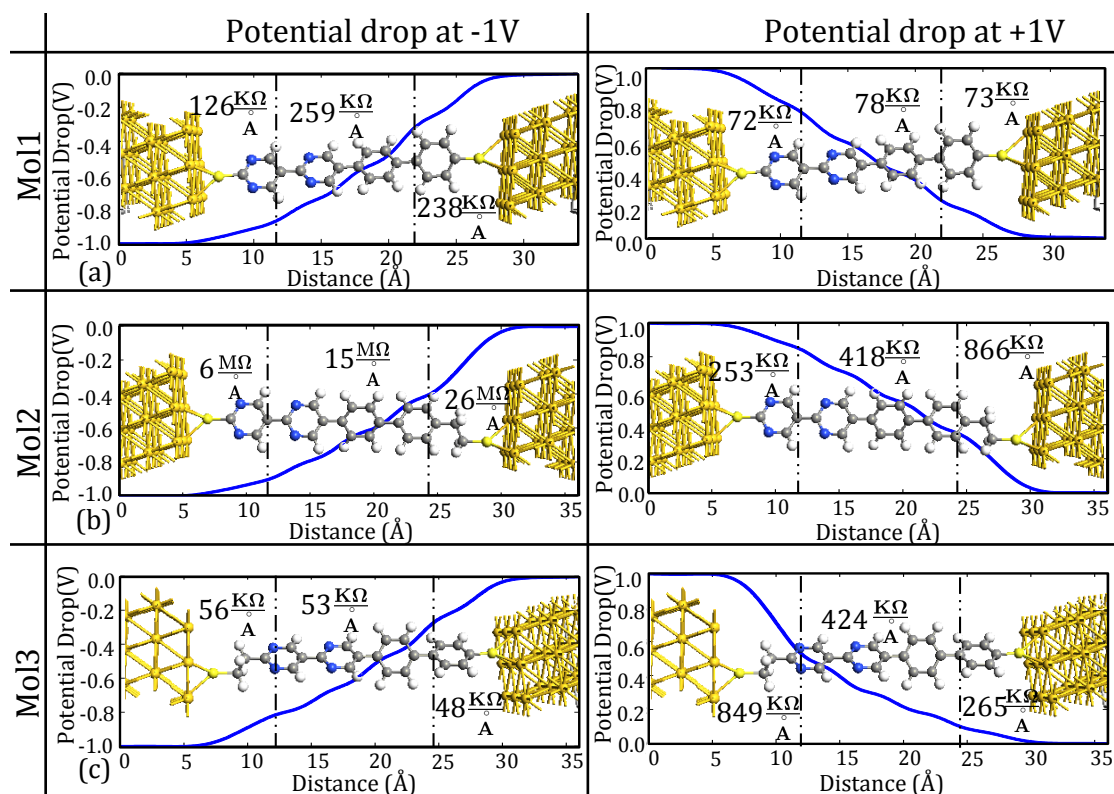
Figure 4.6: The potential drop profile along the three molecules; (left) at voltage bias -1V and (right) at forward bias 1V. The bias is applied on the left electrode. The approximate resistances per unit length for the middle and terminal segments of the molecules are illustrated.

electrode, which leads to an enhancement of the conduction through LUMO. At negative bias, the cathode is connected to the positive electrode, which leads to a current quenching. Despite the reduction in the forward current due to the presence of the barrier, we observe a better rectification as compared to Mol1 (Figure 4.5).

One can change the rectification direction if the dimethyl group is added at the anode of Mol1. This makes the potential drop always high at the anode region, see Figure 4.6c. At negative bias, the anode is connected to the negative electrode, which facilitates the current flow. At positive bias, the anode is connected to the positive electrode and consequently the current is low. As a result, inverse rectification occurs (Figure 4.5).

Adding a dimethyl group indeed controls the potential drop along the molecule as expected and validates our claim. Figure 4.7 and 4.8 show the TS of Mol2 and
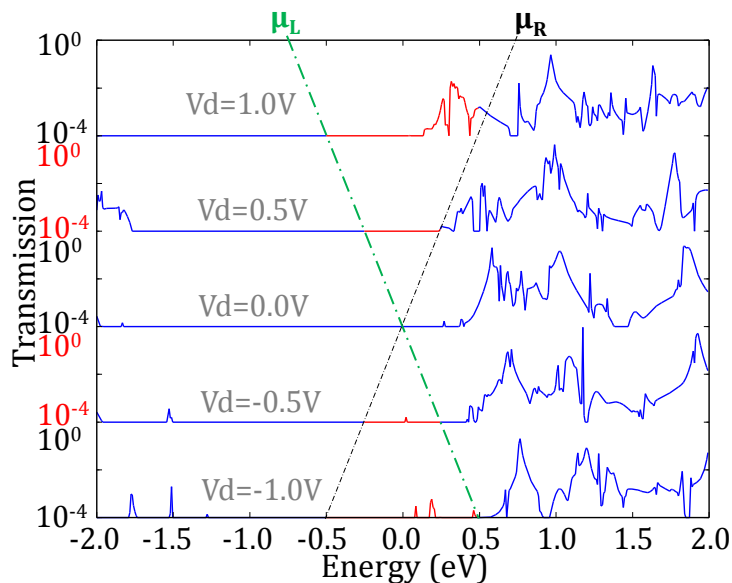
Figure 4.7: Semi-log plot of the TS at various positive/negative biases applied on the left electrode of a device with Mol2.

Mol3 at various positive/negative drain biases. The TS of Mol2 and Mol3 are different from that of Mol1, however the current is carried via LUMO states in the three molecules. In the case of Mol2 (Figure 4.7), the short LUMO peak is responsible for the low current observed.

It is worth noticing that the TS for Mol1 and Mol2 shifts with the applied bias in the same direction of the chemical potential of the left electrode (μ_L), connected to the anode since higher potential drop occurs near the cathode. On the contrary, the TS for Mol3 shifts in the same direction of the chemical potential of the right electrode (μ_R).

Figure 4.9 illustrates the HOMO/LUMO distribution for the three molecules at zero drain bias. The distribution of the molecular orbitals along the molecule can be calculated using the molecular projected self-consistent Hamiltonian (MPSH) [164]. In the three molecules, the HOMO tends to be highly localized at one of the molecules terminals. The LUMO of the three molecules is rather delocalized along the molecules. This emphasizes LUMO dominating conductivity.

Figure 4.10 shows the rectification ratio of the three molecular devices. The average rectification ratio of Mol1 is around 2.8, which agrees with measurement and simulation data in [10, 122, 159, 160]. Mol2 shows a ten-fold enhancement in
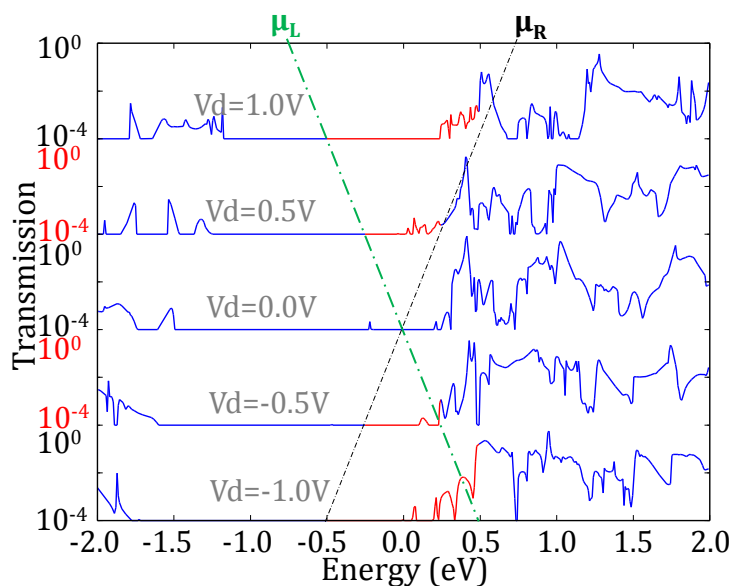
Figure 4.8: Semi-log plot of the TS at various positive/negative biases applied on the left electrode of a device with Mol3.
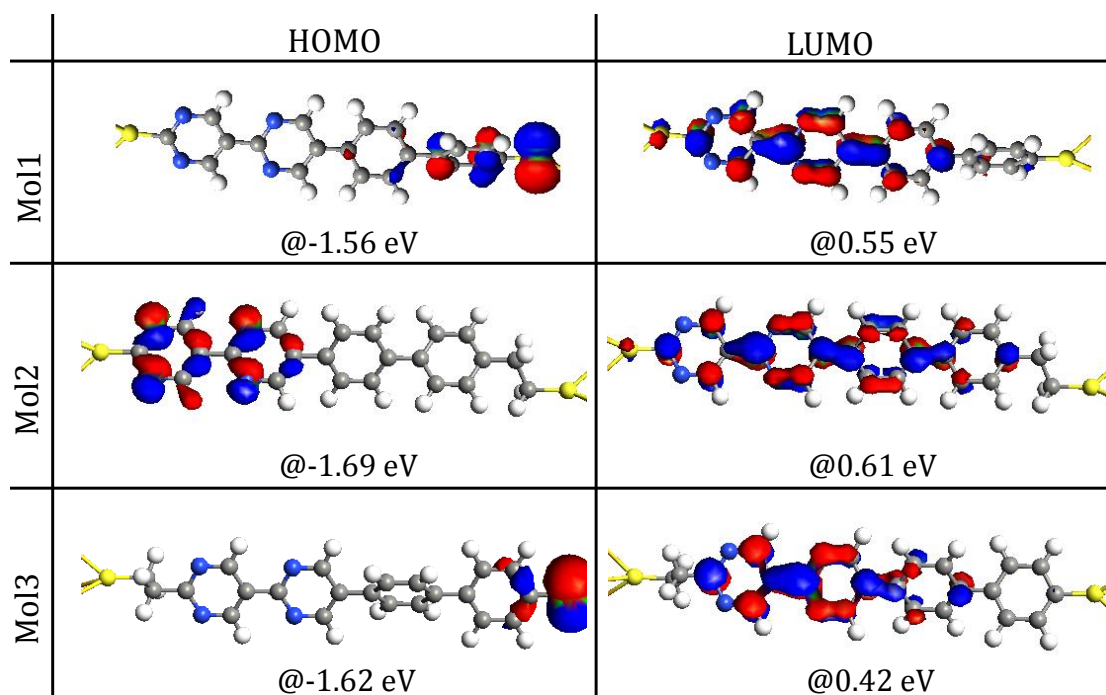

Figure 4.9: The distribution of the HOMO/LUMO molecular orbitals along the three molecules at equilibrium.

the rectification, with rectification ratio exceeding 30 at some biases. Mol3 with inverted rectification direction displays a rectification ratio around 7.
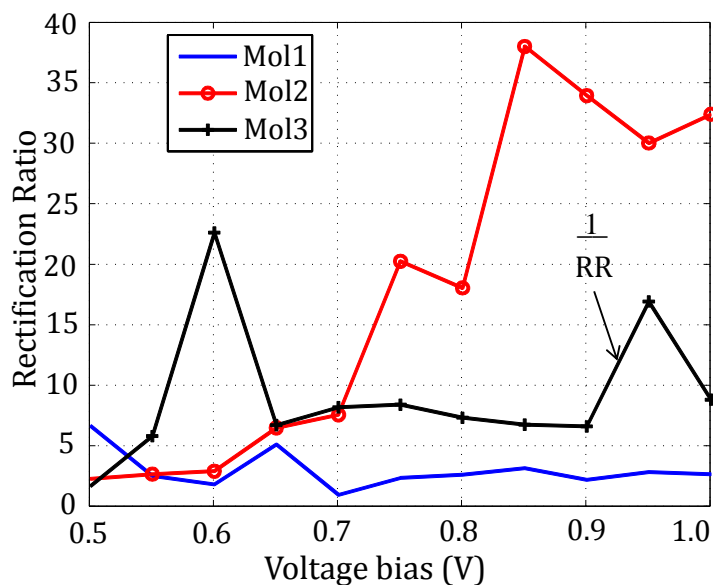
Figure 4.10: The rectification ratio (RR) of the three molecular devices. For Mol3, the RR is inverted since the molecule rectify in an opposite direction to the other two molecules.

These results indicate that adding a dimethyl group to one terminal of the molecule has a stronger effect on the rectification behavior than the inherited asymmetry of the molecule. Moreover, we verify that using the design concept in section 4.3 we can control the transport characteristics in molecular devices.

4.4.2 Oligo-Phenylene Vinylene Molecular Rectifier

Oligo-Phenylene Vinylene (OPV) is among the most famous conjugated molecules due to its delocalized pi-bonds which facilitate the charge's transport across them. Søndergaard et al. realized an OPV molecular wire with oxygen linkers that shows a non-linear response to an external bias with a threshold conductance onset around 1.4 V [139, 165]. The testbed molecule in this subsection is a derivative of this OPV molecule, see Figure 4.11. The employed OPV molecules have an oxygen linker on one terminal and a simple thiolate linker on the other terminal.

In this subsection, we present several atomistic simulation of the molecular device, which elucidate its quantum transport behavior. The main feature here is the rectification, which can reach extremely high values up to three orders of magnitude in the interval from 0.3 V to 1.3 V. We shall elaborate why the
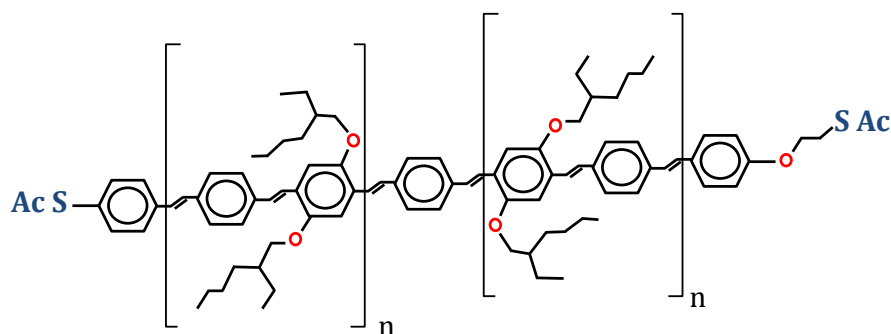
Figure 4.11: The structure of a synthesizable OPV molecule that we target for this study. A simple thiol linker is on the left terminal and an oxygen linker is on the right terminal. The side functionalization groups in the middle of the OPV are usually synthesized for stability and solubility of the molecule and they do not affect the rectification behavior of the molecule based on simulation.

rectification is so strong and why it degrades outside the interval. Besides the interesting response of the device, the analysis clarifies how the atomistic transport characteristic of a device determines its rectification performance.

Studying the device at equilibrium

The electronic properties of a molecular device at equilibrium can be resolved using the MPSH. For the OPV molecule considered here, we find that the HOMO and LUMO are at -1.3 eV and 0.21 eV relative the Fermi-level, respectively. A simple dithiol OPV molecular device, consisting of an OPV with two identical thiol terminals, acts like a molecular wire with a current in the range of few microamperes flow at an applied bias of 1 V [22]. Its transmission spectrum shows a broadening of the LUMO near the E_f which allows current conduction even at low bias, see Figure 4.12a.

By adding an oxygen linker to one terminal of the molecule (in this case the right one), the LUMO broadening disappears. In addition, the peak values of the transmission at the HOMO/LUMO energies are clearly reduced, see Figure 4.12b. This indicates that the oxygen linker induces significant changes to the charge transport behavior of the device, by partially decoupling the molecule from the gold electrode.
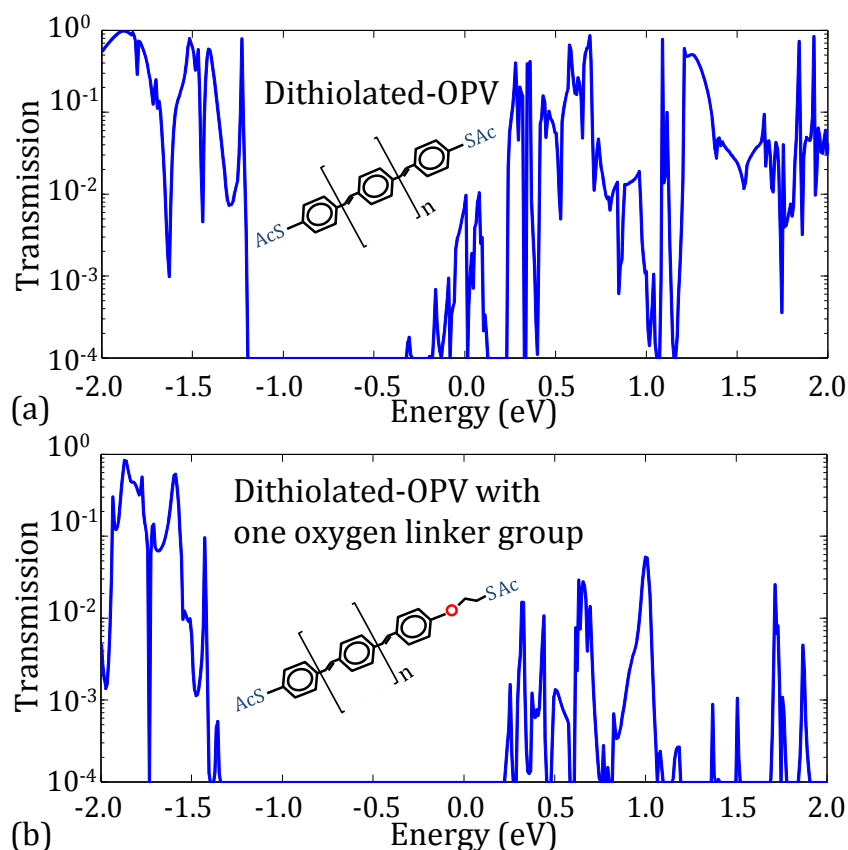
Figure 4.12: The TS of dithiolated OPV molecules (a) without oxygen linkers. (b) with an oxygen linker on one terminal. The Fermi energy is set to be zero. The TS emphasize the role of the oxygen linker in filtering the TS of the OPV and separating the HOMO/LUMO to be at $-1.3\,\text{eV}$ and $0.21\,\text{eV}$, respectively. Besides, the transmission peaks at HOMO/LUMO energies are reduced.

Figure 4.13a shows the distribution of the charge density difference through the molecule at equilibrium (zero bias). Oxygen is characterized by its high electronegativity. Thus, the shared electrons in the polar bonds between the oxygen and the surrounding carbon atoms are attracted toward the oxygen. As a result, negative charge accumulation occurs around the oxygen atom. Figure 4.13b shows the electrostatic potential profile of the device at equilibrium. The charge accumulation creates a potential variation (barriers) at the oxygen linker. Moreover, the oxygen linker includes a dimethyl group which is known for its insulating property [8, 115]. Consequently, it can be expected that when a particular bias is applied to this molecular device, the potential drop would mostly occur at the terminal connected to the oxygen linker.
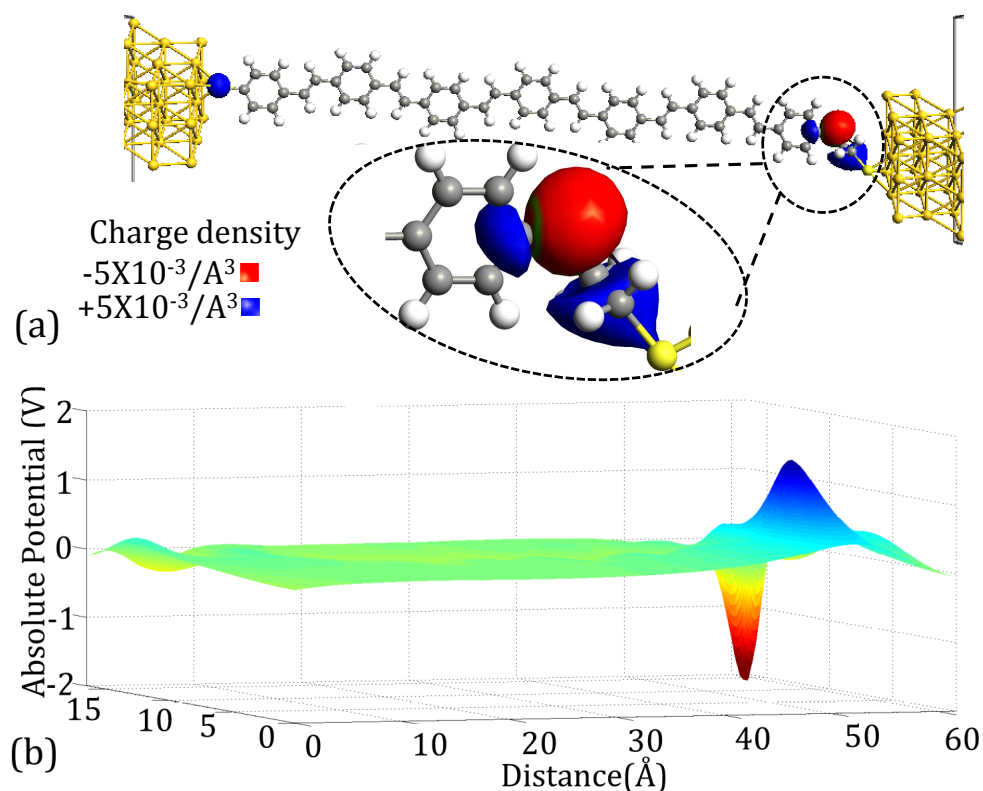
Figure 4.13: (a) The charge density difference distribution through the device at equilibrium (zero bias). (b) A 3d visualization of a contour plot for the absolute electrostatic potential distribution of the device.

Let us now apply the same concept described in section 4.3, yet we have both HOMO and LUMO available at different distance from the Fermi-energy. In Figure 4.14, it is assumed that the potential drop induces abrupt difference between the OPV's MOs and the chemical potential of the right electrode connected to the oxygen linker. Depending on the bias direction, the device starts conducting when the chemical potential of the electrode connected to the oxygen linker meets either the HOMO or the LUMO. This asymmetric conductance-voltage dependency for positive/negative biases would imply a rectification behavior in the interval from the LUMO starting point at forward bias (0.21 V) to the HOMO starting point at reverse bias (1.3 V), as exemplified in Figure 4.14d. In what follows, we verify this simplified picture via atomistic simulation results of the device.
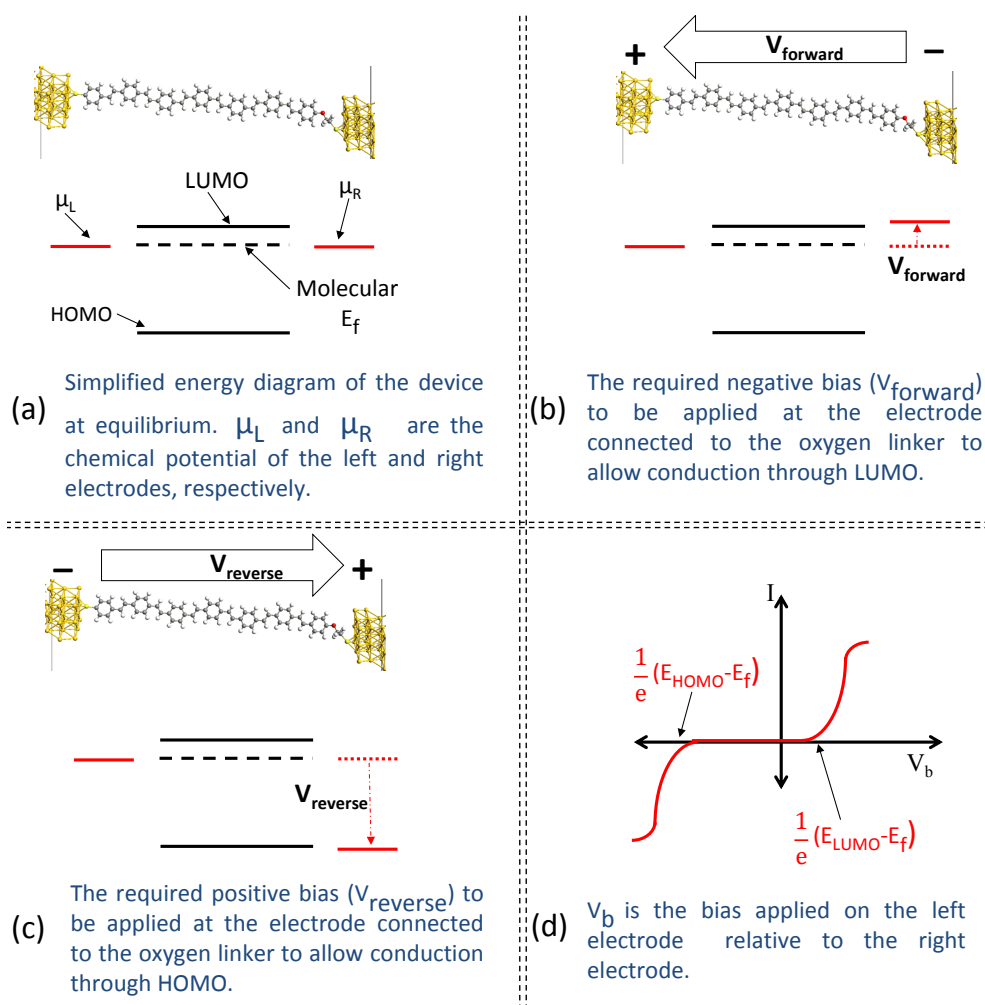
(a) Simplified energy diagram of the device at equilibrium. μ_L and μ_R are the chemical potential of the left and right electrodes, respectively.

(b) The required negative bias ($V_{forward}$) to be applied at the electrode connected to the oxygen linker to allow conduction through LUMO.

(c) The required positive bias ($V_{reverse}$) to be applied at the electrode connected to the oxygen linker to allow conduction through HOMO.

(d) V_b is the bias applied on the left electrode relative to the right electrode.

Figure 4.14: A simplified energy diagram of the device (a) at equilibrium. (b) under bias $V_{forward}$. (c) under bias $V_{reverse}$. (d) the idealistic IV-curve of the device.

Probing the potential drop along the device under bias

Figure 4.15 presents the potential drop profile along the molecule at positive/negative bias of ± 1 Volt. We investigate the potential drop at these biases to clarify the asymmetry of the drop along the molecule. As we shall show later, the current flows through the device at forward bias of 1 V, while it is drastically reduced at reverse bias -1 V.

At reverse bias (Figure 4.15a), the applied potential drops mostly near the oxygen linker. Since no potential drop occurs near the negative electrode, no conduction through LUMO transmission is expected in this case. The potential drop leads to a lowering of the chemical potential of the positive electrode relative to the
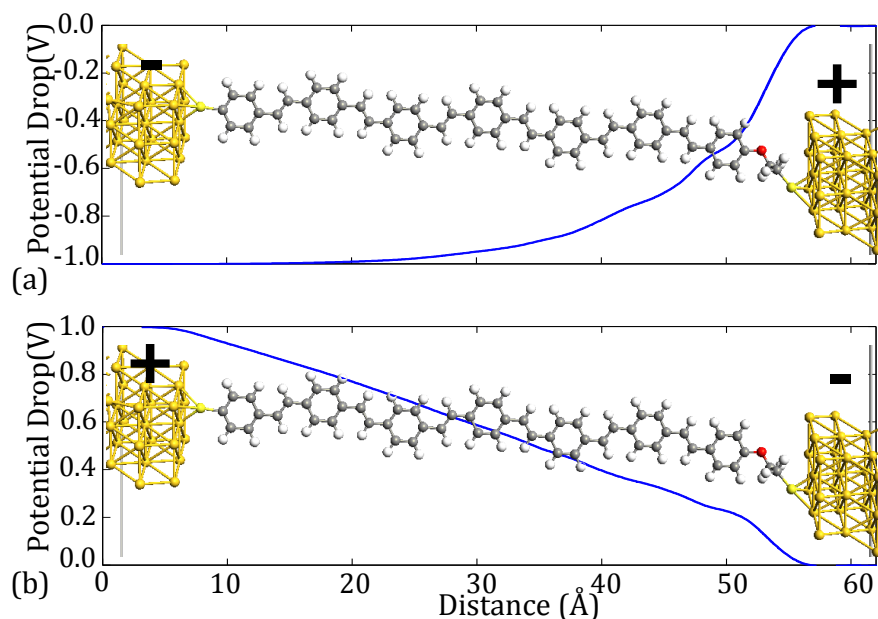
Figure 4.15: The potential drop profile along the asymmetric OPV molecule (a) at reverse bias −1 V. (b) at forward bias 1 V.

MOs. Since the HOMO is about 1.3 eV away from the equilibrium Fermi-energy, the lowering of the chemical potential of the positive electrode is not sufficient to start conduction. Hence, no significant current flows at this negative bias. The only current contribution comes from tunneling from one electrode to the other across the HOMO-LUMO gap. Note that, the potential drop is not abrupt, as assumed in the simplified energy diagram, but it gradually picks up near the oxygen terminal.

At forward bias (Figure 4.15b), the potential drop is smoothly distributed along the whole molecule, with a faster drop near the oxygen linker. Since the LUMO is only 0.21 eV away from the equilibrium Fermi-energy, a small potential value needs to raise the chemical potential of the negative electrode. Thus, the steep drop near the oxygen linker represents the required threshold to start conduction while the remaining potential drop is smoothly distributed along the molecule.

Transmission spectra of the device under bias

Figure 4.16 shows the TS of the device at various positive/negative biases. At negative reverse bias, no molecular orbital is included in the integration window, denoted by the diagonal straight lines, up to voltage bias ≈−1.0 V.
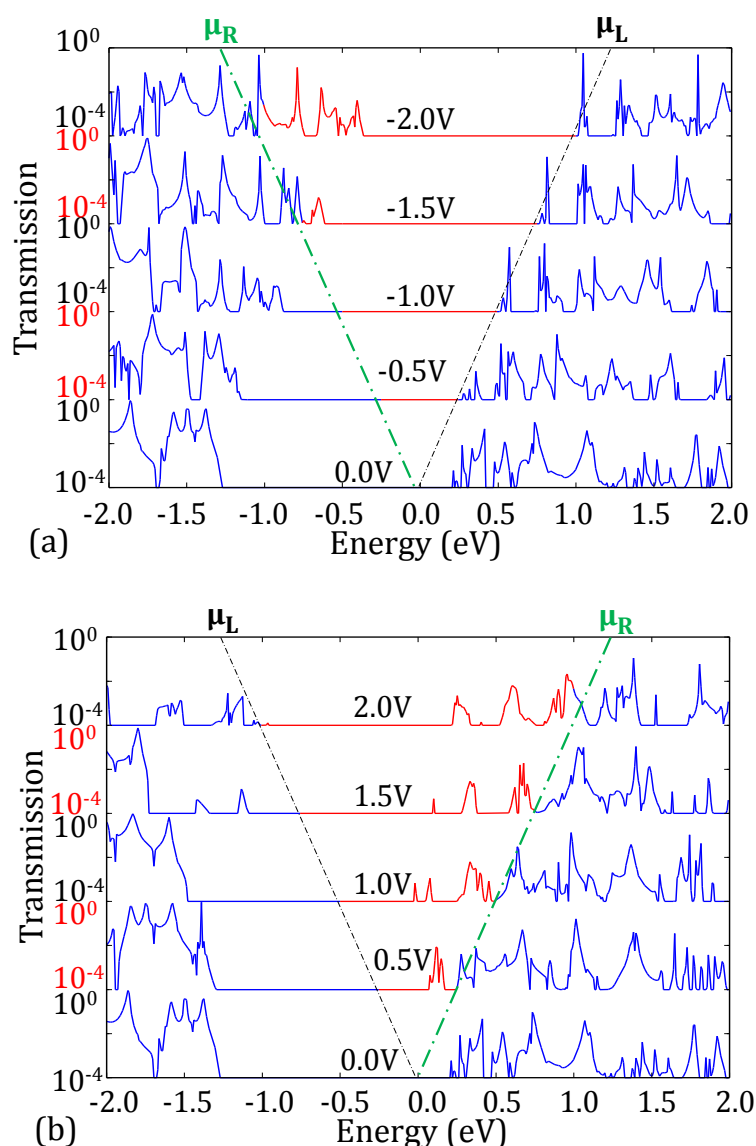
Figure 4.16: The TS of the asymmetric OPV molecule (a) at various reverse biases. (b) at various forward biases. The Fermi-level is set to be zero and the transmission window over which the current is calculated is in red color and surrounded by the dashed lines.

This suggests that almost no current is expected for such bias range. When the reverse bias reaches $-1.3\,\text{V}$, the HOMO level starts entering the integration window. Consequently, a HOMO dominating transmission allows current to start flowing.

At positive forward bias, the LUMO level enters the integration window before 0.5V. Thus, a LUMO dominating transmission leads to current flow at relatively low positive bias $\approx 0.3\,$V.

It is worth to notice that, the TS of the molecule shift under bias in the same direction of the chemical potential of the left electrode (μ_L), which is connected to the molecule via the simple thiol linker (see Figure 4.16). This is because most of the potential drop occurs near the right electrode, connected to the oxygen linker. Since the potential drop at forward bias is uniformly distributed along the whole molecule, the TS show a weaker shift with respect to the reverse bias case.

Analysis of the HOMO/LUMO orbitals

Figure 4.17 illustrates the HOMO/LUMO charge distribution through the OPV molecule at different drain biases. As illustrated in the previous analysis, only HOMO contributes to the reverse bias current, and only LUMO contributes to the forward bias current. The HOMO charge distribution at reverse bias ($V_{ds} = $ -1 V) concentrates on the left portion of the molecule (Figure 4.17c). Figure 4.15a shows that there is almost no potential drop (electric field) at that portion, which explains the weak current at reverse bias. On the contrary, the LUMO charges at forward bias ($V_{ds} = $1 V), also occupying mostly the left portion (Figure 4.17f), are now subject to a high electric field (Figure 4.15b). This in turns leads to an appreciable current.

Influence of molecular length on the device behavior

We illustrate here the influence of the molecular length on the transport characteristic of the device. Figure 4.18 shows the IV curves for an OPV molecular device with 3,7 and 9 phenylene rings, respectively. The curves show that increasing the molecular length has a clear impact on the reverse bias current, which is reduced by orders of magnitude with increasing molecular length. This is consistent with the origin of such current, namely tunneling across the HOMO-LUMO gap [165]. On the other hand, the molecular length has a weak influence on the forward current because the LUMO channel does not depend on the length. Accordingly, the rectification ratio increases by orders of magnitude with increasing the molecular length (Figure 4.19).
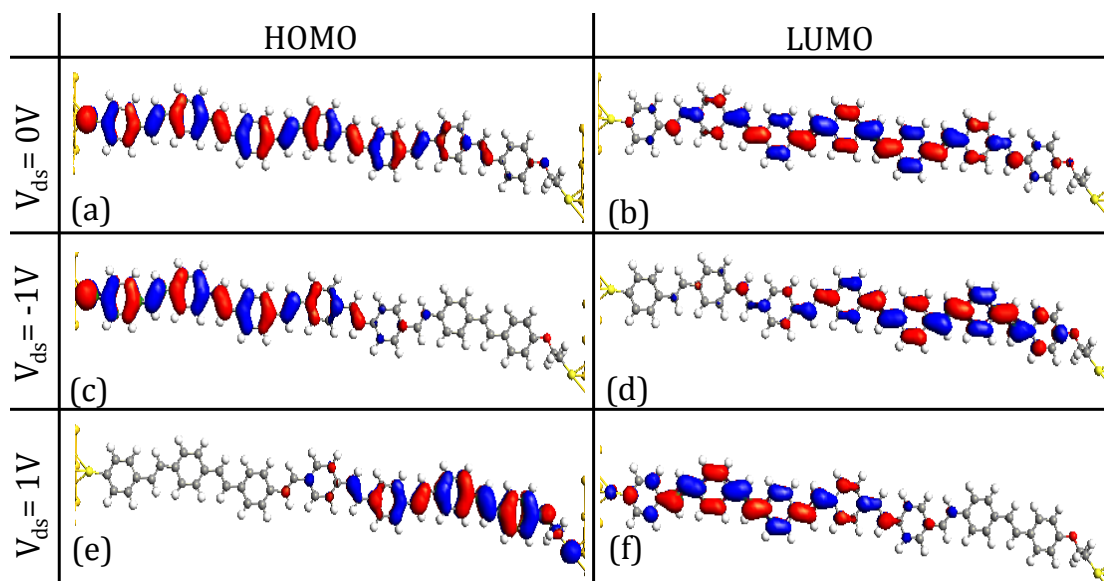
Figure 4.17: The distribution of the HOMO/LUMO molecular orbitals along the device at different drain-source biases.
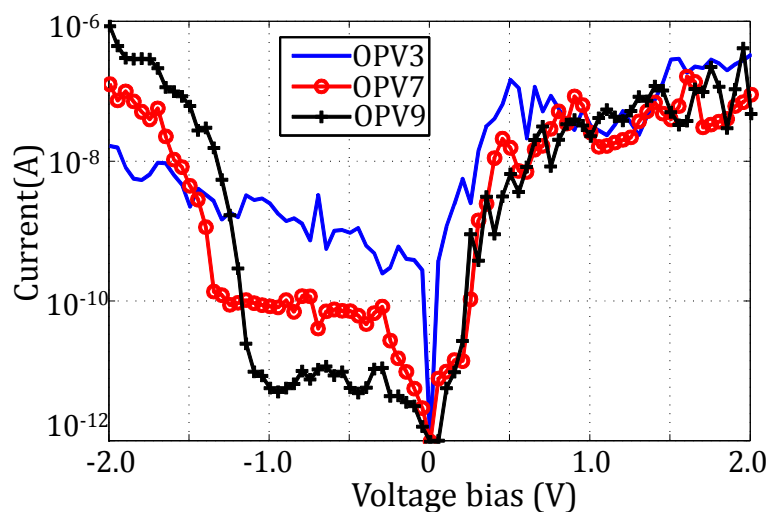

Figure 4.18: The IV curves of the asymmetric OPV molecular devices with 3,7 and 9 phenylene rings.

Another important observation is that the value of the reverse bias, at which the HOMO conductance starts, shifts slightly to lower values with increasing the molecule's length. This behavior is related to the potential drop profile along the molecule. At reverse bias, longer molecules allow relatively higher percentage of the potential drop near the positive electrode. Thus, electrical conduction, due to the alignment of the chemical potential of the positive electrode with HOMO, is achieved at relatively lower bias value for longer molecules.
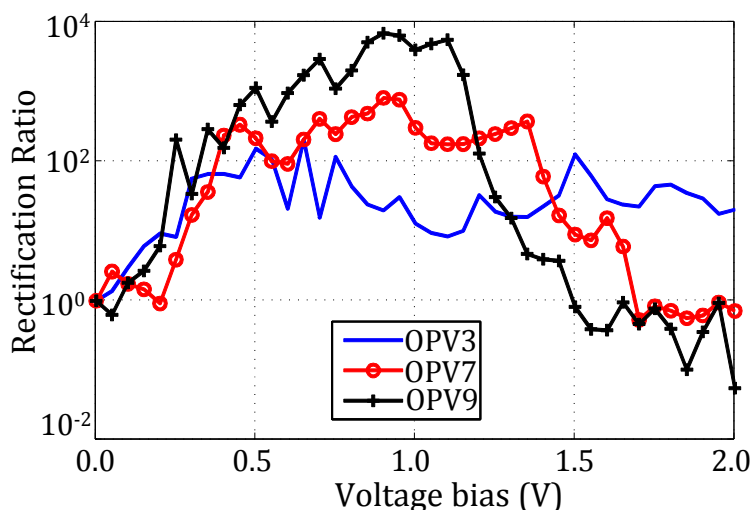
Figure 4.19: The rectification ratio of the asymmetric OPV molecular devices with 3,7 and 9 phenylene rings. The rectification ratio is calculated as $I(V)/I(-V)$.

The study presented in this subsection suggests a novel molecular rectifier that provides a rectification ratio >1000. We simulate molecules with up to 9 phenylene rings (<8 nm length) and show that the rectification ratio is enhanced with increasing the molecular length. For a longer molecule with 17-19 rings, we expect to have a rectification of more than 10^4 which would be a breakthrough record in the field of molecular electronics.

4.4.3 Influence of Doping Variation on Molecular Rectifiers

Aviram and Ratner proposed the first single molecular rectifier which was called afterwards Aviram Ratner diode [4]. The molecule is generally called Donor-Sigma- Acceptor (D-σ-A) diode since it is composed of two electroactive regions, donor (D) and acceptor (A). These two regions are linked by a σ covalent bond which has some sort of insulation since it forms a potential barrier. Several theoretical studies have investigated different parameters affecting the rectification performance of the D-σ-A molecules [118, 166].

Figure 4.20 illustrates the structure of the testbed D-σ-A based molecules with various doping. Mol4 was a typical molecule studied as an example of the D-σ-A molecule in [118]. The remaining molecules are the same but with an increased/decreased number of acceptors(NO_2)/ donors(NH_2). In this subsec-
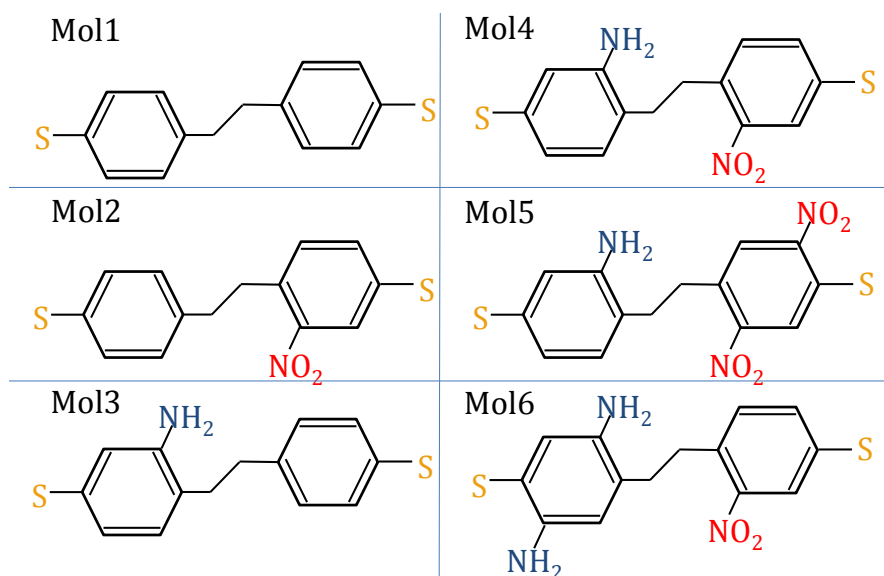
Figure 4.20: The structure of D-σ-A based molecules under investigation.

tion, we shed light on the correlation between the change of doping, and the rectification and other device properties.

Figure 4.21 shows the IV characteristics of the six molecules; Mol1 and Mol3 are plotted in the inset because their current values are small compared to the other molecules. As can be noticed, the addition of the donor group (NH_2) slightly reduces the negative bias current, see Mol3 compared to Mol1. On the other hand, the addition of the acceptor group (NO_2) acts on enhancing the positive bias current, see Mol2 compared to Mol1. This may be attributed to two factors: firstly, the conduction in these molecules is dominated by transmission through the LUMO as shall be elaborated shortly. the second factor is that, an acceptor (NO_2) withdraws some charges from the molecule; thus the LUMO transmission is enhanced and vice versa for a donor.

Figure 4.22 shows the distribution of the HOMO and the LUMO along the six molecules without contact electrodes. For all molecules except Mol1 that has neither donors nor acceptors, the HOMO is localized on the donor region while the LUMO is localized on the acceptor region. This asymmetry in the distribution of the HOMO and LUMO plays an important role in the rectification behavior. High current is favorable when the positive electrode is near the HOMO, and the negative electrode is near the LUMO. This is because the positive electrode tends to withdraw electrons from the molecule while the negative electrode acts as electrons injector.
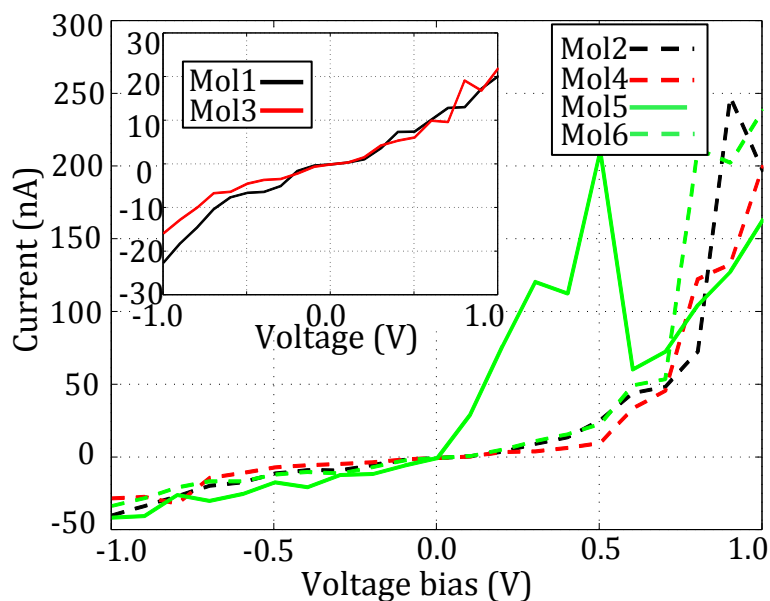
Figure 4.21: The simulated IV-curves of the six molecular devices. Mol1 and
Mol3 are plotted in the inset since their current have relatively
low values. All molecules other than Mol1 and Mol3 show clear
asymmetric curves.

Figure 4.23a shows the TS of the six molecular devices at equilibrium. The TS
are rather similar far from the E_f. However, the main variations occur around
the E_f especially for Mol1 and Mol3 which have lower values of LUMO peaks.
This explains the low current values of Mol1 and Mol3.

In Figure 4.23b, the TS of Mol1 within the integration window at positive and
negative biases are almost equal, which leads to the symmetric current curve.
On the other hand, Figure 4.23c and 4.23d show that LUMO contribution at
positive biases is greater than at negative biases. This results in the asymmetric
current curves of Mol4 and Mol6.

Referring to the illustrated design concept in section 4.3, the amount of current
flowing through a device depends on the potential drop near the negative
electrode (right electrode at positive bias and left electrode at negative bias).
Figure 4.24 shows that, for Mol1, the potential drop near the negative electrode
is equal for both positive and negative biases, whence equal current flows. For
Mol4 and Mol6, the potential drop near the negative electrode is higher in case
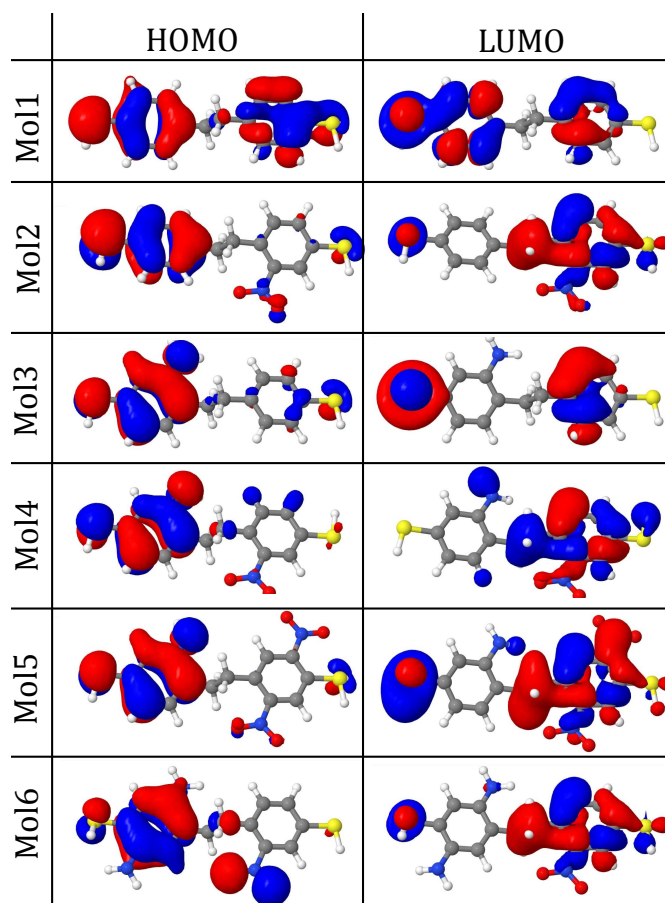of positive bias, whence higher current flows at positive biases.

Figure 4.22: An iso-surface plot for the distribution of the HOMO/LUMO molecular orbitals along the six molecules without the gold contact. A cutoff value of 0.02 is used in the plotting.

It is important to notice in Figure 4.23c,d that the LUMO peaks of Mol4 and Mol6 under bias are relatively shifting in the direction of μ_L. This is because the potential drop near the right electrode is a bit higher than that near the left electrode. Moreover, for Mol1, the TS are not significantly shifting under bias since the potential drop near the electrodes are approximately equal at positive and negative biases.

The dipole moment indicated in Table 4.1 is calculated along the direction of transport. One can notice that, for Mol1, Mol2, Mol3 and Mol4, the dipole increases on adding a dopant, and the effect of NO_2 is higher than the effect of NH_2. For Mol5 and Mol6, interestingly, the addition of the dopant acts on reducing the dipole moment. An explanation for that could be that the same dopant is inserted in the opposite side of a ring, so the net dipole in the transport
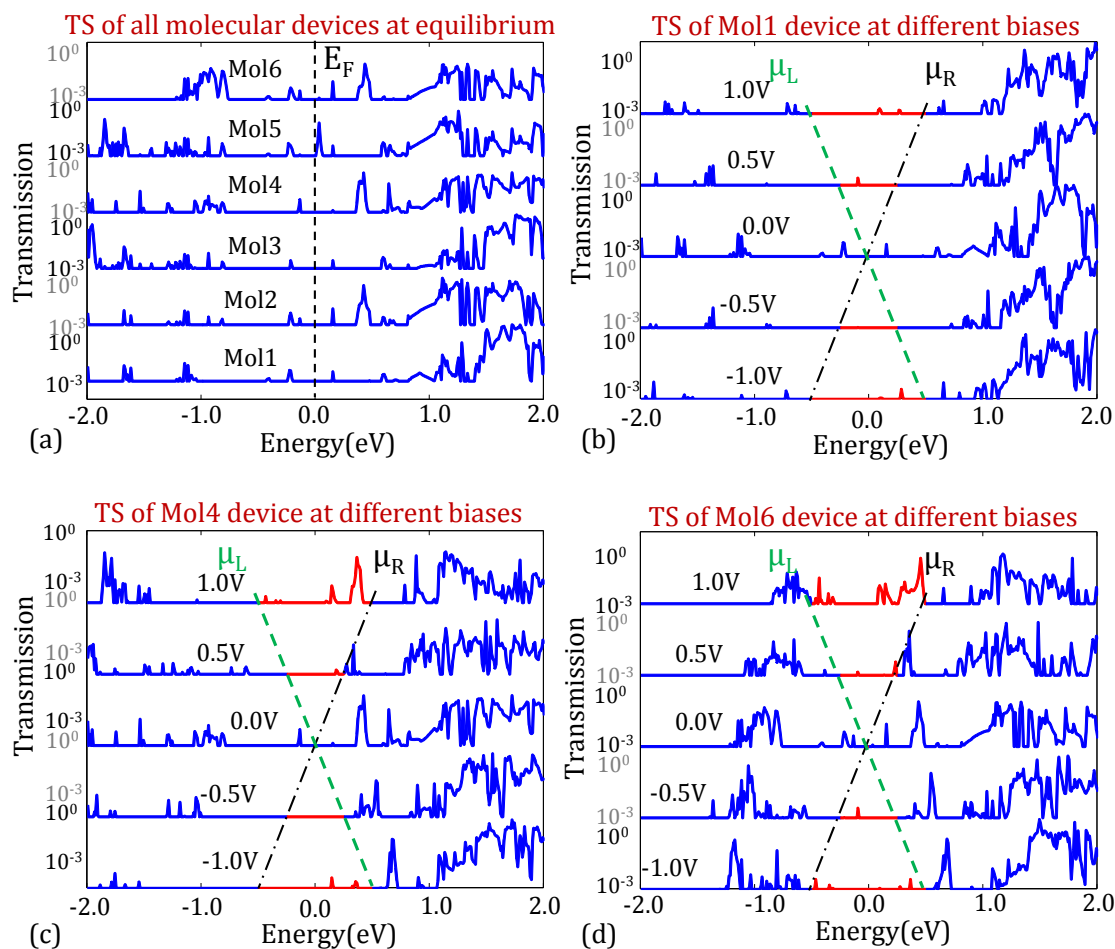
Figure 4.23: (a)Semi-log plot of the TS of the six devices at equilibrium. Semi-log plot of the TS at various positive/negative biases applied on the left electrode of a device with (b) Mol1 (c) Mol4 and (d) Mol6. The transmission window over which the current is calculated is in red color and surrounded by the dashed lines.

direction is reduced. Consequently, the cancellation of the NO_2 in Mol5 leads to lower dipole moment compared to the cancellation of the NH_2 in Mol6.

Figure 4.25 shows the rectification ratio of the six molecular devices. The rectification ratios generally have higher values at higher biases, except for Mol5. The average rectification ratios for all devices in the interval [0.6V,1.0V] are also listed in Table 4.1. The table shows a direct proportional relation between the dipole moment and the rectification ratio of the molecular devices for Mol1, Mol2, Mol3 and Mol4. This dependence is reasonable since the field created by the dipole in the direction of transport would resist the charge flow in one direction and
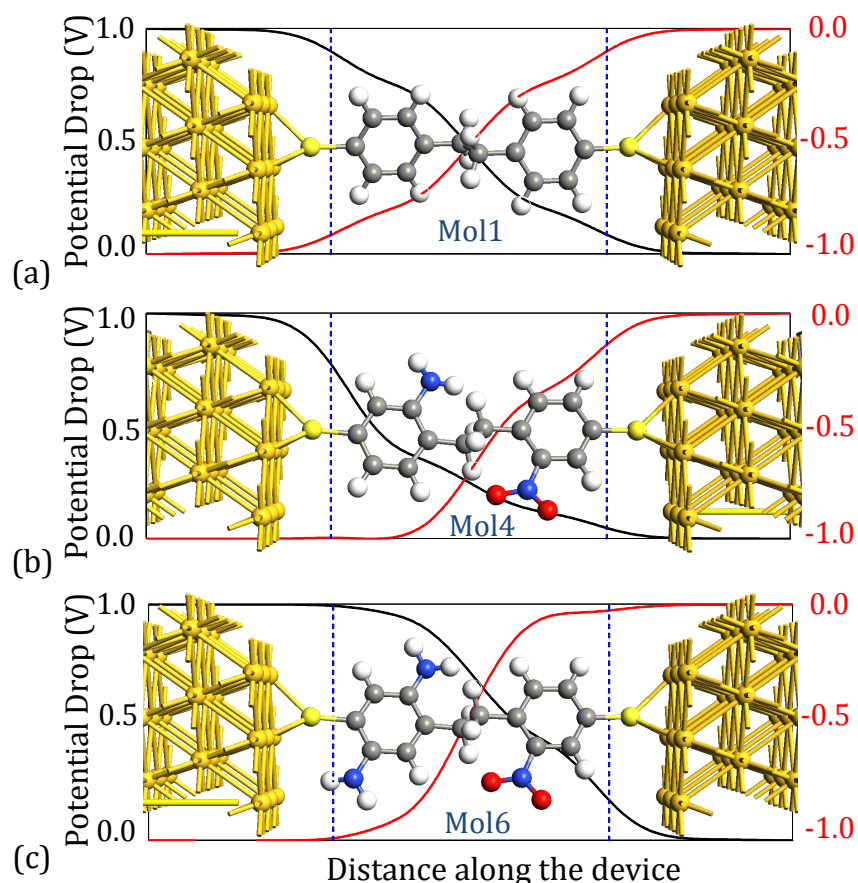
Figure 4.24: The potential drop profile along molecules Mol1, Mol4 and Mol6; (red) at voltage bias -1V and (black) at voltage bias 1V. The bias is applied on the left electrode. The dashed lines to clarify the difference in potential drop near the gold electrodes.

Property	Mol1	Mol2	Mol3	Mol4	Mol5	Mol6
Dipole Moment (Debye)	0.004	2.037	0.977	2.325	0.481	1.942
Average Rectification	1.071	4.093	1.540	4.528	3.243	6.287

Table 4.1: The value of the calculated dipole moment of each molecule in the direction of transport and the average rectification ratio from 0.6 V till 1.0 V for all molecular devices.

enhance it in the other direction. The change in the relation for Mol5 and Mol6 could be related the cancellation occurs in the dipole as we just mentioned.
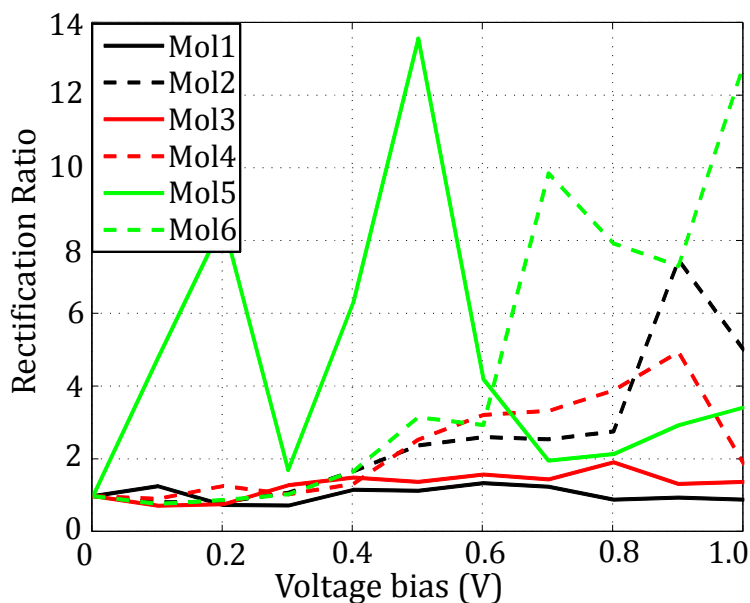
Figure 4.25: The rectification ratio of the six molecular devices.

In the investigation for the effect of doping on the behavior of the D-σ-A diodes, we did not consider the influence of the position where the dopants are inserted. This could have also an impact on the rectification performance since it would affect the dipole moment of the molecules. Moreover, we do not cover the influence of different acceptor/donor dopants other than NO_2/NH_2.

A key outcome from this study is that doping does indeed affect the rectification response of a device yet not always with a direct proportionality correlation. In addition, we noticed that an acceptor enhances the conductivity of a device with a LUMO dominated transmission while a donor reduces this conductivity.

4.4.4 Molecular Devices with Negative Differential Resistance

Various research groups showed that devices built up with carbon chains have interesting properties like NDR behavior [117, 167], spin polarization filtering [81], and can also be used for enhancing rectification performance of molecular diodes [117, 153]. Recently, Yuzvinsky et al. developed a method for realizing a carbon chain through a controllable altering of the diameter of an individual carbon nanotube [168]. Moreover, Chuvilin et al. performed a transformation from graphene nanoribbons to single carbon chains [169].
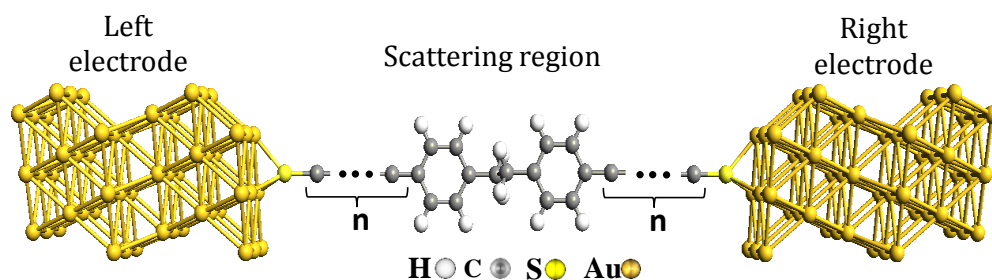
Figure 4.26: The general structure of a symmetric molecular device with n-chain of carbon atoms. The molecule is connected to semi-infinite (111) gold electrodes through thiol-gold bond. The gold electrodes consist of 3×3 atoms/layer.

In this subsection, we provide an atomistically based analysis of devices which show odd/even oscillation in their transport behavior as a function of the number of carbons within the chain. A wide bias range of NDR behavior is observed in case of "odd" carbon chain (CC). Figure 4.26 illustrates the general structure of the testbed molecular devices in this study. We specifically investigate a molecule with 7 CC on both sides as an example for molecules with "odd" chains (**Mol1**) and a molecule with 6 CC as an example for molecules with "even" chains (**Mol2**). The investigation for the employed prototype molecules is motivated by the results in [117, 153], in addition to the realized CCs in [168, 169].

Figure 4.27 illustrates the IV-curves of Mol1 and Mol2 devices. Mol1 shows NDR over a wide bias range with a negative slope around -1 MΩ and a peak to valley ratio greater than 10. On the other hand, Mol2 shows no NDR behavior, yet only a nonlinear increase of small current values with the bias is observed. It is worth noting that the current for Mol1 starts at a relatively high value, more than 3 orders of magnitude, compared to the starting current of Mol2. The same qualitative behavior is observed for all molecules with odd/even CCs in the range 0-7.

Figure 4.28 shows the TS of devices with different number of carbon atoms within the CC ranging from 0-7. The figure illustrates a clear odd/even oscillation in the behavior of the devices. Devices with an "odd" number of carbon atoms are characterized by the existence of several molecular orbitals (MOs) around the Fermi level (E_f) compared to devices with an "even" number of carbon atoms.
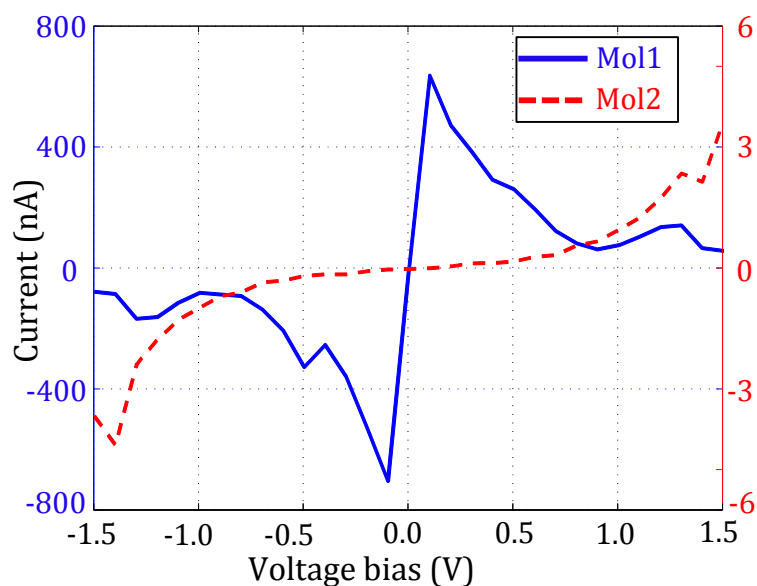
Figure 4.27: The simulated IV-curves of Mol1 and Mol2. The curves are plotted in different scales since there are orders of magnitude difference in current values.
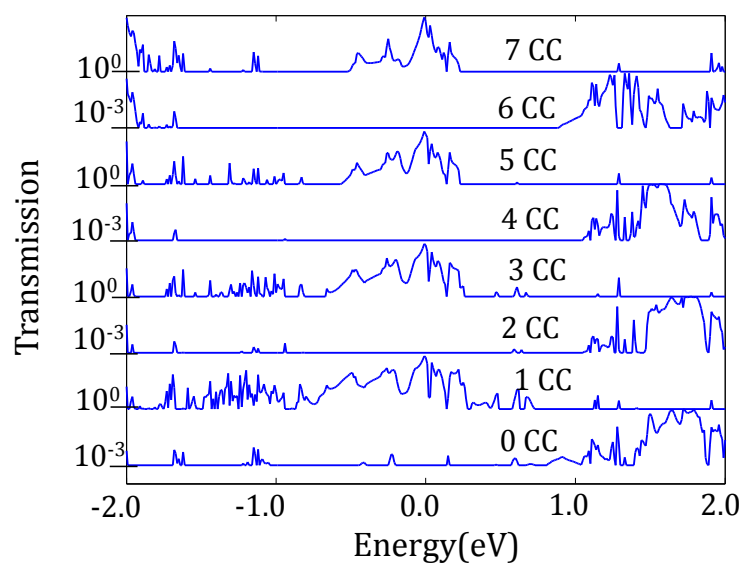
Figure 4.28: The equilibrium (zero bias) TS of symmetric devices with different number of carbon atoms per chain ranging from 0-7.

We suggest that the odd/even oscillation in the TS behavior (Figure 4.28), as well as the NDR behavior of devices with "odd" CCs (Figure 4.27), have the same origin. For an "even" number of carbon atoms, we have an alternation of triple and single bonds as shown in Figure 4.29. Thus, each carbon fulfills the Octet
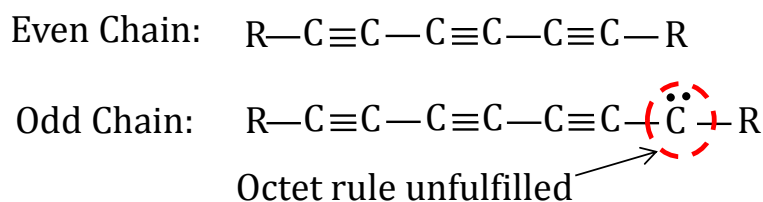
Even Chain: R—C≡C—C≡C—C≡C—R

Odd Chain: R—C≡C—C≡C—C≡C—[C̈]—R

Octet rule unfulfilled

Figure 4.29: A possible bond structure for 6CC (even chain) and 7CC (odd chain). In case of "odd" CC, we assume for simplicity only one atom broke the Octet rule, but in reality the lack of electrons is distributed among all atoms in the chain.

rule i.e. having 8 shared electrons in the outermost level. On the other hand, in case of "odd" number of carbon atoms, there is a lack of 2 electrons in order for the Octet rule to be fulfilled for all atoms.

Note that, SP hybridization for carbon atoms in the chains is adopted for the presented devices. Even for other possible bonding configurations, there is still a lack of 2 electrons within the "odd" CCs and we get similar characteristics on simulating these other devices. Moreover, when we allow hydrogen filling for the "odd" CC, two atoms are added, and the behavior completely changes to be similar to the devices with "even" CC.

Therefore for molecules with "odd" CCs, unoccupied MOs would move downwards with respect to E_f in order to allow a charge exchange between the molecule and the electrode at equilibrium. This in turns would allow the Octet rule fulfillment for the "odd" CCs. It is worth noting that the amount of the peaks in the TS of "odd" CC decays with increasing the number of atoms in the chain. This is because the lack of the 2 electrons is distributed among all atoms in the chain, so the effect reduces with the increase of atoms.

The induced MOs are symmetric with respect to the molecule, and they are localized at each carbon chain because the dimethyl insulating group effectively isolates the two halves of the molecule. At equilibrium, the MOs are at the same energy levels giving the opportunity for high transmission values around the Fermi level, whence high conductivity.

Upon applying a bias, the localized MOs at each side follow the chemical potential of the contacted gold electrode to guaranty the supply of the missing electrons, for Octet rule fulfillment. The projected density of states (PDOS) on
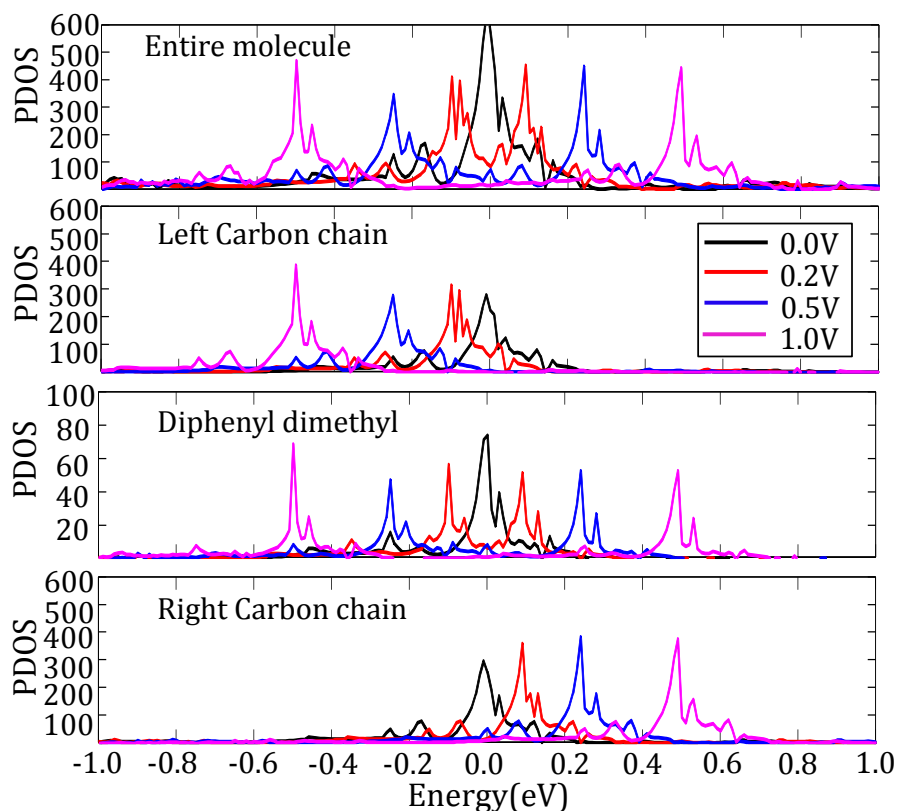
Figure 4.30: The PDOS on the entire molecule, left chain, right chain and central region of Mol1 under different biases. The Fermi-level is set to be zero.

different segments of Mol1 under different biases (Figure 4.30) confirms this argument. At equilibrium, both CCs contribute in the HOMO and the LUMO near E_f. On applying the bias, the PDOS peak of the left CC connected to the positive electrode starts shifting below E_f, acting as HOMO state. Conversely, the PDOS peak of the right CC connected to the negative electrode starts shifting above E_f, acting as LUMO state. These overall shifts lead to the split of the PDOS of the entire molecule and the diphenyl dimethyl segment as well. Since the MOs follow the respective electrode's chemical potential, the PDOS peaks are always near the border of the bias windows.

In general, two factors can provide high conduction in a single-molecule device. The first is the presence of an energy state (or MO) between the chemical potential of the contact electrodes. The second is a delocalization of this MO over the entire molecule. Consequently, the reduction of the overlapping PDOS between all segments of the molecule causes a reduction in the resonance tunneling
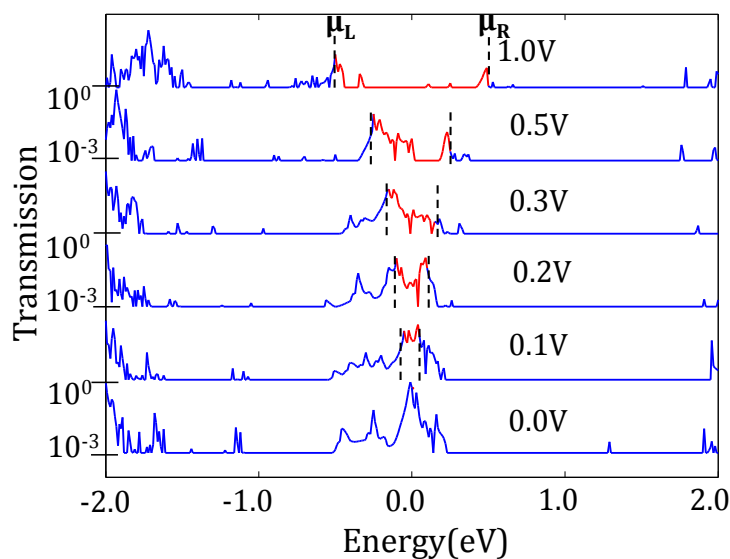
Figure 4.31: The TS of Mol1 (7CC) under various applied biases. The Fermi-level is set to be zero and the transmission window over which the current is calculated is in red color and surrounded by the dashed lines.

through the molecule. Figure 4.31 illustrates the TS of Mol1 under different biases. We can notice that the transmission peak around E_f splits, and its height continuously diminishes with increasing the bias. Correspondingly, the output current decreases, leading to the NDR behavior.

The IV-curves, TS and PDOS of the device were calculated using the DFTB+NEGF code, but the gold surfaces were not included in the scattering region. We redid the simulation with the gold surfaces and we got very similar results, but the code did not converge at some high biasing values. It is worth mentioning that, these devices were also simulated using the EHT+NEGF and DFT+NEGF from Quatumwise Atomistix, and the NDR response was observed in both calculations.

Another way to visualize and explain this special transport behavior of Mol1 in comparison to Mol2, is by illustrating the distribution of frontier MOs of both molecules under different biases, and their energy relative to the E_f, see Figure 4.32 and Figure 4.33. At equilibrium, LUMO and HOMO energies for Mol2 are far from E_f (Figure 4.33). Thus, the delocalization of the HOMO/LUMO

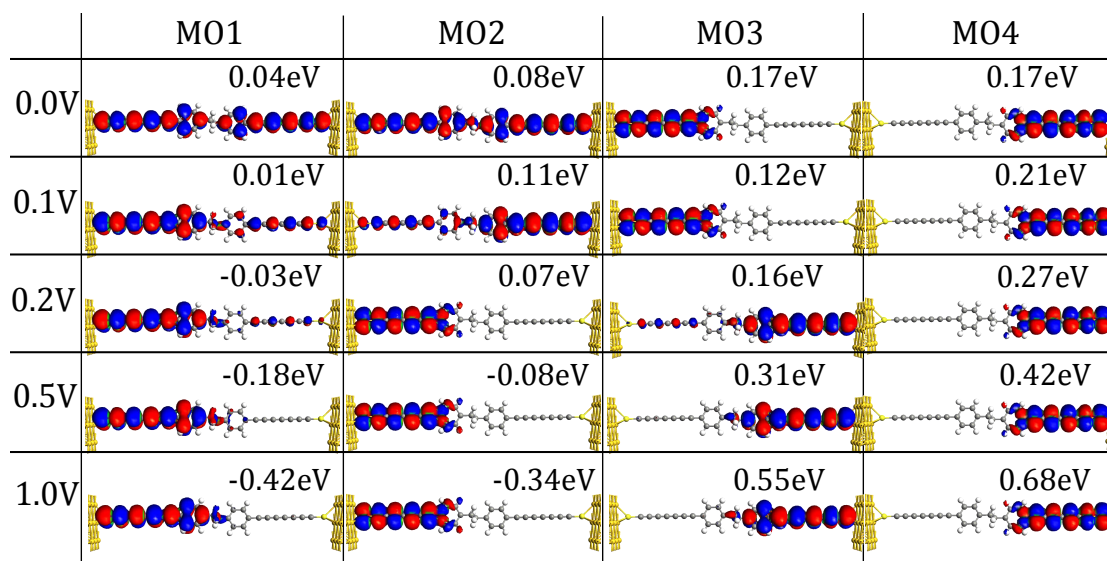|	MO1	MO2	MO3	MO4
0.0V	0.04eV	0.08eV	0.17eV	0.17eV
0.1V	0.01eV	0.11eV	0.12eV	0.21eV
0.2V	-0.03eV	0.07eV	0.16eV	0.27eV
0.5V	-0.18eV	-0.08eV	0.31eV	0.42eV
1.0V	-0.42eV	-0.34eV	0.55eV	0.68eV

Figure 4.32: An iso-surface plot for the distribution of the frontier MOs of Mol1 under different biases. The first four frontier MOs are illustrated. The energy position of each MO relative to E_f is denoted. A cutoff value of 0.02 is used in the plotting.

	HOMO	LUMO
0.0V	-1.49eV	0.76eV
0.1V	-1.45eV	0.74eV
0.2V	-1.39eV	0.71eV
0.5V	-1.31eV	0.66eV
1.0V	-1.12eV	0.53eV

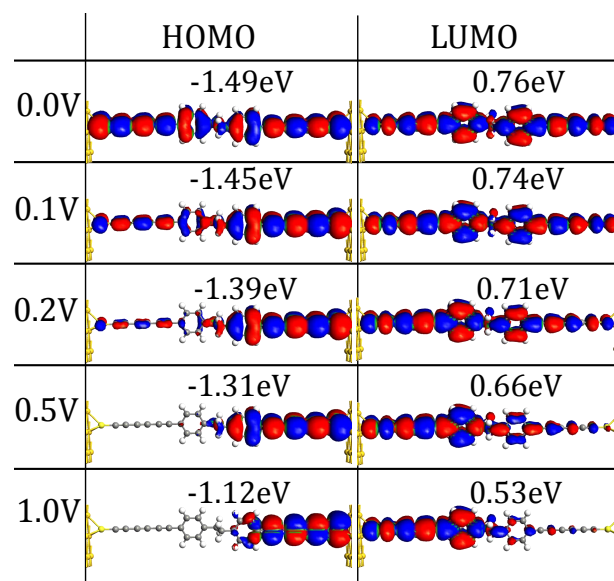**Figure 4.33:** An iso-surface plot for the distribution of the frontier MOs of Mol2 under different biases. Only HOMO and LUMO are illustrated. The energy position of each MO relative to E_f is denoted. A cutoff value of 0.02 is used in the plotting.

cannot provide conductivity at small bias in this case. As the bias increases, the HOMO/LUMO moves towards E_f, whence the conductivity is enhanced.

Consistent with the previous analysis, the frontier MOs of Mol1 are already aligned with E_f at equilibrium (Figure 4.32). In addition, they are delocalized along the molecule [4]. Thus, high conductance is expected even at low bias. As the bias increases, the frontier MOs stay mostly within the bias window, however, they start to be localized at opposite sides of the molecule. This, in turn, leads to the observed reduction in the conductivity.

As explained previously, MOs at each side of Mol1 follow the chemical potential of the contacted gold electrode, upon applying the bias. Thus, the MOs localized near the left (positive) electrode (MO1 and MO2) are HOMO levels, while the MOs localized near the right (negative) electrode (MO3 and MO4) are LUMO levels. For Mol2, since the HOMO/LUMO are away from E_f, a positive applied bias on the left electrode depletes the left portion of the HOMO levels, while the right (negative) electrode depletes the right portion of the LUMO levels. This explains the opposite HOMO/LUMO localization symmetry of Mol1 and Mol2 under bias.

Various studies relates molecular NDR behavior to an intrinsic increase in the resistivity of some segments of molecules due to charging or conformational changes [22,64,170]. Figure 4.34 shows the potential drop profile along Mol1 and Mol2 under biases 0.5 V and 1 V. The potential drop profile at both biases is the same. This indicates that the relative resistivity of each segment of the molecule with respect to other segments is kept constant; therefore, no space-charge or conformational effect is taking place in this case.

For Mol2, the potential drop is along the whole molecule with a steeper drop around the dimethyl group since only sigma bonds exist on this region. On the other hand, for Mol1, the potential drop is confined in the middle region around the dimethyl group. This is related to the continuous presence of high DOS within the bias window along the "odd" CC segments, which guarantees a high conductivity for them.

Question remains regarding the feasibility of actual realization of such molecule with "odd" chains of carbon atoms. Further work should address the experi-

---

[4]Note that, MO1 and MO2 (MO3 and MO4) are almost at the same energy value, so they are integrating each other at 0V and 0.1V. They correspond to the broadening in the HOMO (LUMO), respectively.
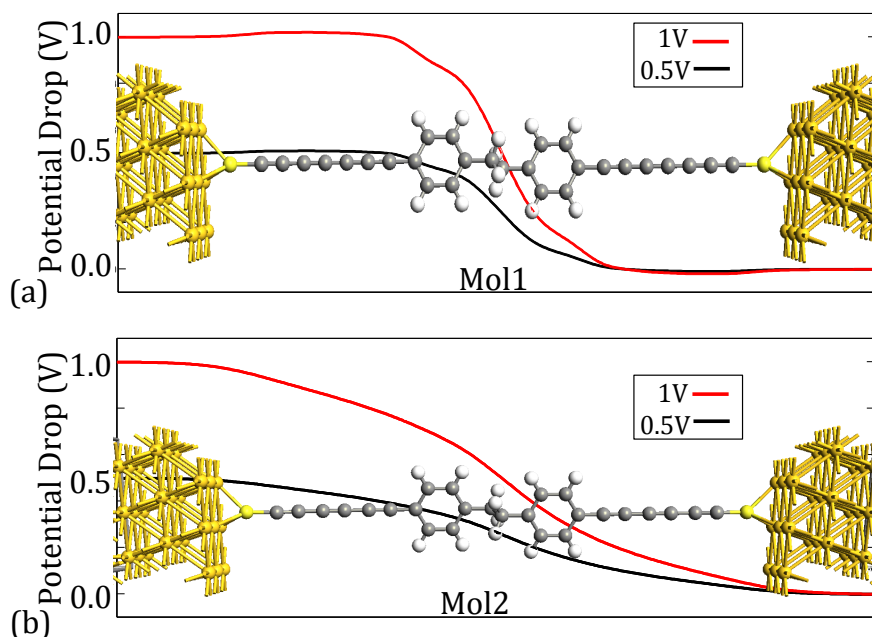
Figure 4.34: The potential drop profiles along Mol1 and Mol2 under biases 0.5 V and 1 V.

mental side for synthesis of the molecule and realization of the device since this could provide a breakthrough achievement in the field molecular electronic.

4.5 Conclusion

Molecular rectifiers are required in the realization of crossbar arrays application since they allow the selectivity of each cell [18, 171]. We studied three different species of molecular rectifiers and illustrated important factors that affect the rectification in these molecules. We showed the feasibility to control the rectification direction and magnitude of molecular devices merely through varying their linker groups. In addition, we proposed an asymmetric OPV molecular rectifier that shows a rectification ratio of more than three orders of magnitude while preserving high on current. Although the synthesis of asymmetric molecules is feasible and realized by some groups [8, 92], it requires a non-trivial huge amount of effort. We hope that the asymmetric OPV molecular rectifier is realized soon and its performance is verified experimentally.

Furthermore, we studied a two terminal molecular device with a wide range of NDR and a peak to valley ratio greater than 10. The NDR behavior has many applications in low power memories as well as high speed circuits and

systems [128, 129]. The tesbed device has chains with an "odd" numbers of carbon atoms in both sides, which make the realization of such device still questionable. We believe that the systematic analysis of the device and the clearly built relationships between the different transport characteristics can be exploited in the explanation of other devices exhibiting NDR.

5 Three Terminal Molecular Devices

5.1 Introduction

Molecular electronics is an interdisciplinary between two major fields of research namely physical chemistry and electrical engineering. Molecules synthesis constitutes the first step in building a molecular device; the complexity of this step usually depends on the complexity of the molecular structure itself. After that, comes another challenging step which is the preparation of contacts for the molecule to be attached. There are currently several different techniques for that purpose [100, 139, 172]. Finally, molecular characterization and analysis need to be performed in order to allow further design of molecular electronic devices [69, 173].

The semiconducting behavior of conjugated molecules has triggered the attention of many research groups [22, 108–110]. Oligo-Phenylene Ethylene (OPE) and Oligo-Phenylene Vinylene (OPV) are among the most famous species due to their delocalized pi-bonds which facilitate the charge's transport across them. Moreover, they are mechanically very stable and rigid which are favorable properties for contacting molecular devices [174]. Tsio et al. prepared a Quinone-modified OPV which can be electrochemically controlled [175]. This was implemented through applying an oxidation/reduction process to the molecule to switch between two conduction states with ratio up to 40. Søndergaard et al. realized an OPV molecular wire with oxygen linkers that displays a non-linear response to an external bias with a threshold conductance onset around 1.4 V [139, 165]. We used derivatives of this OPV molecule in the analysis carried out in this chapter (Figure 5.1).

This chapter is organized as follows: we first illustrate the methodology applied in the study of the testbed three terminal molecular devices. After that, we discuss the device characteristics of a gated molecular OPV wire that shows

For a simple thiol linker group
  R ≡ S Ac
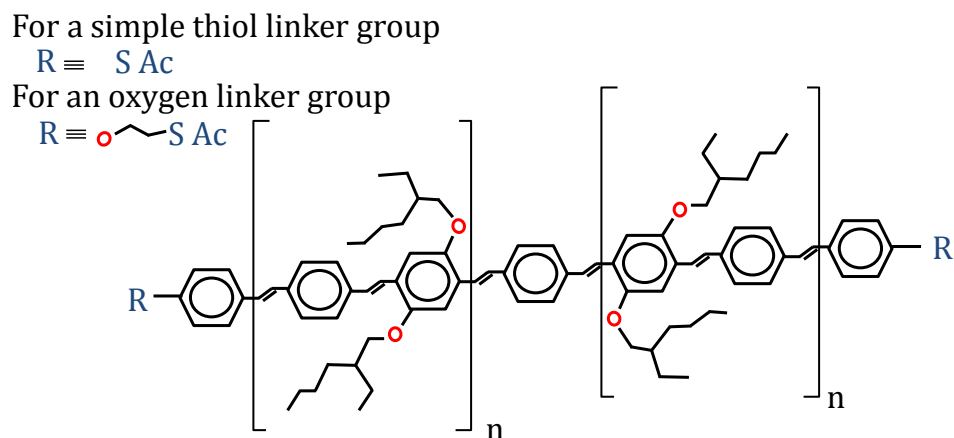For an oxygen linker group
  R ≡ o〜S Ac

Figure 5.1: The general structure of a synthesizable OPV molecule. The side functionalization groups in the middle of the OPV are usually synthesized for stability and solubility of the molecule and they do not affect the rectification behavior of the molecule based on simulation.

a negative differential resistance (NDR), in addition to the gate conductance dependency. Moreover, we show the atomistic simulation results for another gated OPV molecular device with oxygen linkers. The provided simulation analysis of this device matches the experimental measurement and it helps in understanding the device response. Finally, we provide a study on three-leg OPE molecules and we investigate their feasibility as building molecular transistors and standalone logic gates.

5.2 Methodology

Similar to the two terminal devices, we apply the same procedure of geometric optimization of molecules and the placement of the molecules in contact with the gold electrodes via the thiol-gold bond. NEGF formalism in combination with Extended Hückel Theory from Quantumwise ATK is employed in the simulation used in the study of the gated OPV devices [60,61]. The employed boundary conditions in the Multi-grid Poisson solver are Dirichlet along the transport direction and Neumann in the directions perpendicular to the transport.

In the last subsection, the atomistic analysis in the study of the three-leg OPE molecular devices is based on NEGF coupled to DFT and its tight-binding approximation from DFTB+NEGF code [47,147,157]. Since the transport in this case is along the three electrodes, the boundary conditions in the real-space
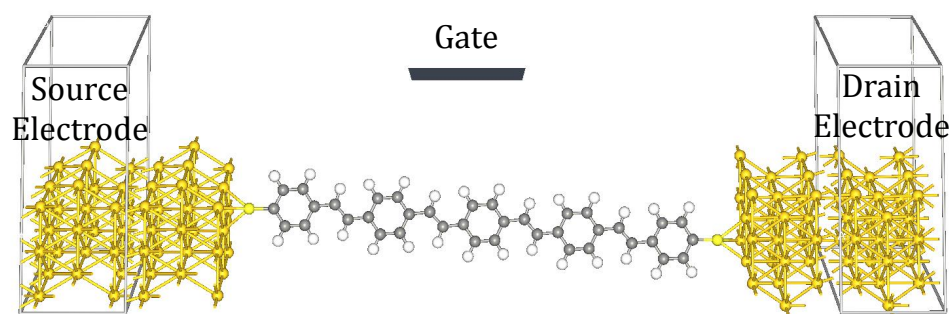
Figure 5.2: The structure of the gated OPV molecular device. The molecule is attached to two (3×3) (111) gold electrodes. Metallic gate is 1 nm away from the molecule and a free space dielectric is assumed in between.

Multi-grid Poisson solver are Dirichlet in the directions of a plane containing the three electrodes and Neumann in the direction perpendicular to the plane.

5.3 Results and Discussion

5.3.1 Gated Molecular Device with Negative Differential Resistance

In this subsection, we analyze the transport behavior of an OPV molecular device with a back-gate, where an NDR behavior and an obvious gate dependency are noted. The main objective of the section is to give possible explanations for these transport characteristics by shedding light on various atomistic simulations of the device.

Figure 5.2 shows the simulation setup of the employed OPV molecular device with gate electrode. Figure 5.3 shows the output characteristic curves of the gated OPV molecular device in linear[1] and logarithmic scale.

Device Analysis at Equilibrium

Figure 5.4 shows the distribution of charge density difference through the molecule at equilibrium (zero gate and drain bias). Positive and negative charges accumulate near the two thiol-gold terminals of the device forming

---

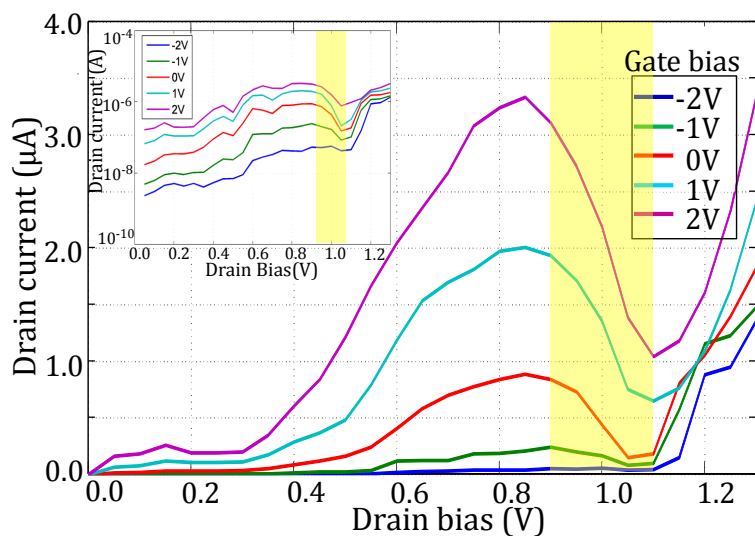[1]The linear curves are plotted using MATLAB after curve smoothing.

Figure 5.3: The simulated I-V curves of the OPV device at various gate bias in linear scale. The inset is the I-V curves in Logarithmic scale. The highlighted is the region where the NDR is noted.
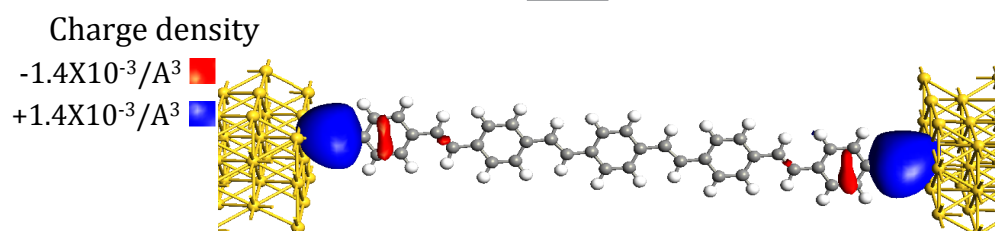

Figure 5.4: Distribution of charge density difference through the molecule at equilibrium.

electric dipoles in these regions. Since the gold contacts have a lot of weakly bounded electrons, the shared electrons between the OPV molecule and the thiol-gold terminals are attracted to the OPV. As a result, a fraction of positive charges accumulates near the thiol region and negative charges would spread through the OPV's atoms, especially those near the terminals. The created electric dipoles play a vital role in the transport behavior of the device. This is because the dipoles would have anti-symmetric polarities relative to an electric field generated by the drain-source bias.
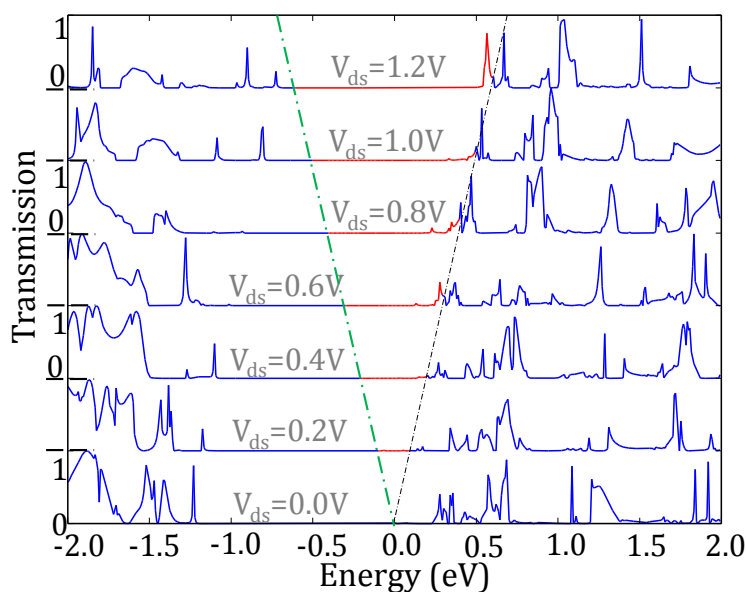
Figure 5.5: The simulated TS at zero gate bias with different drain biases. The transmission window over which the current is calculated is in red color and surrounded by the dash lines. The fermi level is set to be at zero.

Device analysis under drain bias sweep

Figure 5.5 shows the transmission spectra (TS) of the device at various drain-source biases. It is clear that the current is dominated by resonance tunneling through the LUMO. Interestingly, the LUMO broadened area within the integration window is reduced at drain bias 1.0 V relative to that at 0.8 V. This is translated to a reduction in the current value which leads to an NDR behavior. The NDR behavior is mainly observed in the range of drain-source bias 0.9 V to 1.1 V.

We refer back to the concept discussed in section 4.3 to explain the observed NDR behavior in this device. For a device whose conduction is dominated by LUMO tunneling, the conduction is enhanced with the increase of the potential drop near the negative electrode. Figure 5.6 shows three potential drop profiles over the molecule at zero gate bias. The profiles correspond to the drain biases: 0.9 V, 1.1 V and 1.3 V. These correspond to bias values before, within and after the NDR region, respectively. Although the molecule has a symmetric structure, the potential drop through it does not show this symmetry. The resistance of each terminal is polarity-dependent, and the terminal of molecule near the
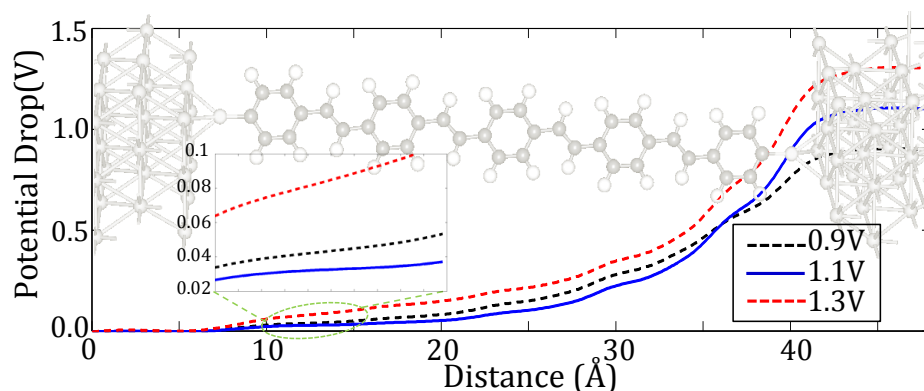
Figure 5.6: Potential drop through the OPV molecular device at $V_g = 0\,V$, and $V_{ds} = 0.9$, 1.1 and 1.3 V. The inset is a zoom-in for the potential drop near the negative electrode.

positive electrode shows higher resistivity[2] . We suggest that the dipoles created near thiol-gold regions could be the origin of this potential drop due to their anti-symmetric action, similar to back-to-back PN junctions, toward the applied field.

As can be noticed in Figure 5.6 the potential drop near the negative electrode at drain bias 1.1 V is less than that at 1.3 V, and interestingly it is also less than that at drain bias 0.9 V. The NDR behavior of the device can be attributed to the reduction in potential drop near the negative electrode besides broadening and shifting of the LUMO away from the Fermi-level. Moreover, the slopes of the potential drop at drain biases 1.1 V and 1.3 V are similar, however it is less steeper near the positive electrode at drain bias 0.9 V. This could point out an important non-linear dependency between the applied drain bias and the dipole near the positive electrode, where a change is introduced to the dipole resulting in increasing resistivity within the NDR interval. Consequently, the resistivity of the dipole near the positive electrode increases in the NDR interval up to drain bias 1.1 V. This results in lower potential drop near the negative electrode; thus the LUMO dominated current is reduced. After the NDR region, the resistivity remains constant. Thus, increasing the bias would increase the potential drop near the negative electrode, hence the LUMO dominated current increases again.

---

[2]An identical behavior is observed when the positive bias is applied on the left electrode.

The peak to valley ratio of the NDR is reduced as we go from positive to negative gate bias. This originates from the fact that negative gate bias pushes the LUMO away from the Fermi-level as we will elaborate in the next subsection. Thus, the contribution of LUMO in the transmission is reduced, and the magnitude of current in the NDR interval shows less notable reduction. It is worth mentioning that after drain bias 1.3 V the simulation usually shows significant current variations. The thiol-gold bond already shows a variation in its resistive property within the NDR region. Thus, the variation in the magnitude of current at higher drain biases might be attributed to the need for dynamic molecular geometry change, which is not accounted in the simulation. Zhitenev et al. stated that experimental measurement of a gated molecular devices shows stable and reproducible characteristics for drain bias up to 1 V, after that numerous switching in the current values is also observed [137]. They related this switching to an electromigration that may occur inside the metallic electrodes [137, 176].

Device analysis under gate bias sweep

Similar to macroscopic devices, a positive gate bias leads to a negative charge accumulation in the central region of the molecule (Figure 5.7a). These negative charges come from the gold contacts since no observed positive charges arised within the molecule to compensate the excess negative charges.

Since electrons are dominating the transmission, increasing the gate bias results in increasing the molecule's conductance, hence the current increases. Moreover, the TS change directly with the gate bias variation (Figure 5.8). The LUMO is pushed towards the Fermi-level with increasing the gate voltage. This provides another mean to illustrate the exponential increase in the current with increasing the gate bias. Similarly, one can deduce that a negative gate bias would result in a positive charge accumulation in the central region of the molecule (Figure 5.7b), which in turns reduces the electron mobility through the molecule.

On simulating the conductance as a function of the gate bias and at fixed drain bias 0.4 V, a clear impact of the gate bias on the conductance behavior is found (Figure 5.9). A direct proportional relation is observed in the gate bias range -3.5 V, to 4 V. Remarkably, the gate-conductance relation is inverted below gate bias -3.5 V; the conductance starts increasing again although the gate bias decreases.
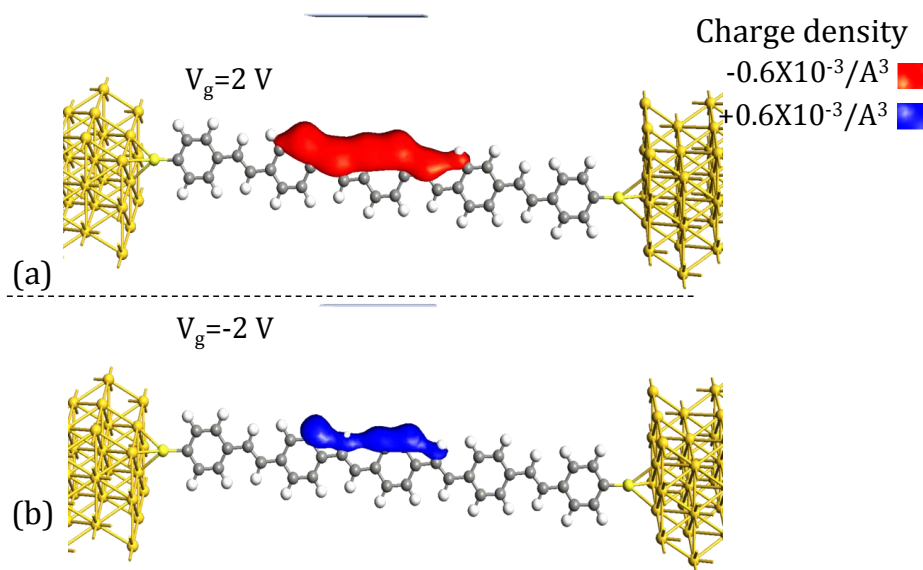
Figure 5.7: The charge density difference, at zero drain bias while gate bias is (a) $V_{gs} = 2V$ and (b) $V_{gs} = -2V$. This is relative to the charge density difference of the device at equilibrium.

The origin of this inversion in the gate-conductance relation is related to the position of HOMO and LUMO. A negative gate bias results in shifting the HOMO towards the Fermi-level and the LUMO away from the Fermi-level. At gate bias -3.5 V, the Fermi-level is almost in the midway between the HOMO and the LUMO. Further increase in the negative gate bias allows higher HOMO transmission, hence the conductance value increases (Figure 5.8). This inversion behavior in the gate-conductance relation is interesting for applications in which logic gates are built with single molecular devices. A detailed illustration for such applications can be found in [177, 178].

5.3.2 Dithiolated Oligo-Phenylenevinylene Gated Device

This subsection focuses on simulation and characterization of an OPV molecular FET. The validity of the results is supported by its agreement with the experimental measurements conducted on the same molecule. The employed OPV molecule has oxygen linkers, which are found to enforce an interesting nonlinear current characteristics. We will first give background information for the fabrication process and measurement results. After that, we will specify the device setup that we use for modeling the real device, and present the atomistic simulation results of the device.
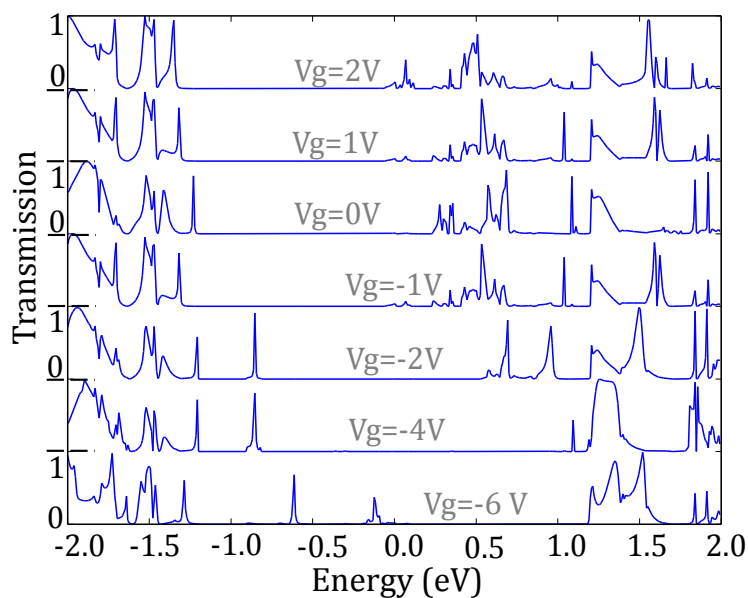
Figure 5.8: The simulated TS at zero drain bias with different gate biases. The fermi level is set to be at zero.
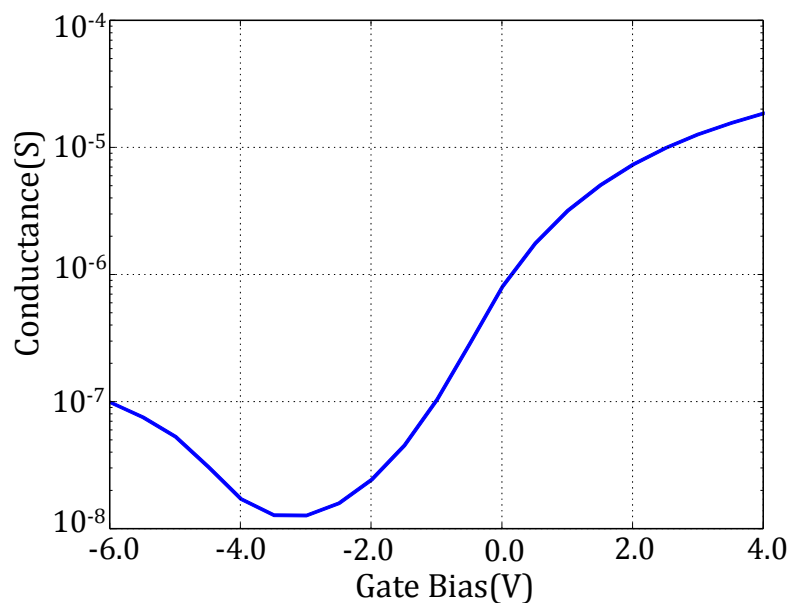

Figure 5.9: The conductance of the molecule as a function of the gate bias at fixed drain bias 0.4 V.

Experimental procedure and measurement data[3]

The choice of oligomers of poly-phenylene vinylene molecules returns to their easy synthesization process and their moderate stability [165]. Stepwise Horner-Wadsworth-Emmons reaction for a bifunctional OPV-monomer is used in the synthesization of OPVs with 3-19 phenyl units (up to 12 nm length) with various linkers. Detailed explanations, about the synthesization of the OPV and the addition of the different linkers to it, can be found in [165].

For realizing the molecular FET device, an InAs nanowire of 50 nm diameter is grown with a 5 nm segment of InP [139]. This InP segment acts as an insulating barrier that disconnect the InAs conducting segments (Figure 5.10a). The nanowire is then mechanically transferred onto a substrate of p-doped silicon with SiO2 layer over it to act as the back gate of the molecular device. Further development are applied to the nanowire for treatment and smoothing [139].

The wire is functionalized by adding few droplet of the OPV solution on the insulating InP segment. After that, the tetrahydrofurane solvent is evaporated, hence the OPVs are left unbound to the wire in the form of thioacetates [165]. Further process is then performed to bind the OPV to the conducting segments. Ag and Ti are used as ohmic contact for the drain/source InAs segments and the P-doped Si gate. Figure 5.10b shows the SEM image of the device, whereas Figure 5.10c shows the schematic circuitry setup of the device.

The characteristic curves of the molecular device for different gate and drain biases are shown in Figure 5.11. The curves show threshold values for the drain biases at which the current starts increasing rapidly. Moreover, increasing the gate bias reduces the threshold value, and a complete switch-on of the device is achieved at gate bias 3 V. *Applying a negative drain bias results in increasing the effective gate bias; this explains the high current at the negative drain bias (asymmetric curves).* It is worth mentioning that based on the molecule geometry and size; it is

[3]Prof. Frederik Krebs group in Technical University of Denmark (Denmark) was responsible for the synthesis of the molecule. Prof. Lars Samuelson group in Lund University (Sweden) was responsible for the development of the nanowire. Prof. Marc Tornow group in Technische Universität Braunschweig (Germany) was responsible for the electrical characterization and measurement.
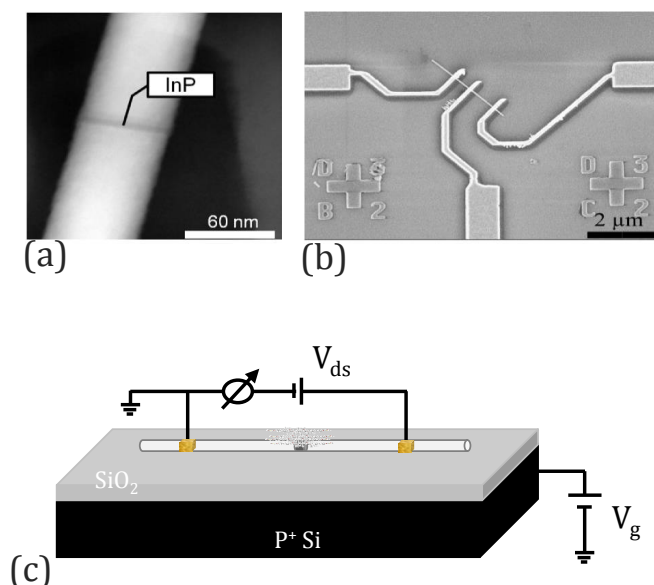
Figure 5.10: (a) Scanning electron microscopy (SEM) image of InAs/InP heterostructure nanowires, adopted from [139]. (b) SEM image of an individual 2.8 long wire contacted by three metal leads as ohmic contacts.(c) Schematic circuitry setup of the device.

expected that around 300 OPVs are aligned over the InP region [139]. This means that the current flows through a single OPV in the range of few nano-Amperes.

Simulation setup

The device setup in the simulation differs from the experimental one. Gold (111) electrodes with 3×3 atoms/layer are employed. The thiolate terminals of an OPV molecule with 7 phenyl rings are replaced by thiol-gold bonds. The position of the metallic gate is chosen by trial-error until we reach the best matching to the experimental results. The gate is around 1 nm away from the molecule (Figure 5.12). Although the final simulation setup is different from the real one, the general characteristics of the simulated device match the experimental results. The main concern of this subsection is to explain the quantum transport characteristics of the device.

The simulation at high gate and drain bias of this device shows a lot of fluctuation and low convergence rate. Thus, we present the results in the interval where the values are stable to some extent. We provide an explanation to the realized device characteristics employing the available atomistic simulation results. Centaurus modeling tool was used to model the electrical properties of
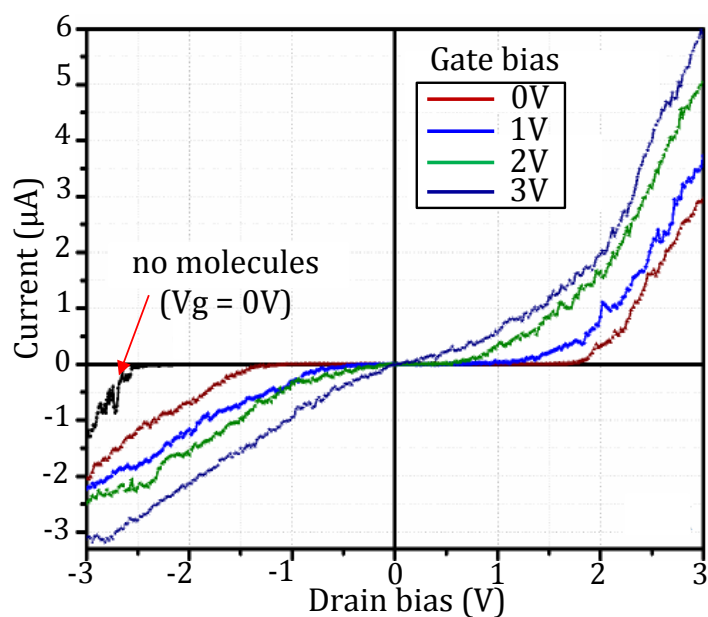
Figure 5.11: The measured I-V curves of the nanowire before and after surface functionalization with OPV molecules, adopted from [139].
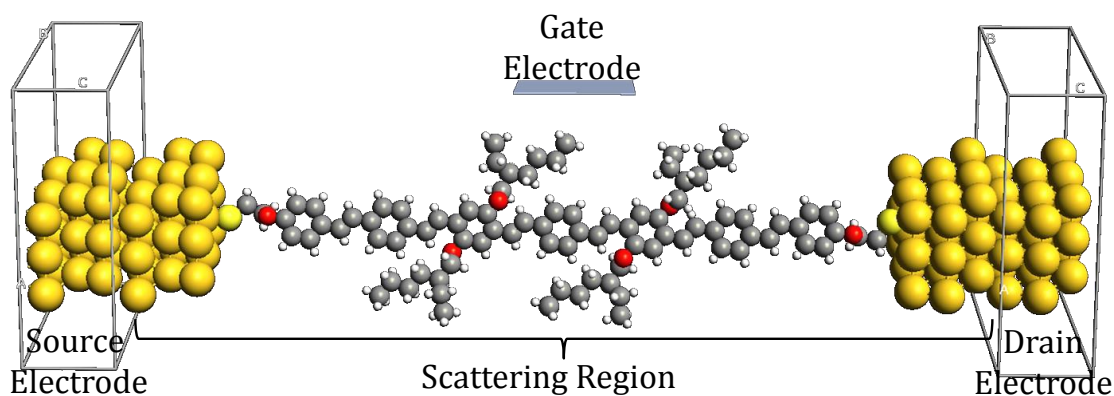
Figure 5.12: The gated OPV molecular device setup. The drain/source electrode regions are illustrated by the wire boxes. The metallic gate is placed at around 1 nm away from the molecule.

the complex gated structure of the InAs/InP nanowire on the silicon substrate without the molecules[4]. The effective gate biases, that alter the molecules energy levels, are found to be in consistence with the the atomistic simulation.

---

[4]This task was implemented by Bogdan Popescu and Dan Popescu at Technische Universität München.

Figure 5.13: The simulated I-V curves of the OPV device at various positive gate biases.

As an illustration of the simulation results, Figure 5.13 shows the output characteristic curves of the gated OPV molecular device. As can be noticed, the output curves based on the simulation matches the experimental results qualitatively.

Device analysis at equilibrium

Figure 5.14 shows the charge density distribution and the electrostatic potential profile of the device at zero gate and drain bias. 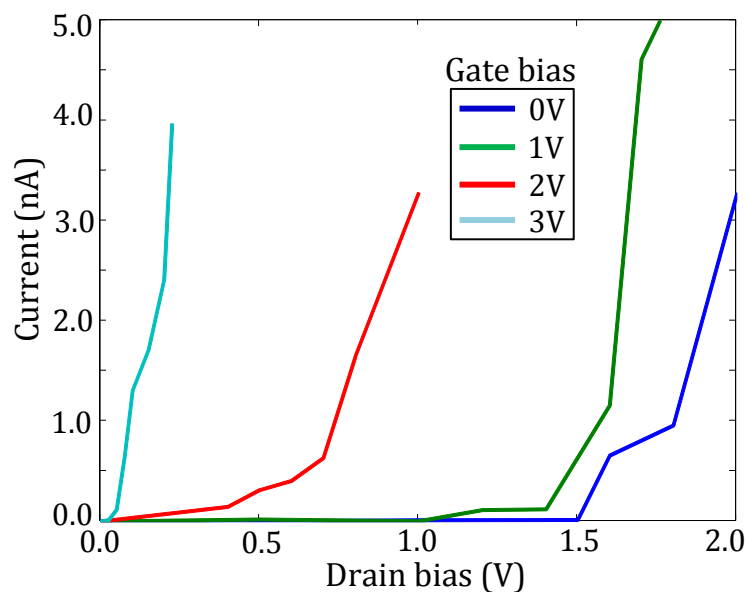Oxygen is characterized by its high electronegativity. Thus, the shared electrons in the polar bonds between the oxygen and its neighboring carbon atoms are attracted to the oxygen. As a result, negative charges accumulate over the oxygen atom (Figure 5.14a). This corresponds to a potential well by solving Poisson equations (Figure 5.14b). The potential barriers and wells in the middle region of the molecule are due to the side functionalization groups. They do not have a big impact on the charge transport along the device. We simulate the molecule with/without the side functionalization groups and the results are similar for this device.

The main feature of these oxygen linkers is the potential well created by the oxygen atom. To illustrate the influence of the oxygen linkers on the behavior of the molecular device, Figure 5.15 shows the TS of three OPV devices with
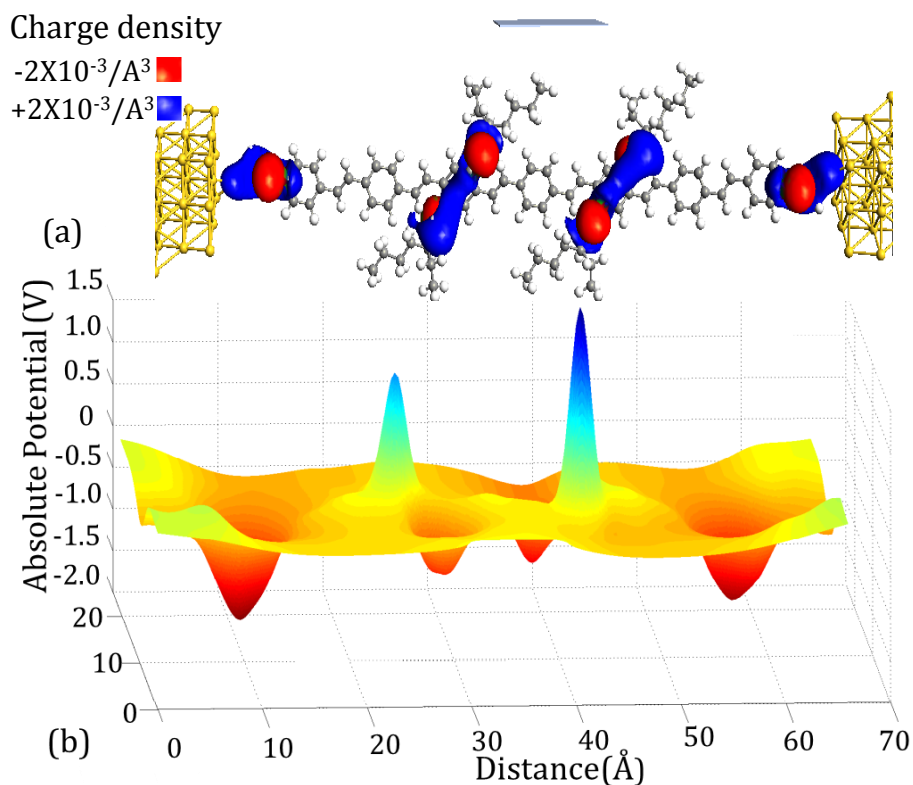
Figure 5.14: (a) The charge density distribution through the device at zero gate and drain bias. (b) A 3d visualization of a contour plot for the absolute potential profile of the device.

different linkers, at equilibrium. As can be noticed, the three devices have HOMO and LUMO peaks at position around -1.5 eV and 0.2 eV, respectively. This could be attributed to an inherent feature of the OPV itself. Interestingly, the addition of the oxygen linker leads to a reduction in the transmission peak values, and the broadening is also quenched. This indicates that the terminal with oxygen linker decouples the molecule from corresponding electrode. A resolution of 0.001 eV is used in the calculation of the TS of the OPV with oxygen linkers, to be able to capture the transmission peaks.

Device analysis under drain bias sweep

It is worth noticing that the applied voltage is on the right electrode unless otherwise stated. The current flow occurs if at least one of the next two conditions is fulfilled. If the applied voltage acts on relatively increasing the chemical potential μ_L of the negative electrode such that it exceeds the LUMO of the molecule, a current through LUMO transmission will flow. If the applied voltage
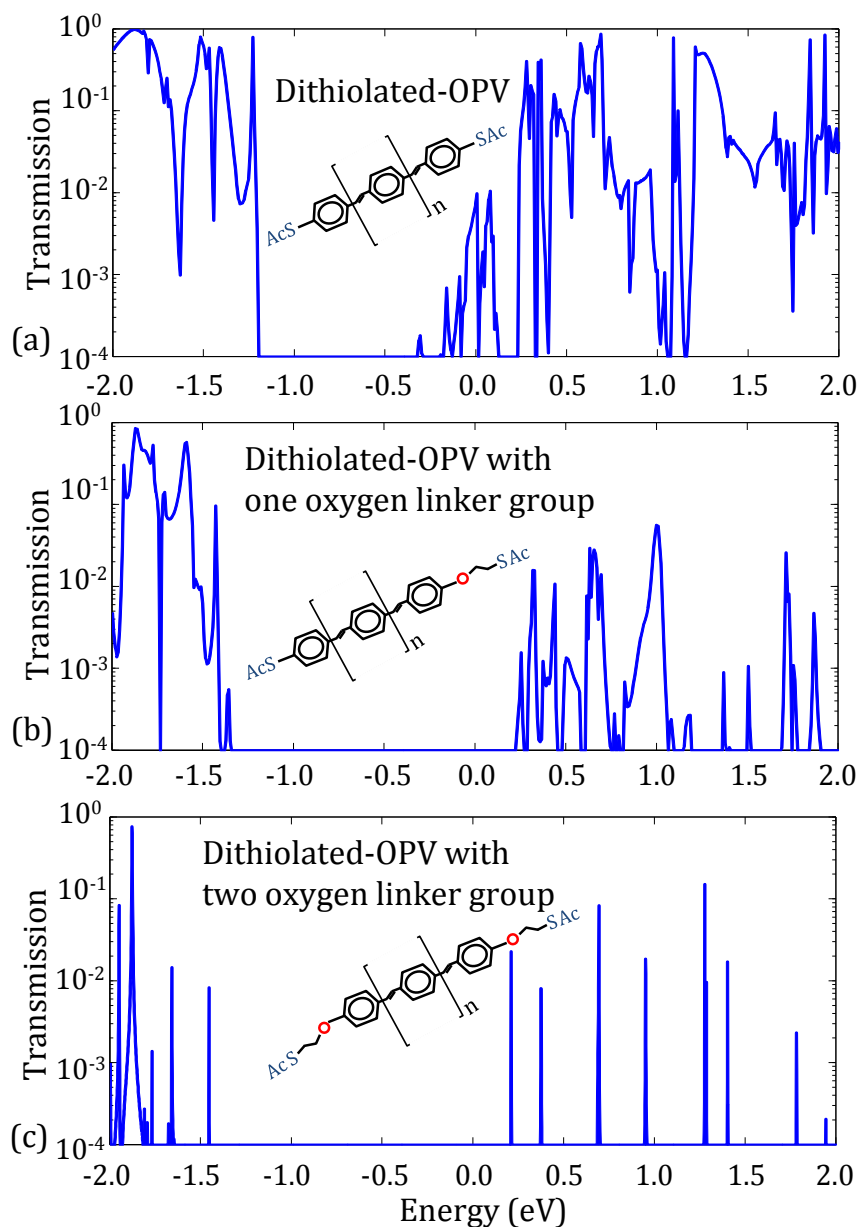
Figure 5.15: The TS of dithiolated OPV molecules (a) without oxygen linker groups. (b) with an oxygen linker group on one terminal. (c) with oxygen linkers group on both terminals. The Fermi energy is set to be zero.

acts on relatively lowering the μ_R of the positive electrode such that it goes beneath the HOMO of the molecule, a current through HOMO transmission will flow. One may expect that conduction could occur through LUMO transmission at relatively small bias ≈ 0.21V. This expectation is valid only if a potential drop of 0.21V takes place near the negative electrode. Nevertheless, it is found that
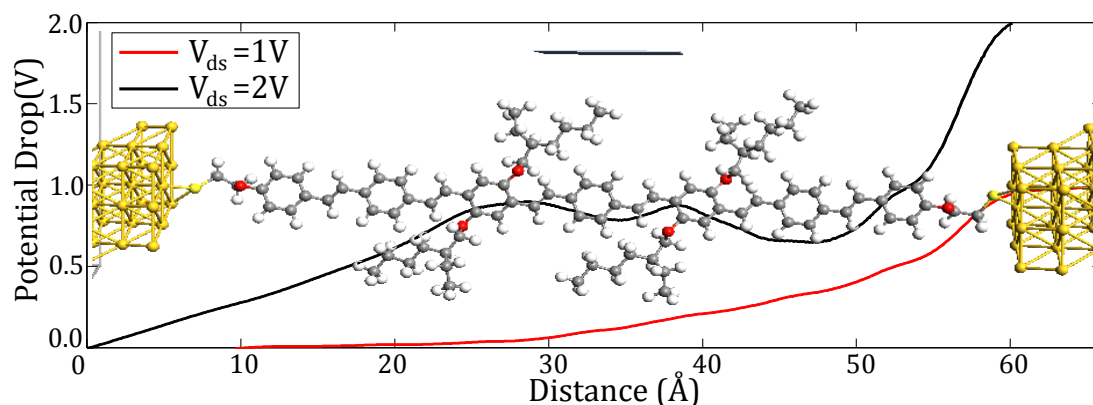
Figure 5.16: The electrostatic potential drop through the molecule at $V_g = 0$V and $V_d = 1$V and 2V.

almost the whole potential drop occurs near the positive electrode before the threshold value (Figure 5.16).

We need to refer to the asymmetric OPV molecular rectifier in which the potential drop is mainly at the oxygen linker regardless to the bias polarity (subsection 4.4.2). The forward current starts at low bias through LUMO when the negative electrode is the one connected to the oxygen linker. Conversely, the reverse current starts at higher bias through HOMO when the positive electrode is the one connected to the oxygen linker.

The testbed OPV molecule with oxygen linker on both sides can be modeled as two back-to-back diodes of the asymmetric OPV. When a drain-source bias is applied along the devices, the same current flows through both diodes according to Kirchhoff current law. Consequently, the drop of applied bias below threshold is mostly at the reversely biased diode, near the positive electrode. After threshold, the bias is distributed along the whole device but still the greatest drop near the positive electrode (Figure 5.16). At a bias lower than the transistor threshold, the charges can bypass the forward biased diode, but they accumulate at the reverse biased one (Figure 5.17).

At zero gate bias, the threshold is achieved through HOMO transmission at drain bias around 1.5 V. The LUMO is found to contribute also in transmission after certain drain bias. Figure 5.18 shows the TS for different drain voltage values at zero gate bias. The HOMO transmission dominates the transmission window after the threshold. The shifting of the TS under drain bias follows the
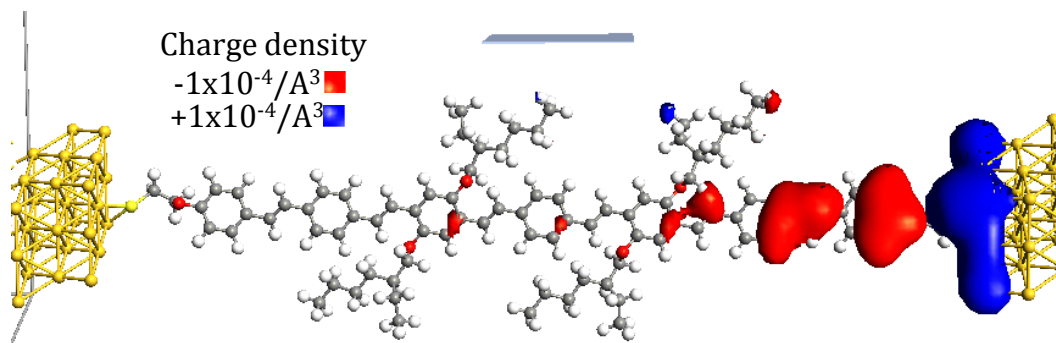
Figure 5.17: The charge density difference through the molecule at $V_g = 0V$ and $V_d = 1V$.
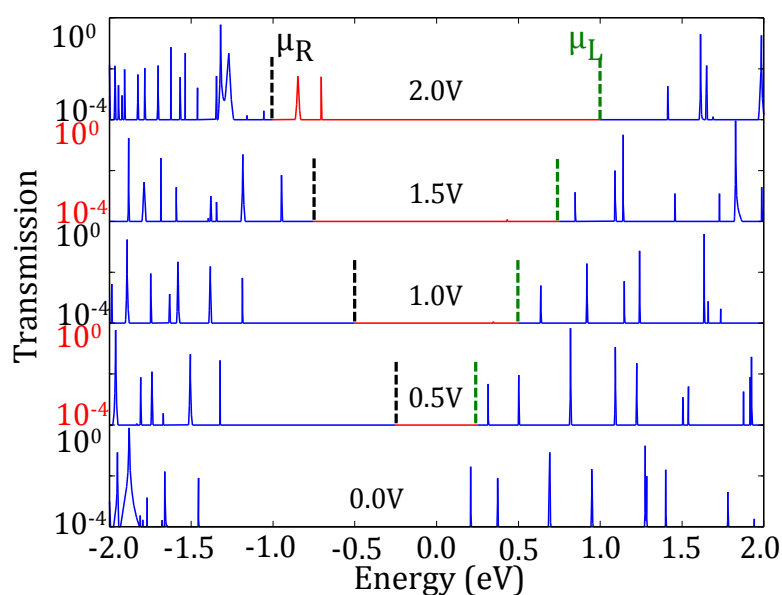
Figure 5.18: The TS at zero gate bias with different drain biases. The transmission window over which the current is calculated is in red color and surrounded by the dashed lines.

chemical potential of the left electrode (μ_L) because most of the potential drop is near the right electrode.

The inset of Figure 5.19 shows the drain voltage sweep -including negative values- at zero gate bias to show the symmetric operation of the device. The negative drain voltage is simulated by reversing the polarity of the drain-source electrodes. As can be noticed, the threshold voltage is the same at both sides, and the characteristics after the threshold are quiet similar.
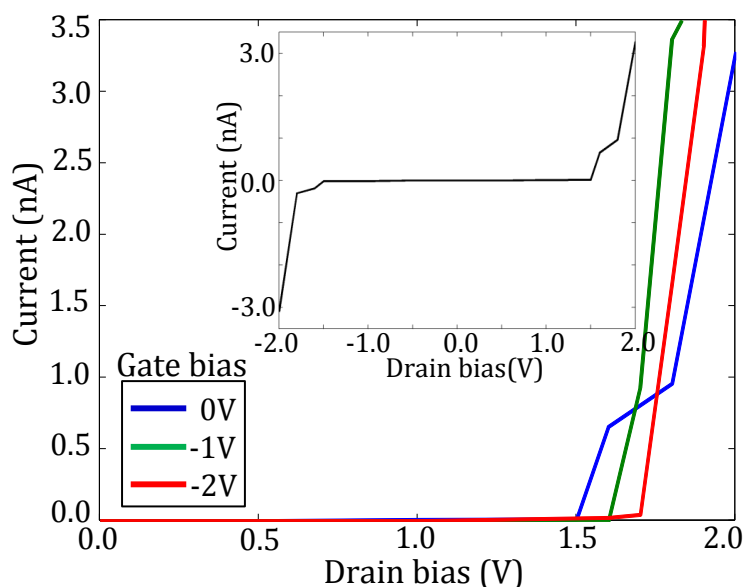
Figure 5.19: The simulated I-V curves of the OPV device at various negative gate biases. The inset is the drain voltage sweep including negative values at zero gate biasing.

Device analysis under gate bias sweep

A positive gate bias imposes a forward bias for the two back-to-back diodes, hence negative charge accumulation occurs in the inner part of the molecule (Figure 5.20a). Conversely, a negative gate imposes a reverse bias for the two back-to-back diodes, hence almost no charge accumulation occurs in the inner part of the molecule and only some charge accumulate near the oxygen linkers (Figure 5.20b).

Figure 5.21 shows the TS of the device under various gate biases and at zero drain-source bias. The energy levels are pushed down under a positive gate bias, however the accumulation of negative charges within the molecule results in raising in the energy levels. These competing effects lead to the weak shift in the TS under positive gate biases. For negative gate biases, there is almost no charge accumulation, hence only the effect of rising the energy levels with the negative gate bias occurs. Interestingly, the onset conduction switching at negative gate bias is slightly changing (Figure 5.19), although the HOMO is shifting toward the Fermi-level. This is because the potential drop becomes no more confined near the positive electrode.
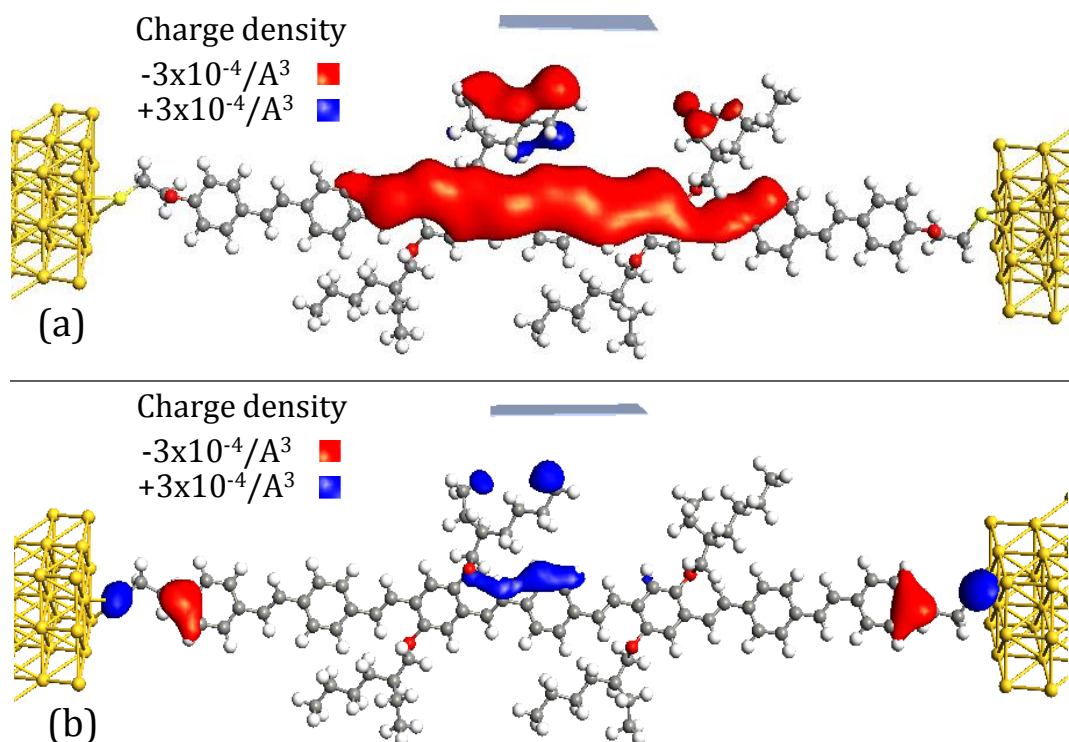
Figure 5.20: The charge density difference through the molecule at zero drain bias and gate bias: (a)$V_g = 2$V, (b)$V_g = -2$V.

Figure 5.22 illustrates the HOMO and LUMO distribution through the OPV molecule at various gate and drain biases. At equilibrium, the HOMO and LUMO are delocalized along the molecule. In consistence with the TS, the HOMO and LUMO position are at -1.45 eV and 0.21 eV, respectively. Under drain bias 2 V, the HOMO and LUMO are localized at left and right segments of the molecule, respectively. This is because a positive applied bias on the right electrode depletes the right portion of the HOMO levels, and the left (negative) electrode depletes the left portion of the LUMO levels.

The distributions of both HOMO and LUMO, under gate bias 3 V, are similar to those at equilibrium. However, their energy positions shift down; the LUMO is almost align with the Fermi-level. Thus, small applied drain bias would allow current to flow by tunneling through the LUMO.

5.3.3 Three-Leg Molecular Devices

In this subsection, we theoretically study three-leg oligo-phenylene ethynylene (OPE) molecular devices exploiting the interesting behavior of the previously
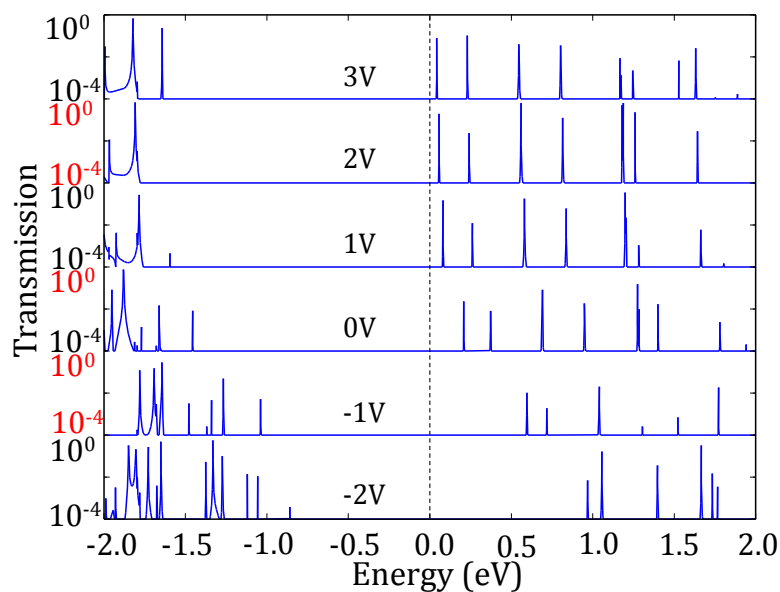
Figure 5.21: The TS at zero drain bias with various gate biases.

	HOMO	LUMO
V_g= 0V V_{ds}= 0V	-1.45 eV	0.21 eV
V_g= 0V V_{ds}= 2V	-0.36 eV	1.04 eV
V_g= 3V V_{ds}= 0V	-1.64 eV	0.04 eV
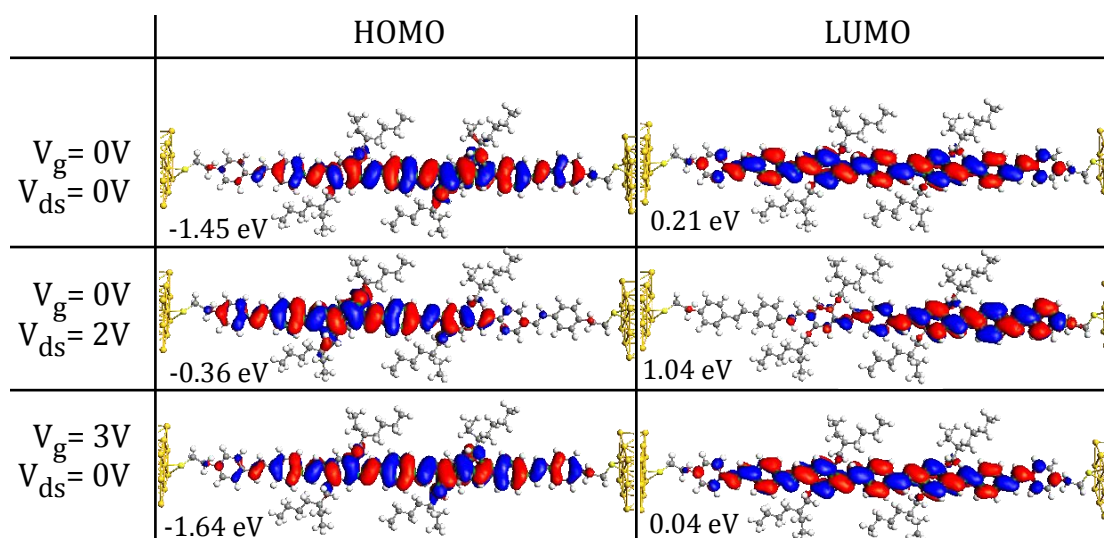
Figure 5.22: An iso-surface plot for the distribution of the HOMO and LUMO of the OPV molecular device under different biases. The energy position of each MO relative to E_f is denoted. A cutoff value of 0.02 is used in the plotting.

studied OPV molecular rectifier. We proposed two different device applications namely; a molecular transistor and a standalone NAND logic gate. Our choice for OPE specifically is because three-leg OPE molecular structures are
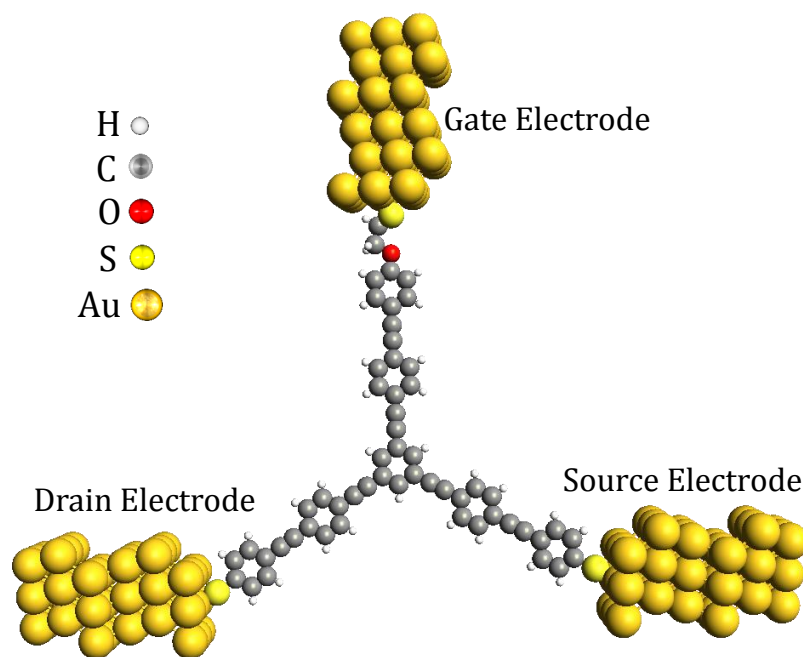
Figure 5.23: The typical structure of three-leg molecular device. The shown molecule is the three-leg molecular transistor (Mol1). Each leg of the molecule is bounded to gold electrodes through thiol-gold bond. A (111) gold with 3×3 atoms/layer is employed.

already synthesized[5], but the final devices setup and characterization are still in progress.

Molecular transistor

We hereby illustrate a study on derivatives of the three-leg molecules that work as molecular transistors. Figure 5.23 shows the proposed molecular transistor structure. We use a leg with an oxygen linker as the gate for the three-leg transistor while using thiol linkers in the other two legs.

On simulating the device, the output current characteristic of the device with two phenyl rings per leg is as illustrated in Figure 5.24. There is a drain current modulation with the gate bias. Since the oxygen linker partially decouples the gate electrode from the molecule, the effect of the gate is almost only electro-

---

[5]This was informed to us in private communication with prof. Marc Tornow at Technische Universität München. The molecules are synthesized by group of prof. Marcel Mayor at Universität Basel.
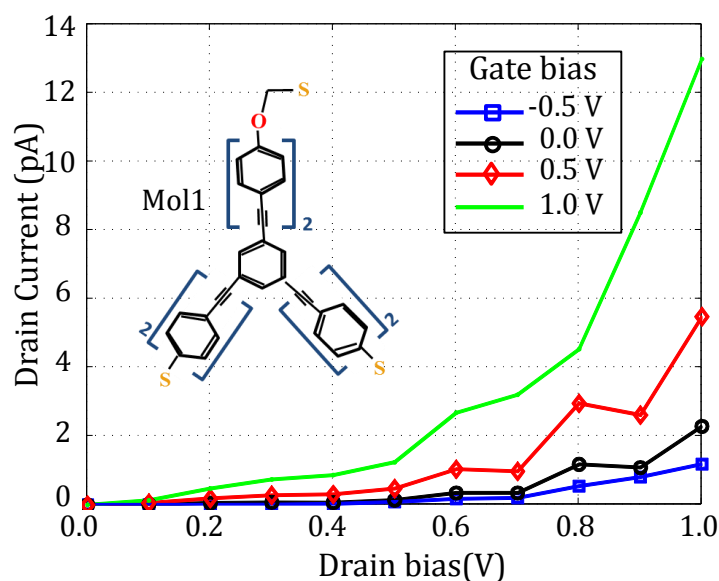
Figure 5.24: The output characteristic curves of Mol1 Device where all legs are meta connected to each other as in the inset.

static. Thus, the gate performance in this three-leg molecular device is similar to the back-gate in the molecular devices discussed in the previous subsections. However, the gate electrode here is in the same plane with the source and drain, which provides a chance for new applications and architectures.

Unfortunately, the values of drain current are relatively low in the order of few pico-Amperes. The main factors that influence the magnitude of current are the length of the molecule and the type of connection of the molecular legs with respect to each other at the central ring. Figure 5.25a shows the IV-curves for simple two terminal dithiol-OPE devices with 3,5 and 7 phenyl rings (all rings are Para connected). Increasing the length of the molecule leads to logarithmic reduction in the magnitude of current. A similar length-conductivity dependency was also observed by other studies in the literature [179,180].

The legs of the molecule can be connected in Ortho, Meta or Para configuration with respect to each other. Figure 5.25b demonstrates the impact of the three different configuration on the magnitude of current, for a simple two terminal dithiol-OPE device. It can be noticed that the Para configuration allows the highest current which is about three orders of magnitude higher than that from the Meta configuration. This is consistent with the results reported in [181]. We suggest that the source and drain legs of the molecule should be Para connected
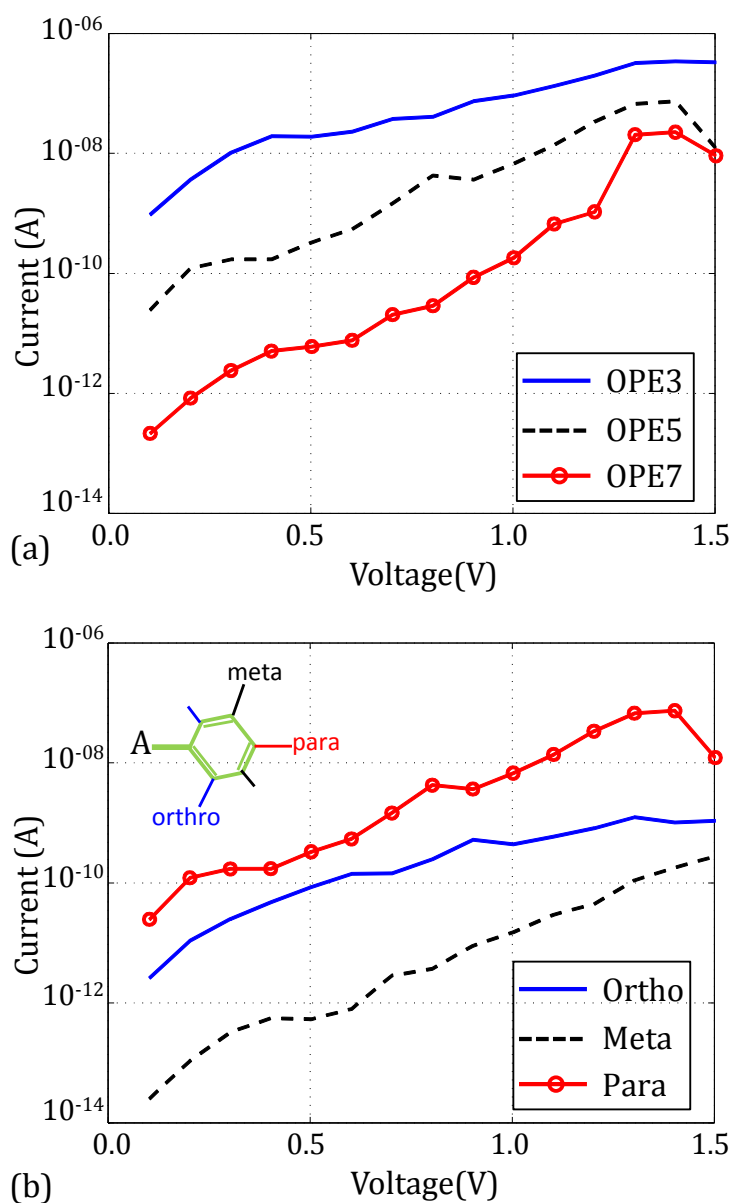
Figure 5.25: The IV curves of two terminal dithiol-OPE devices (a) with different number of phenyl rings and all are para connected. (b) with different connections between the two-legs at the central phenyl ring. The inset in (b) illustrates the different connections with respect to node A in a phenyl ring.

while preserving the gate leg to be in the Ortho and Meta configuration with respect to the source and drain, respectively.

Figure 5.26 shows a new molecular structure of the device (Mol2), and the corresponding output current characteristics. It is obvious that the magnitude
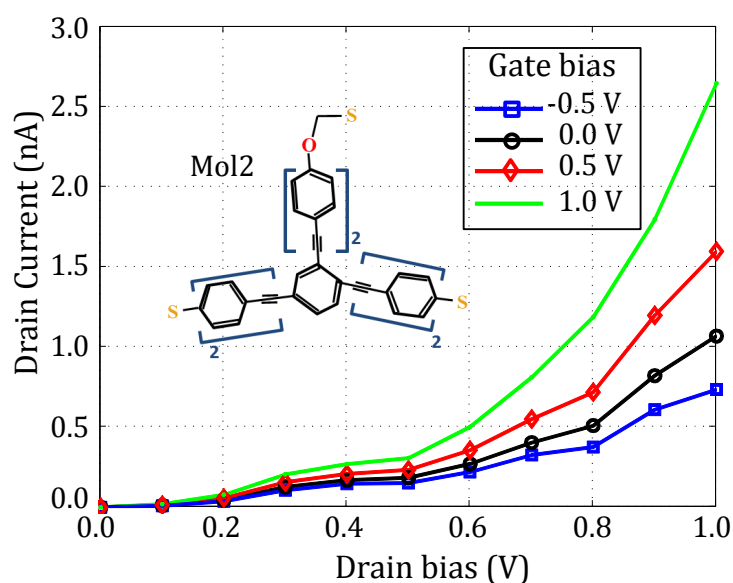
Figure 5.26: The output characteristic curves of Mol2 where the source-drain legs are para connected as in the inset.

of current is enhanced by more than two orders of magnitude with respect to the previous case. Furthermore, the gate bias influence on the drain current modulation is still observable. We also investigate the influence of changing the length of the gate leg (Mol3) and the length of the drain/source legs (Mol4). The output current curves for Mol3 and Mol4 are illustrated in Figure 5.27. For Mol3, changing of the gate length does not affect the magnitude of current, and the correlation between the gate bias and the current does not differ from Mol2. This is due to the fact that the influence of the gate electrode is found mainly on the leg attached to it and a very weak effect on the central phenyl ring. For Mol4, longer drain and source legs leads to a reduction in the values of current by more than one order of magnitude.

For the case of Mol2, Figure 5.28 shows the influence of the gate bias on the drain-source TS at zero drain-source bias. It is obvious that the current is dominated by resonance tunneling through the LUMO which is closer to Fermi-level. The increase in gate bias leads to shifting of the LUMO towards the Fermi-level, in addition, the magnitude of some LUMO peaks increases. Although the gated-leg has direct bond with the gold electrode, the shifting of the TS due to the gate is not very strong. This can be attributed to the decoupling caused by the oxygen linker.
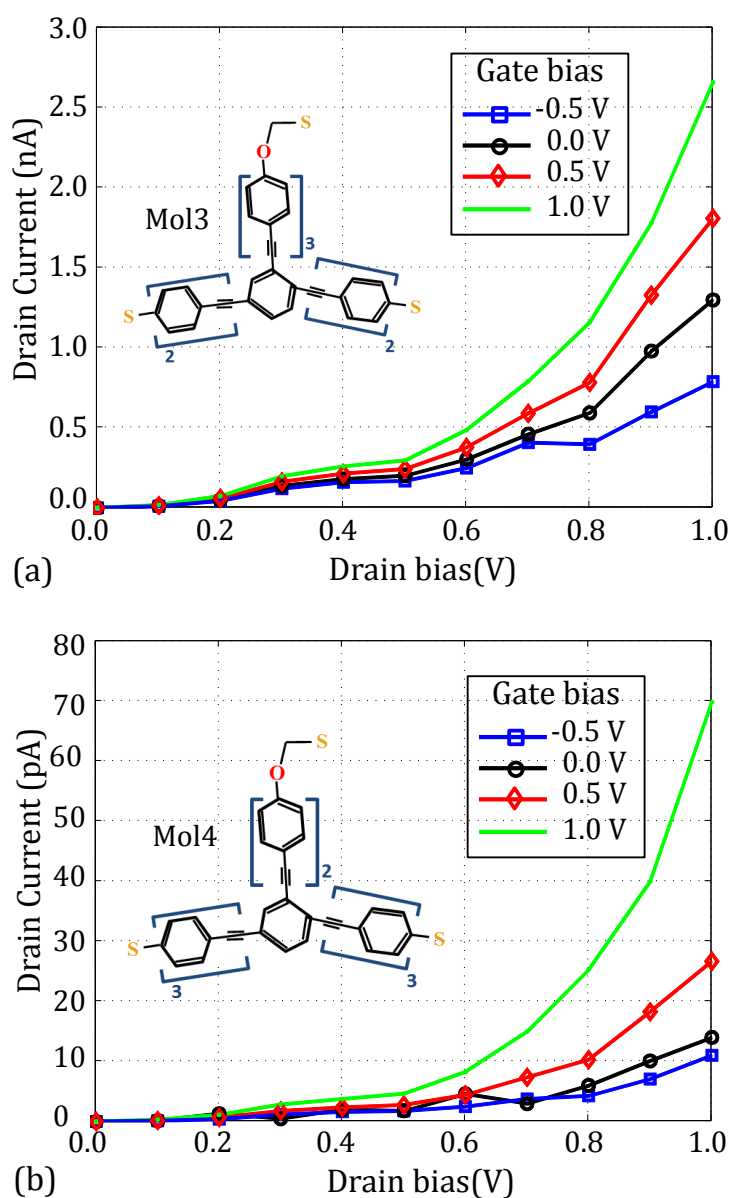
Figure 5.27: The output characteristic curves of a device with (a) Mol3 in which the source and drain legs are 3 rings instead of 2 for Mol2. (b) Mol4 in which the source and drain legs are 3 rings instead of 2 for Mol2.

Figure 5.29a shows the electrostatic potential profile of the device under gate bias 1 V and zero drain-source bias. The effect of the gate bias vanishes before the central phenyl ring, and this leads to the weak modulation of the source-drain TS. Figure 5.29b shows the potential drop profile of the device at drain source bias 1 V and zero gate bias. Unlike for the gate bias, the drain bias has a stronger
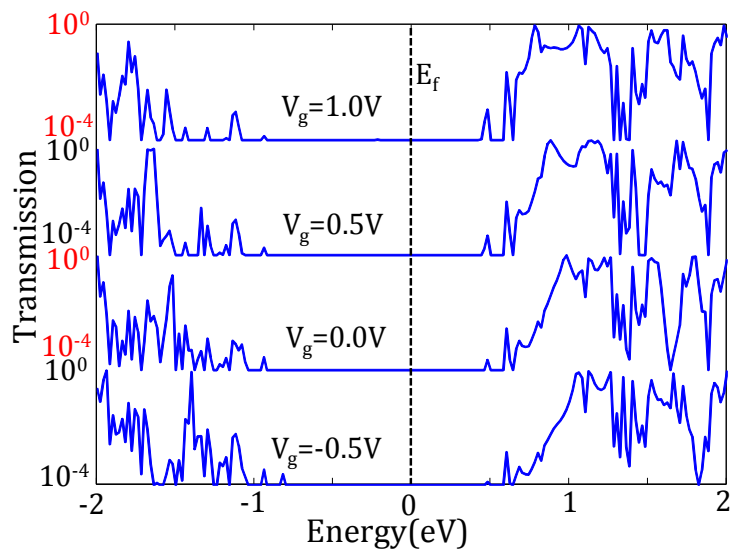
Figure 5.28: The TS of Mol2 at zero drain-source bias and different gate bias.
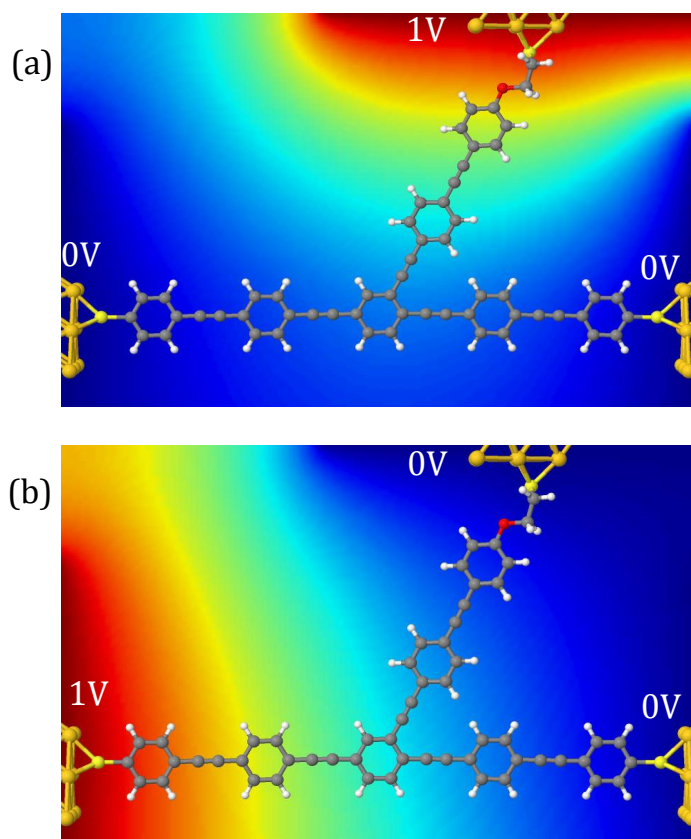
Figure 5.29: The potential profile distribution of Mol2 device (a) under gate bias 1 V and zero drain-source bias. (b) at drain-source bias 1 V and zero gate bias.
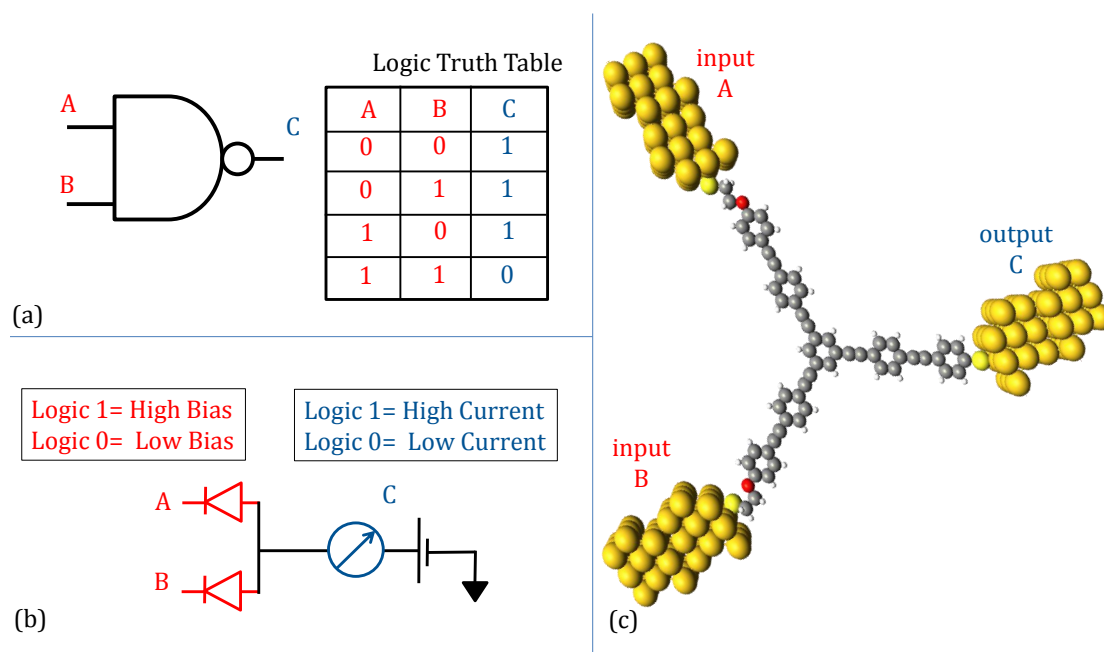
Figure 5.30: (a)The symbol of NAND logic gate and the corresponding logic truth table. (b) Implementation of standalone NAND logic gate using diodes and the interpretation of the input/output signals. (c) The proposed structure of the three-leg molecular NAND Logic gate device.

influence on the potential profile at the source-leg. This is mainly due to the absence of the oxygen linker, in comparison to the gate leg.

Standalone NAND logic gate

In this subsection, we elaborate the feasibility of a standalone NAND logic gate using a single three-leg molecular device. Figure 5.30a shows the symbol and the logic truth table of a conventional NAND logic gate. A standalone NAND logic gate can be implemented using diodes as shown in Figure 5.30b. In this implementation, we interpret the input logic as follows: a high voltage (1.3 V) for a logic '1' and a low voltage (0 V) for a logic '0'. On the other hand, we interpret the output logic as follows: a high current for a logic '1' and a low current for a logic '0'.

Figure 5.30c illustrates the employed structure of the three-leg molecular device equivalent to the NAND logic gate with diode implementation. Figure 5.31 shows the reading of the current flowing through the output leg of the molecule
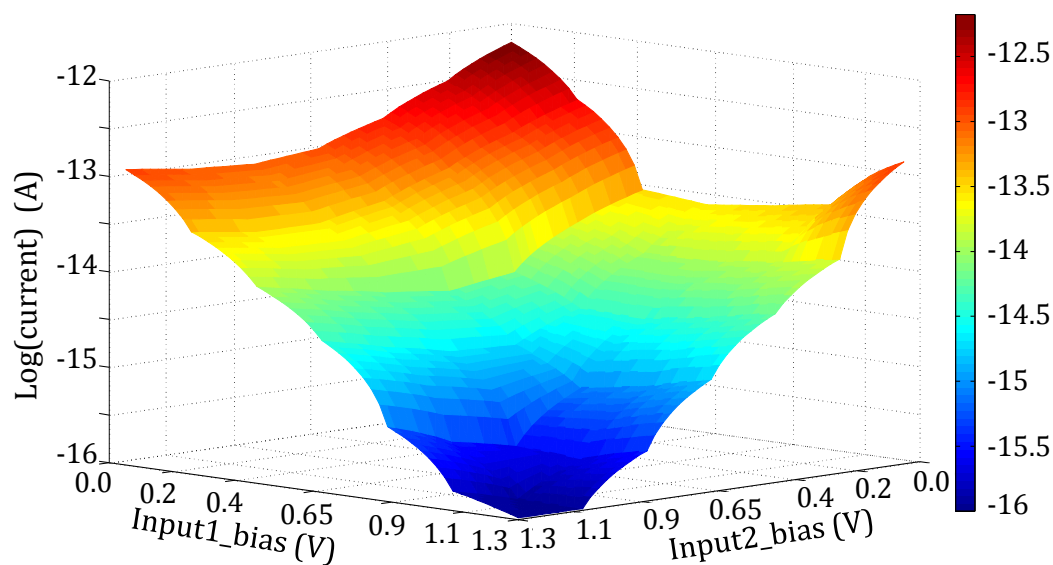
Figure 5.31: The output current reading from the standalone molecular NAND logic gate for different combinations of input biases. The reading terminal 'C' is connected to 1.3 V voltage bias.

at different biases combinations applied to the input legs of the molecule. The results show correct functionality of the molecule. Moreover, for input bias variation up to 0.2 V, one can still distinguish the output logic where $I_{high}/I_{low} > 200$. It is worth noting that the current flow from one input to the other is about four orders of magnitude lower than the output current (I_{high}).

A standalone OR may be realized with the same molecular structure just by changing the input convention to be -1.3 V for logic '1', and 0 V for logic '0' while connecting the output reading-leg to bias voltage of 0 V. A standalone OR (or NAND) logic gate can also be achieved with a three-leg molecule without oxygen linkers. Employing the logarithmic reduction of current with length of the molecule, we can let the two input legs of the molecule relatively long while having a short output leg connected to ground. The current due to an applied bias to any of the input legs will have only a single path which is through the output leg of the molecule. Thus, high current is read from the output leg if any of the input biases is high, and low current is read only if both input biases are low.

5.4 Conclusion

Molecular transistors are key components for functional electronic systems. In this chapter we studied different molecular transistor using conjugated OPV and OPE molecules. An electrostatically gated OPV device with oxygen linker was realized in [139,165]. Our simulation on the same device reproduces qualitatively the measurement current curves, and illustrates the factors behind the nonlinear current behavior and gate-conductance dependency. Moreover, we studied another gated OPV device without oxygen linkers that shows a NDR at particular drain bias interval in addition to an interesting gate-conductance dependency. The remarkable characteristics of the two gated OPV devices promote them as good candidate components for building large-scale molecular circuits and systems.

Not only did we investigate the use of an electrostatic gate electrode, but also a direct coupled gate which is feasible in three leg molecular devices. We utilized the rectification performance of the asymmetric OPV rectifier to build three-leg molecular devices with various functionalities. We showed that we could build up a functional molecular transistor as well as stand-alone logic gates. Three-leg OPE molecules are already synthesized, but the specification of anchor linker groups in each leg still needs investigation. Also the realization of atomic size electrodes that can hold the three leg molecules is still in process.

6 Towards Circuit Modeling of Molecular Devices

6.1 Introduction

Modeling and simulation tools play a crucial role in the rapid development of semiconductor technologies as they reduce the required prototype cycles and costs. Molecular electronic is one of the promising technologies currently gaining a lot of interest in the research community. Theoretical studies in the field of molecular electronics have been concerned with the understanding and explanation of the physics behind the quantum phenomena observed at this very small scale.

Despite of the existence of outstanding publications for modeling molecular devices [8, 149, 150, 182], none of them targets the circuit modeling of molecules. One of the far goals of device modeling is to provide the essential inputs for circuit models. The main advantage of developing concrete circuit models for molecules is that it facilitates the prediction of the behavior of logic and memory systems with sets of molecules rather than single-molecule systems. Previous successful attempts were made to provide a circuit analogy for the first-principle calculations which are applied on the study of molecular devices [183]. Nevertheless, such model only provides analytic expressions for the circuit equations and do not attempt any circuit simulation. A circuit model for bistable molecular crossbars was provided in [18].

In this chapter, we take a direct step toward providing a circuit model for molecular devices. The proposed model in this study as well as other physical modeling in literature [8, 150, 182] help in fast assessment for the characteristics of the molecular device. However, unlike other models, our model allows us to predict the behavior of a system with different molecular devices connected

together in a form of circuit. The chapter is organized as follows: we first explain the theory behind the proposed model. After that, we show how the proposed modeling is applied and shed some light on the employed atomistic simulation that we used to further verify our models. Finally, we show the results of our circuit model on four molecular devices and validate these results vs. available experimental and/or atomistic simulation results.

6.2 Proposed Model

Shared electrons in a covalent bond are known to be attracted to atoms with the highest electronegativity. As an example, the charge distribution in H_2O molecule displays a negative charge accumulation on O and a positive charge accumulation on H since O has a higher electronegativity than H. Moreover, as known from electromagnetic, a positive electrostatic potential acts on attracting negative charges.

Assuming that an atom gained a positive electrostatic potential, the neighboring atom will not be affected unless the potential is high enough to change the electron sharing distribution between the two atoms. In other words, such potential (V_a) should exceed a given threshold value (V_{th}). This threshold depends on the polarity of the bond; an atom with strong electronegativity (high ionization potential) would have a high V_{th}. Moreover, V_{th} depends on the type of bond between the atoms. Electrons in a pi-bond are loosely attracted to both atoms, which implies a low V_{th} compared to sigma-bond electrons. Generally, the degree of variation in the electron sharing distribution between neighboring atoms depends on the magnitude of ($V_a - V_{th}$).

When a given atom gains positive charges due to losing electrons, this translates via solving the Poisson equations to an increase in its potential. Under equilibrium condition (no current is flowing), such potential is exactly $V_a - V_{th}$. In case of a chain of atoms this process repeats till the potential difference between neighboring atoms is less or equal to V_{th}. If this chain is contacted with electrodes, and the applied bias is greater than the sum of all thresholds, then current flows. Note that, the previous discussion holds not only for single atoms but also for molecules.
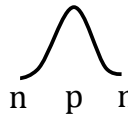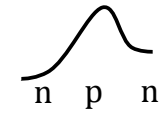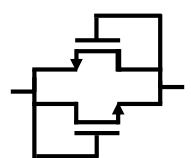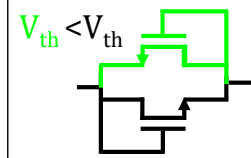
Atoms in neutral state	C $\underline{\quad}$ $\underline{\color{red}O}$ C $\underline{\quad}$	C $\underline{\quad}$ $\underline{\color{green}N}$ C $\underline{\quad}$
Charge redistribution after bonding	C—O—C	C=N—C
Potential energy profile	n p n	n p n
Equivalent transistor model		$V_{th} < V_{th}$

Figure 6.1: A simple scheme to illustrate the choice of NFET in modeling the atoms or molecules.

When an electrostatic potential bias is applied to a metallic electrode (e.g. a gate) which is separated by an insulating dielectric from an atom/molecule, only part of this electrostatic potential would affect the atom/molecule (weak coupling). This is also the case if a molecule is only weakly bounded to its neighbors, for instance via a linker such as an Alkyl chain, which acts like an insulator [8, 115]. The coupling is then reduced, and the potential of one molecule slightly affects the next molecule.

It is suggested that atoms/molecules behaving as described above can be modeled as an n-type field effect transistor (NFET). A positive gate bias of the molecular NFET represents the tendency to attract electrons. Such gate potential is directly affected by the potential of its neighboring atoms and the coupling between them. To account for both neighboring atoms in a chain, two parallel NFET are used.

Figure 6.1 illustrates the reason behind choosing NFET transistor and employing two transistors. As can be noticed the charge redistribution due to the polar covalent bond creates regions similar to the macroscopic NPN junction. Since the control mechanism at the atomic level is electrostatic, a FET transistor is employed rather than a bipolar one. An atom is directly influenced by its neighbor atom; thus a gate terminal controlling the modeling transistor is directly
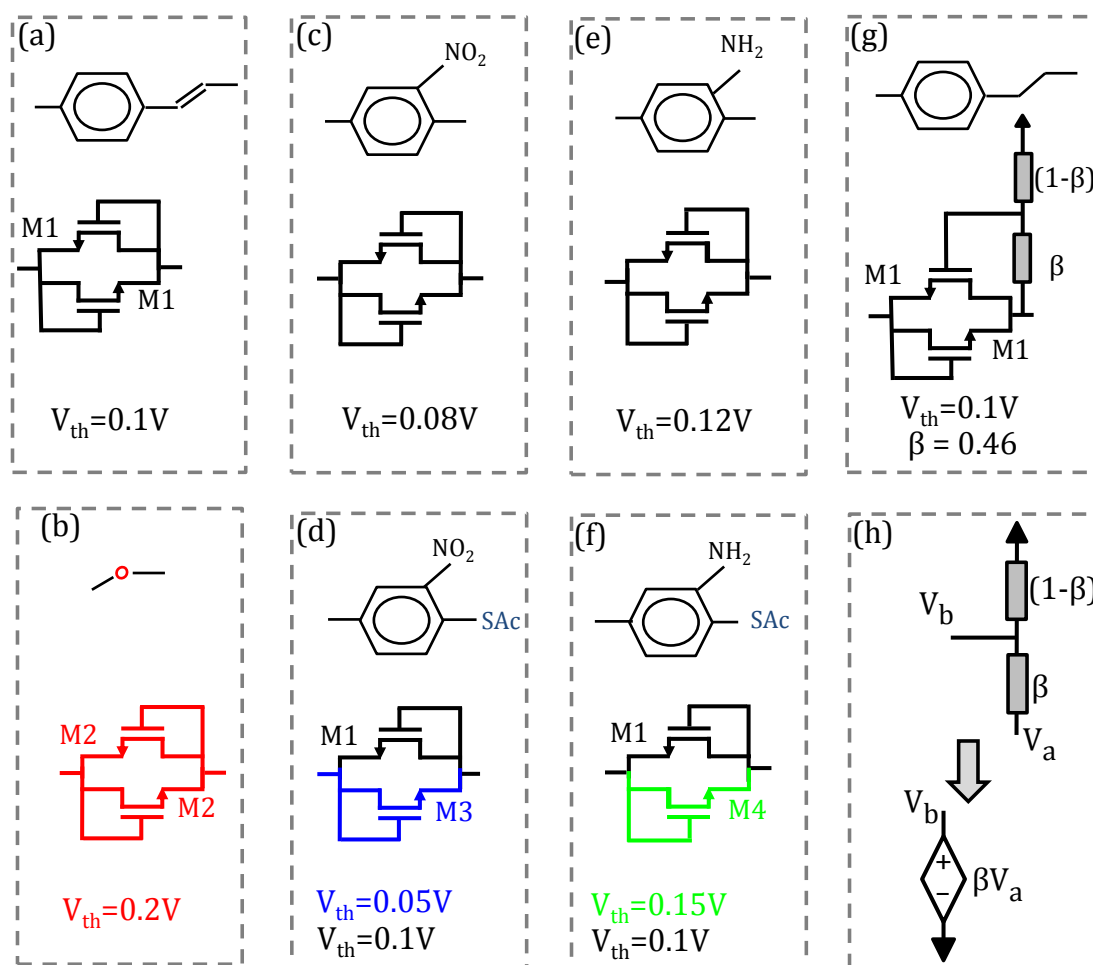
Figure 6.2: Circuit models for the various molecules which are employed as building blocks to study the different molecular devices. NO2 and NH2 are examples of acceptor and donor dopants, respectively. SAc refers to thioacetate which is known to create a good bonding to the contact electrodes (e.g. a thiol-gold bonding).

connected to transistor's side (drain) terminal. To account for two neighboring atoms in a chain, two transistors (not always identical) are employed.

Figure 6.2 illustrates the circuit model for the various molecules which are used in this chapter as building blocks to study the different molecular devices. For a chain of a simple phenyl ring with the ethylene chain connected to it (Figure 6.2a), charges transfer smoothly due to the presence of delocalized pi-bond between neighboring carbon atoms. Thus, a transistor with small threshold value (M1, $V_{th} = 0.1$ V) can model such molecule. This value is chosen based on experimental and first-principles studies which indicate that a di-thiol benzene

molecular junction start conducting at small applied bias (≈ 0.1 V) [184, 185]. An atom like Oxygen, which is characterized by high electronegativity (besides the presence of only sigma bonds with the neighboring atoms/molecules in a chain) is modeled with a higher threshold value (M2, $V_{th} = 0.2$V), see Figure 6.2b.

When a phenyl ring is doped by an acceptor (high electronegative), the acceptor acts on attracting electrons which is equivalent to applying a positive gate bias. This positive offset in the gate bias can be translated to a reduction in the threshold value ($V_{th} = 0.08$ V), see Figure 6.2c. In fact, if this acceptor-doped phenyl ring is near one contact electrode, the attracted electron will come mostly from the electrode since it has a plenty of weakly bounded ones. Thus, the reduction in the threshold is only in the corresponding transistor direction (M3, $V_{th} = 0.05$ V), see Figure 6.2d. Similarly for a phenyl ring doped by a donor (low electronegative), the same argument suggests an increase in the threshold value, see Figure 6.2e,f. It is worth nothing that the type of dopants and the number of dopants molecules also affects the threshold values of the transistors.

Another important molecule component in molecular devices is the insulating alkane chain (e.g. dimethyl chain connected to a phenyl ring in Figure 6.2g). Alkane chains are characterized by their insulating behavior since only saturated sigma bonds exist between the carbon atoms resulting in a very low current at small applied bias [115]. This translates to a weak coupling between molecules interconnected by such insulating chain. This is modeled by a voltage divider since only a part of the bias (coupling coefficient $\beta = 0.46$) is transferred to the interconnected molecule. It is worth mentioning that insulating chains usually start conducting at high bias especially for short chains (strong electric field); this is simply handled by increasing the coupling coefficient at high applied bias. For instance, we can assume $\beta = 0.8$ when the bias exceeds 1.5 V.

In Figure 6.2h, we illustrate how a voltage divider sub-circuit can be substituted by voltage-dependent voltage source, in order to simplify the circuit. For a direct connection, we can use a voltage dependent voltage source of exact equal value of the voltage ($V_b = V_a$). The logic behind this shorthand simplification is to facilitate the addition of any external electrostatic effect like in case of external gate.

Circuit simulations in this study are made using LTSpice with level 1 FET-models[1] [186]. It is worth noting that the chosen values for threshold voltages are found to give the best fitting results for the molecule-modeled circuits developed in this study. We also used an atomistic simulation, in order to have a deeper understanding of the quantum transport behavior in the molecular devices. This understanding could help in verifying/disproving our proposed modeling theory. The atomistic simulation is based on a non-equilibrium Green's function (NEGF) formalism coupled to extended Hückel theory (EHT) by ATK [60, 61]. Detailed information about the methodology used in the atomistic simulation was presented in the previous chapters.

6.3 Results and Analysis

In this section, we will illustrate the results of applying our modeling methodology on four different devices with two-terminal molecules. We target such simple structure molecular devices, in order that the methodology can be verified and understood in an easy way. Modeling results are verified by comparing to atomistic simulation and real measurement of the same devices. The first and last subsections deal with oligo-phenylenevinylene (OPV) molecule derivatives which was synthesized in Ref [165]. After that, we will model a molecular device with no covalent linker to one electrode [72]. Finally, we will model a sample molecule from the well-known donor-sigma-acceptor (D-σ-A) family of molecular rectifiers [4].

6.3.1 Modeling of an Asymmetric OPV Molecular Rectifier

In this subsection, an asymmetric OPV molecular device is investigated. The molecule has an oxygen linker on one terminal and a simple thiol linker on the other terminal. Figure 6.3 shows the OPV molecular device and the corresponding circuit model.

---

[1]The employed model is NMOS with typical parameters value ($Kp = 5 \times 10^{-7}, Vth = V_{th}, lambda = 0, gamma = 0.586$), where V_{th} value depends on the corresponding modeled molecule in Figure 6.2. The bulk node for all transistors is connected to the lowest voltage node in the circuit.
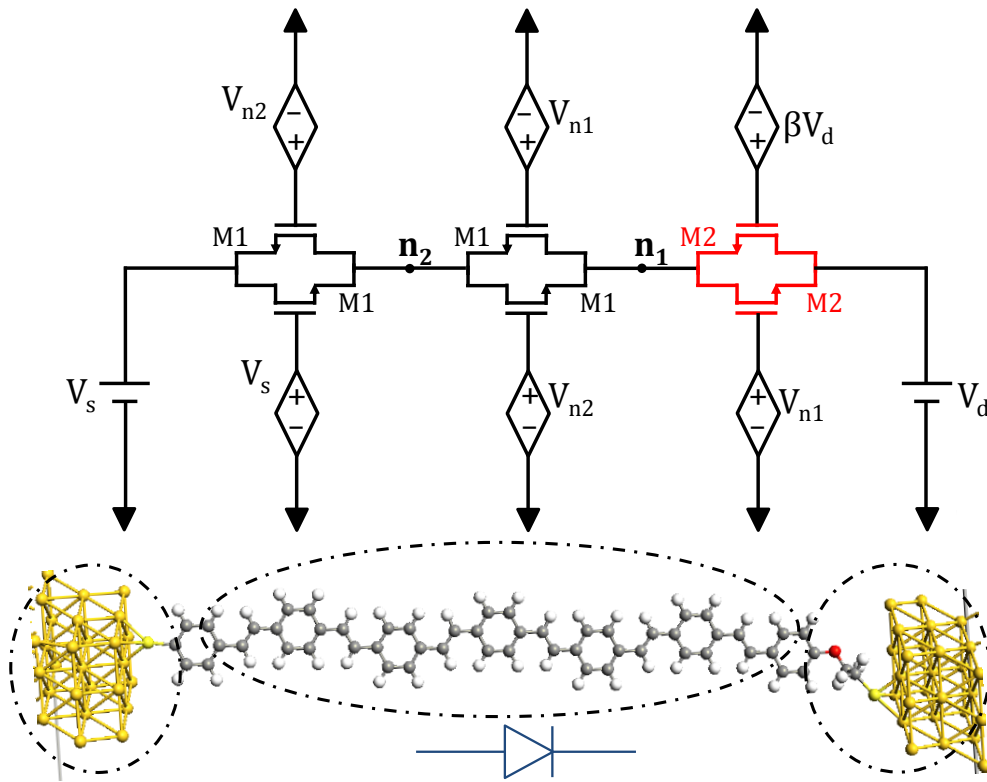
Figure 6.3: The proposed model for an asymmetric OPV molecular device with an oxygen linker on the right terminal. A complete coupling between thiol and gold is assumed since there is no insulators in-between.

According to the circuit model: at reverse bias, when the positive voltage is applied to the electrode connected to the oxygen linker, the condition for current flow is:

$$V_{ds} > \frac{V_{th,O}}{\beta} + 2\ V_{th}, \tag{6.3.1}$$

at forward bias, when the positive voltage is applied to the electrode connected to the simple thiol linker, the condition for current flow is:

$$V_{sd} > V_{th,O} + 2\ V_{th} \tag{6.3.2}$$

Since $\beta = 0.46$ and $V_{th,O} > V_{th}$, an asymmetric current voltage curve is expected in which the device switched-on at higher bias voltage during the reverse bias compared to the forward bias (Figure 6.4).

An atomistic simulation for the asymmetric OPV molecular device is performed to allow the verification of the circuit model results [20]. Figure 6.4 shows that the I-V characteristic curve of the device using the atomistic simulation nicely matches the results of the modeled circuit. A clear rectification behavior can
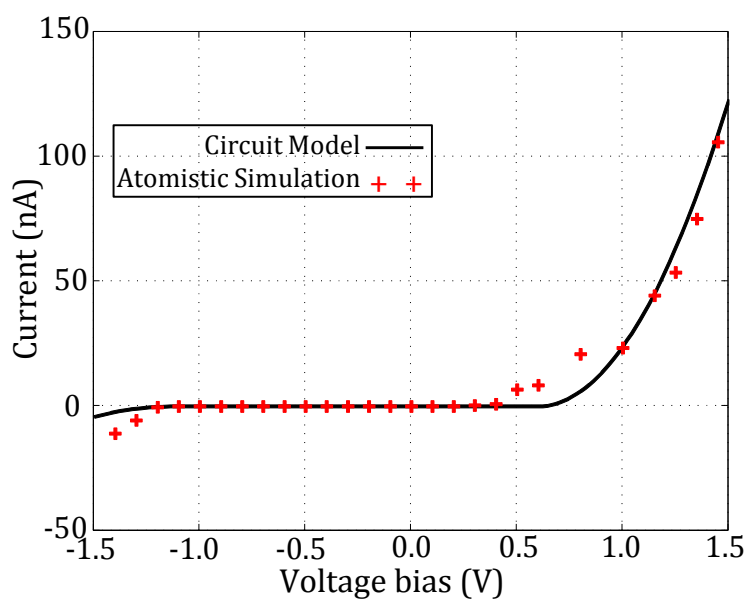
Figure 6.4: The SPICE simulated I-V curve of the circuit model of the asymmetric OPV device (solid line) and the atomistic simulated data points (plus symbols) of the same device.
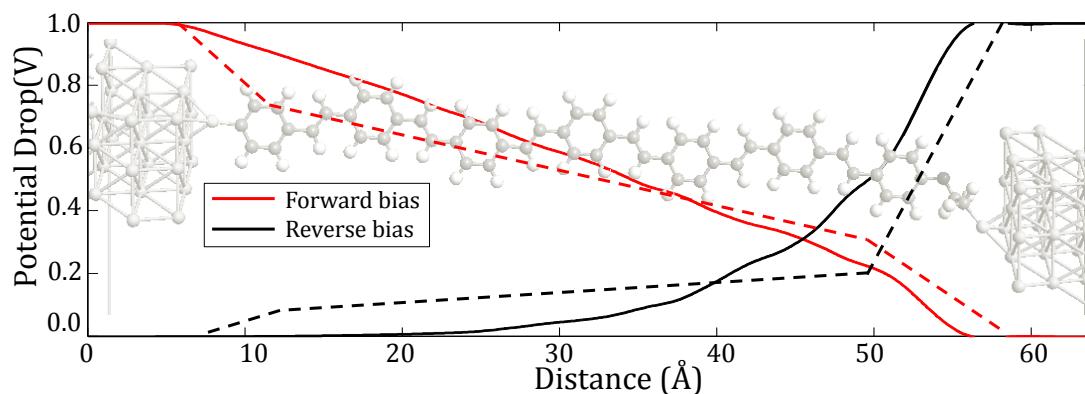
Figure 6.5: The electrostatic potential drop along the asymmetric OPV molecule for an applied voltage 1 V to the right electrode (reverse bias), and an applied voltage 1 V to the left electrode (forward bias). Solid lines are using the atomistic simulation. Dashed lines are for the circuit model simulation.

be noted in both curves. Shoulders showing up in atomistic simulations are sometime an artifact due to convergence to local minima.

Based on the circuit model, one can conclude that the oxygen linker region plays the main role in the potential drop profile along the device under bias. The corresponding transistor with high threshold voltage is indeed the most

difficult to be switched-on. Thus, almost the whole potential drops over the oxygen-modeled transistor at reverse bias. At forward bias, the potential drop is divided more equally between each segment of the device. All transistors are switched-on, and the potential drop over each of them is far greater than the threshold value.

Figure 6.5 illustrates the potential drop profile along the device at forward/reverse biases employing the atomistic simulation (solid lines) and the circuit model (dashed lines). For the circuit model, the uniform potential drop along each molecule's section equals to the potential drop between the source/drain of the corresponding transistor subcircuit. The potential profiles are in good agreement with our expectation from the circuit model. At reverse bias, almost the whole potential drop is around the oxygen linker. At forward bias, the potential smoothly drops along the molecule with a bit steeper drop near the oxygen linker.

6.3.2 Modeling of Molecular Device with no Covalent Linker to One Electrode

We further verify the validity of the proposed circuit modeling method by comparison with a molecular device reported in the literature. Kushmerick et al. proposed a molecular rectifier employing an Oligo-Phenylene-ethynylene (OPE) molecule with a thiol-gold on one terminal and no bond to gold on the other terminal (Figure 6.6) [72]. This molecular structure with asymmetric terminals leads to a rectification such that the thiol terminal acts as the anode.

Since atoms in this structure (Carbon and Sulfur) possess nearly equal electronegativity, transistors with equal $V_{th} = 0.1\,\text{V}$ are used for the circuit modeling of each part of the device. The unbounded terminal of the device imposes the special behavior of the device. The unbounded terminal is modeled by weak coupling coefficient (β_2) to the molecule. Thus, similar to the OPV rectifier discussed in the previous subsection, a rectification occurs since a low current flow when the positive voltage is applied at the unbounded terminal of the molecule. The current voltage characteristics from the circuit model simulation matches the experimental measurement of this OPE device (Figure 6.7).
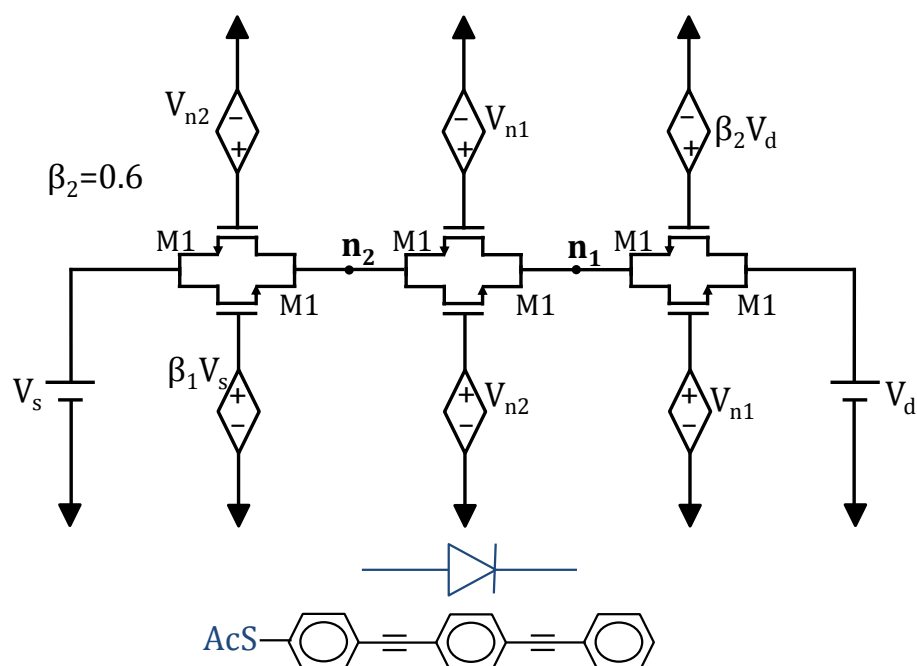
Figure 6.6: An asymmetric OPE molecule with a thiol-gold on one terminal and no bond to gold on the other terminal. The unbonded terminal would result in a weak coupling (β_2) between the electrode and the molecule. $\beta_2 = 0.6$ found to provide best fitting of the model to the measurement data.

6.3.3 Modeling of a Donor-sigma-Acceptor Rectifier

D-σ-A molecular rectifiers are one of the first proposed molecular rectifiers [4, 151]. In general, a (D-σ-A) molecule is composed of two electroactive regions, acceptor (A) and donor (D). The two regions are linked by a σ-type covalent bond which introduces a potential barrier and acts therefore as an insulator. In this subsection, we show a possible circuit modeling of such type of rectifiers. We take as an example the D-σ-A molecular device [23,118]. The device is shown in Figure 6.8 together with the corresponding circuit model.

Figure 6.9 illustrates the circuit simulated I-V curve of the model. The asymmetric behavior in the IV curve is clear; the current is favorable when the positive electrode is next to the donor region. Based on the assumed model, the donor is responsible for the reduction in current at reverse bias while the acceptor is responsible for the enhancement of current at forward bias. These findings are
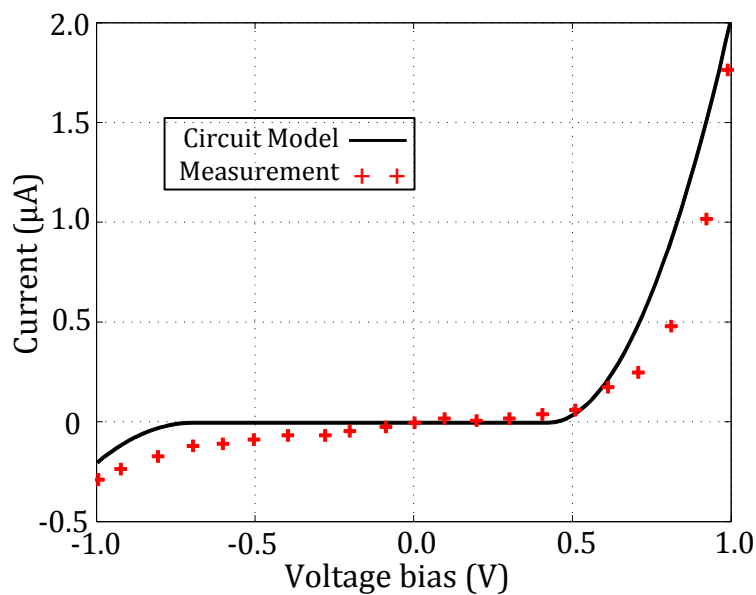
Figure 6.7: The SPICE simulated I-V curve of the circuit model of the OPE device with no covalent linker to one electrode (solid lines) and the measurement data points (plus symbols) adopted from [72].
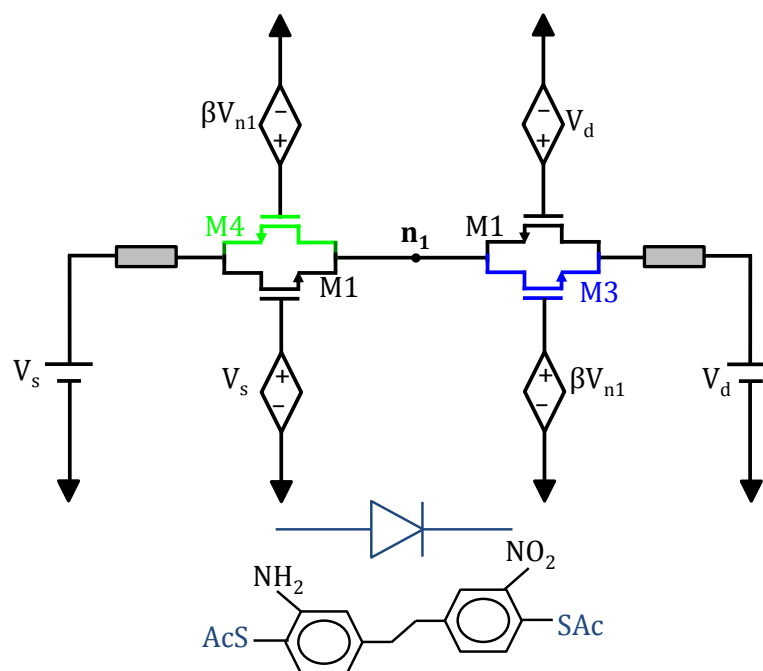
Figure 6.8: The structure of an D-σ-A molecule. The insulating σ bridge leads to a weak coupling for the transistor in both directions.

in agreement with the conclusion in Ref [23], which examines the influence of dopants on the D-σ-A molecules' charge transport.
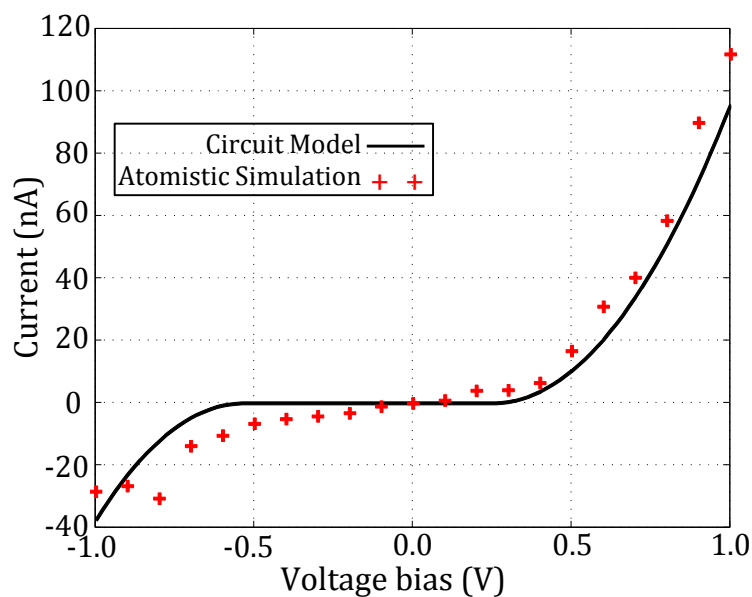
Figure 6.9: The SPICE simulated I-V curve of the circuit model of the D-σ-A molecular device (solid line) and the atomistic simulated data points (plus symbols).

6.3.4 Modeling of a Gated OPV Molecular Device

Figure 6.10 shows a gated OPV molecule, which was synthesized and measured in Ref [139, 165], and the corresponding circuit model. The electrostatic coupling of the gate to the molecule is introduced in the circuit model via the coupling parameter α. We assume equal weak gate coupling for all transistors, $\alpha = 0.08$ to allow the best fitting of the modeled curves to the measurement. This value is reasonable since there exists a 100 nm oxide layer separating the gate from the molecules (for the methyl linker 3 nm long the coupling is 0.46).

Figure 6.11 shows the output I-V curves from the circuit simulation of the modeled molecular device. The curves show a perfect agreement with the device measurement data [139]. For a further verification of the modeled circuit, an atomistic simulation of the molecular device was performed as discussed earlier in Chapter 5. The inset of Figure 6.11 illustrates the output I-V curves from the atomistic simulation. The results show a qualitative agreement with the measurement; the drain-source switching threshold is reduced with the gate bias increase.
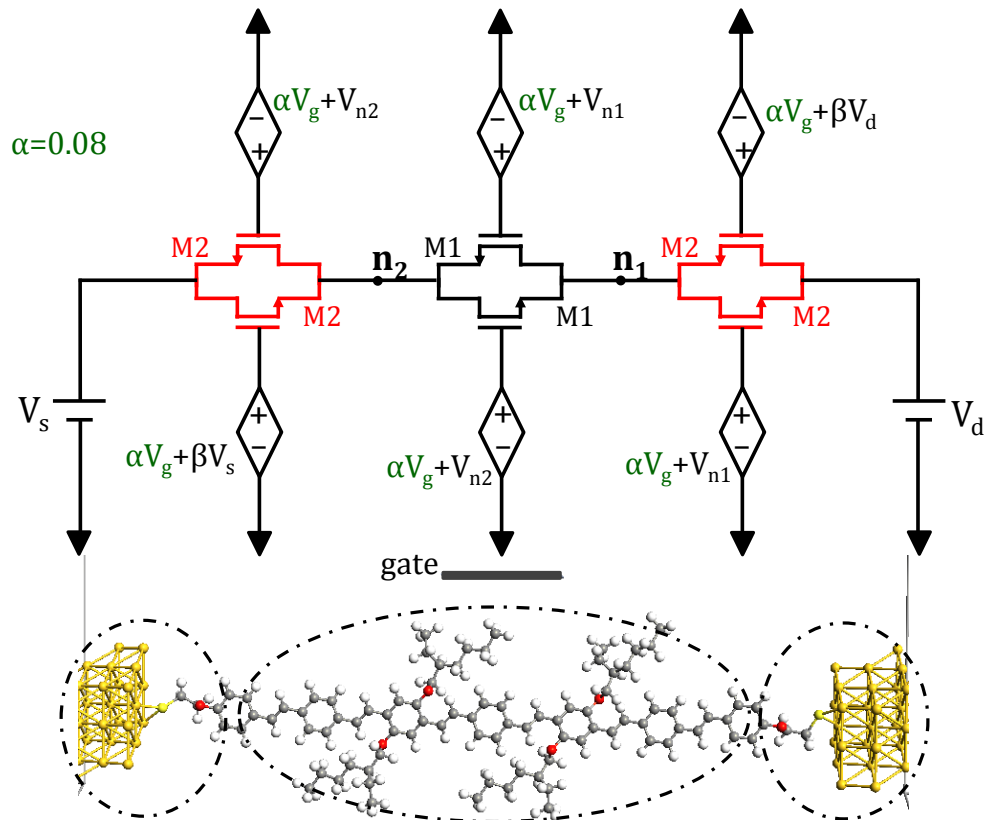
Figure 6.10: The proposed circuit model for the OPV molecule with the oxygen linker groups on both terminals.

The circuit model allows us to reach a quantitative agreement with measurements, also concerning the magnitude of current since we can adjust the width of the transistor. This corresponds to the experimental fact that an unknown number of molecules conduct at the same time [139].

One important feature that can be investigated in both circuit model and atomistic simulation is the potential drop profile along each section of the molecular device. Figure 6.12 demonstrates the potential drop profile at zero gate bias using a drain source bias of 1 V and 2 V, which correspond to bias values less and greater than threshold bias value, respectively.

Interestingly, both the circuit simulation and atomistic simulation shows that the potential drop along the molecule is mostly near the positive (right) electrode, before and after threshold. This behavior can be explained from the circuit model with the high threshold voltage and the weak coupling of the transistor linked to the positive (right) electrode. It is worth noting that the left side transistor,

117
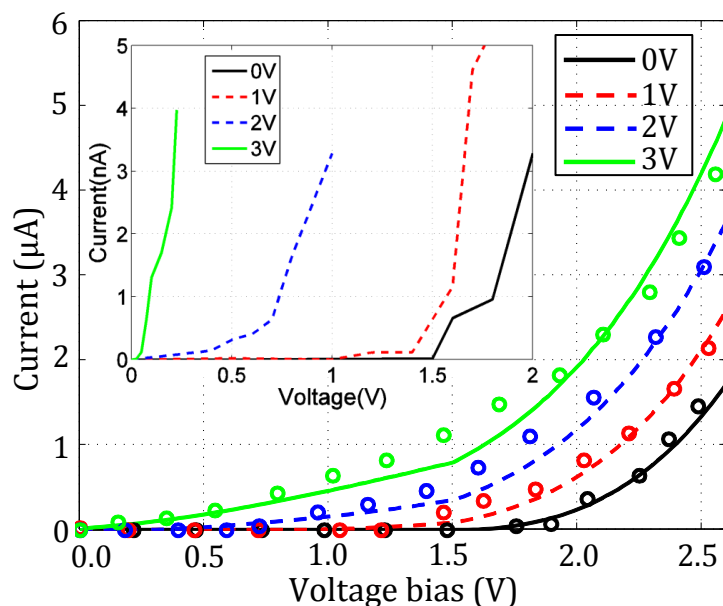
Figure 6.11: (a)The SPICE simulated I-V curves of the circuit model for the OPV device (solid lines) and the measurement data points (small circles) adopted from [139]. The inset is the atomistic simulated I-V curve of the OPV device.
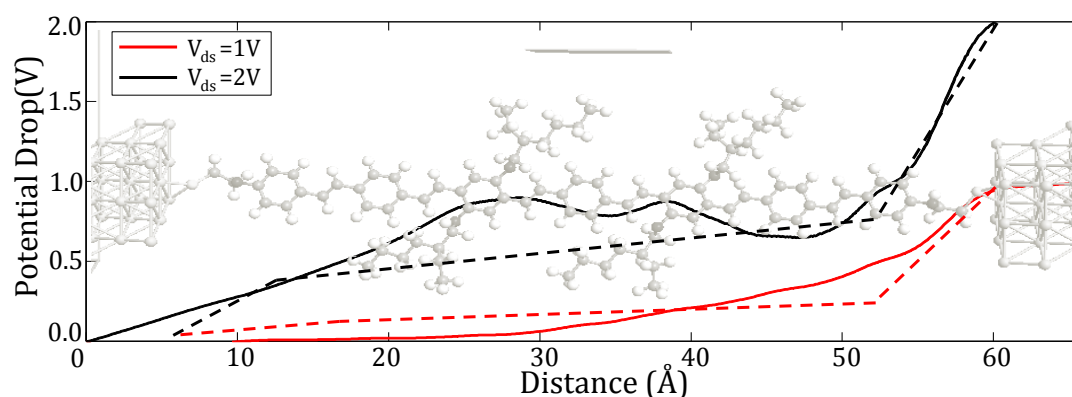
Figure 6.12: The electrostatic potential drop through the molecule at zero gate bias and $V_{ds} = 1$V, and 2V. Solid lines are using the atomistic simulation. Dashed lines are by simulating the circuit model.

modeling the oxygen linker to the negative electrode, is not weakly coupled for this bias direction.

The molecule is further investigated for positive/negative gate biases employing the atomistic simulation tool. Figure 6.13 show the results in which the positive gate bias results in more charge accumulation than the negative gate bias. Similar to macroscopic devices, the charges are coming from the semi-

infinite gold electrodes contacted to the molecule. The proposed model does not consider negative potential, thus the highest negative value would be the zero reference for the circuit. Since the coupling between molecule and oxygen differs from the coupling between the electrode and oxygen, the amount accumulated charges would depend on the direction of charge flow. In other terms, the oxygen-equivalent transistor would play the key role in the charge flow to/from the gold electrode. The device is symmetric, so we focus only on the right oxygen-equivalent transistor, and the left one would act exactly the same. The insets in Figure 6.13 demonstrate the equivalent biasing state of the oxygen equivalent transistors at positive and negative gate biases. The condition for oxygen transistor to be switched on under positive gate bias is

$$\alpha \, V_g > V_{th,O} \tag{6.3.3}$$

On the other hand, the condition under negative gate bias is

$$\beta \, \alpha \, V_g > V_{th,O} \tag{6.3.4}$$

Consequently, the positive gate bias would allow higher switching compared the negative gate bias. Thus, our circuit model implies similar behavior to that found by the atomistic simulation, under positive/negative gate biases.

6.3.5 Model Validity

Other molecules, built up from the different sub-molecules discussed in Figure 6.2, can be modeled by the proposed circuit model [8, 126, 182]. The main advantage of the model is to allow simulation of several devices connected together as found in realistic circuits and systems. However, it is worth noticing that intermolecular coupling as in quantum cellular automata is neglected in the present approach [187].

Further improvement for the proposed model can be explored. For instance, direct contact-to-contact tunneling may be modeled by an adequate value resistor connected between the source/drain voltage suppliers. One challenge that should also be addressed is that it is known that ionization energy increases with its rank (i.e. 2nd ionization energy $> 1^{st}$ ionization energy) [188]. This implies that modeling transistors should not have a constant V_{th}, because it
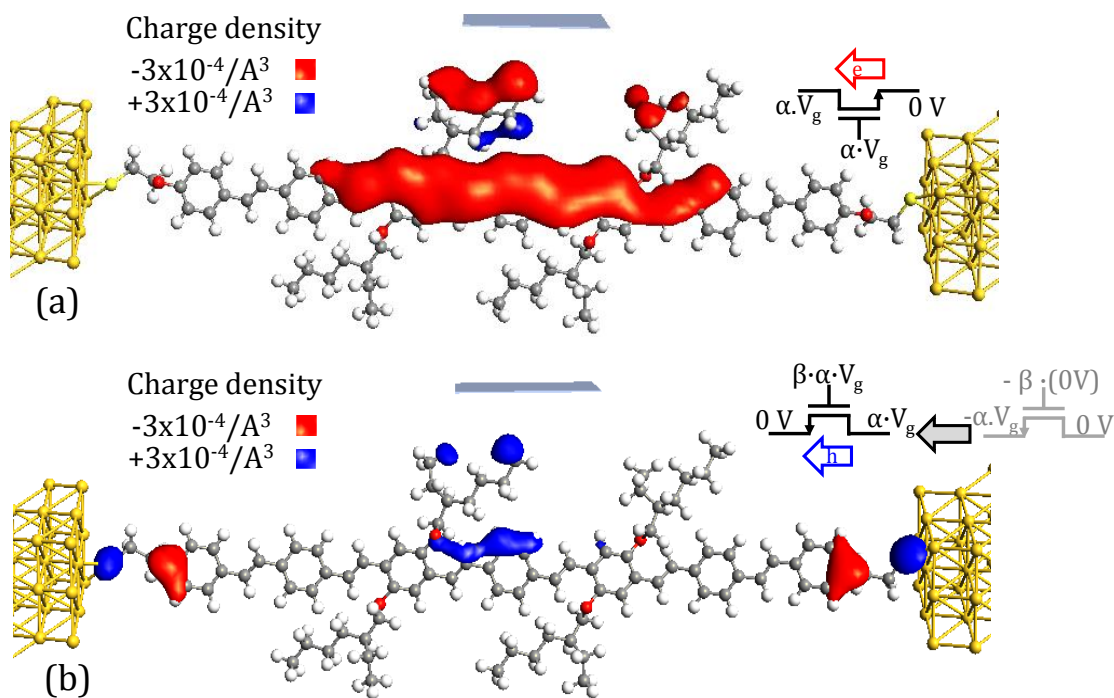
Figure 6.13: The charge density difference through the molecule at zero drain-source bias and different gate biases. (a)$V_g = 2V$, (b)$V_g = -2V$. The charge accumulation at $V_g = 2V$ is more than that at $V_g = -2V$, although the absolute potential differences between the molecule and the electrodes are the same. The bias configuration of the oxygen-modeled transistor is shown in the insets of each sub-figure.

should notably increase after particular biases. This may explain the negative differential resistance behavior observed in some molecular devices [22, 137].

It is important to note that, the model describes at present only static characteristics and does not account for any molecular dynamics. Also, we currently do not account for interference effects that occur due to different connection at the phenyl ring (ortho, meta and para connections).

6.4 Conclusion

We have introduced a technique for modeling molecular devices in terms of circuit elements. The model is applied to state of the art molecular devices. The results reproduce qualitatively the experimental and the atomistic simulation performed on the testbed molecular devices. Our formalism provides a

circuit-based tool which can help the design of complex molecular devices and circuits.

This work builds an interesting bridge between two strongly developing scientific fields; organic chemistry on one hand and electronics on the other hand. We hope that the availability of circuit models could speed up the implementation of complex molecular systems as happened decades ago with silicon technology.

7 Conclusion and Outlook

In this chapter, we shall give a brief summary of the thesis and draw the main conclusions from its results. We shall also state an outlook regarding possible extension to the provided work. Single-molecule device technology is emerging as a candidate that can compensate the limitation in the current silicon technology regarding the device size. As known from history, a development of any technology requires an intensive (almost complete) understanding of the physics behind its devices operation. Therefore, theoretical studies need to be applied, alongside with the experimental ones, in order to allow the analyses of the various transport and electrical properties of the device.

This thesis constitutes a theoretical study on single-molecule devices. We first studied two terminal devices specifically molecular rectifiers. The study highlights important factors that affect the rectification performance of devices. One of the main outcomes is that tailoring the potential drop profile along the molecule can control the transport characteristic in molecular devices. We proved that rectification direction and magnitude of the molecular rectifiers could be varied solely with the resistivity of linker groups. This conclusion provides important insights for controlling the transport behavior and optimizing the rectification in molecular devices. A novel molecular rectifier was suggested and it was shown to provide a rectification ratio >1000. The device composed of a simple OPV molecule with a simple thiol linker on one terminal and an oxygen linker on the other terminal. We simulate molecules with up to 9 phenylene rings (<8 nm length) and show that the rectification ratio is enhanced with increasing the molecular length. For a longer molecule with 17-19 rings, we expect to have a rectification of more than 10^4 which would be a breakthrough record in the field of molecular electronics.

We also examined several correlations between the doping variation on one hand and the transmission spectra, potential drop profile along the molecule,

the dipole moment and the HOMO/LUMO distribution on the other hand. This facilitates the understanding of the impact of doping on the charge transport behavior within the D-σ-A molecular devices. One key outcome here is that doping does indeed affect the rectification performance of a device yet not always with a direct proportionality correlation.

In addition to molecular rectifiers, we also applied a first-principles atomistic study on devices with a wide range of NDR and a peak to valley ratio greater than 10. The devices are composed of a diphenyl-dimethyl connected to carbon chains from each side, which are then linked to gold electrodes through thiol-gold bond. The devices show an odd/even oscillating behavior: the NDR appears only for "odd" numbers of carbon atoms in the chain. In this study, we were able to explain the basic principles behind this NDR behavior via different atomistic analysis which clearly support and confirm each other.

The studies covered also three terminal molecular devices. We studied an OPV gated device with oxygen linker on both sides which was realized in [139, 165]. We were able to reproduce qualitatively the measurement current curves and give a thorough justification for the nonlinear current behavior and gate-conductance dependency. The provided explanation is consistent with the conclusions regarding the relationships between the different transport properties.

Further, we investigated an OPV gated molecular device without oxygen linker groups. The device shows a direct output-current variation with the gate bias. Interestingly, an inversion in the relation of gate-conductance is observed at gate bias -3.5 V and this performance could give a potential application for the device in building different logic gates [177, 178]. Additionally, the device shows a NDR for drain-source bias between 0.9 V and 1.1 V.

The interesting rectification performance of the OPV rectifier was employed to build three-leg molecular devices with various functionalities. The studied devices are based on OPE molecules since a collaborating group already synthesized three-leg OPE molecules. We showed that we could build up a functional molecular transistor as well as stand-alone logic gates (e.g. NAND and OR gates).

Finally, we have introduced a novel technique for modeling molecular devices in terms of circuit elements. We applied the model to state of the art molecular devices. The obtained results are in a good agreement with the experiment and the atomistic simulation performed on the testbed molecular devices. This formalism can help the design of complex systems and circuits composed of several single-molecule devices. Moreover, the model builds an interesting bridge between two strongly developing scientific fields, namely organic chemistry and electronics.

The work accomplished in this dissertation can be extended in different aspects. Physical realization and experimentally verification of the proposed devices, specifically the OPV diode and the device with interesting wide range of NDR, will help in gaining more insights of the devices. For the three-leg molecular device, although the molecules are synthesized, we hope that we shall soon be able to realize suitable three contact electrodes which are non-trivial in such atomic-scale dimensions.

The provided analysis and the established relationships among the different transport characteristics should be further verified. This can be achieved through application to other molecular devices or through design of novel devices. Last but not least, the circuit modeling methodology needs further development to account for additional phenomena as discussed earlier in chapter 6. We believe that the availability of circuit models would speed up the implementation of complex molecular systems similar to what happened decades ago with silicon technology.

Appendix A: Estimation for Molecular Devices Operation Parameters

First we will fix the value of some parameters that we will use in estimating the operation parameters of molecular devices. Based on the experimental and theoretical studies carried out on various molecular devices, the output current at an applied bias of 1 V mostly ranges between [0.1 nA,0.1 μA] [10,111,165]. The estimated average cross-sectional area of the molecules is around 5 Å^2 [111].

Current Density

The current density, which is the current per unit area, ranges between 2×10^9 A$/m^2$ and 2×10^{12} A$/m^2$. For the sake of comparison the current densities of carbon nanotubes and copper are 3.2×10^{10} A$/m^2$ and 3.2×10^5 A$/m^2$, respectively [111].

Operating Speed

To the best of our knowledge the speed of single-molecule devices was not investigated in experimental studies. For devices with a film of molecules, a transition time around 80 ns was reported [189]. We, hereby, present an attempt to predict the average speed of single-molecule devices. We assume having a two terminal device. The frequency is calculated as

$$frequency = \frac{1}{\tau} = \frac{1}{RC},$$
(0.1)

where R and C are the resistance and the capacitance of the whole device. The resistance of the device is nonlinear, so we will just assume the resistance at bias 1 V, which would be (R=V/I) ranging from 10 GΩ to 10 MΩ. It is worth mentioning that the Resistance at lower bias is one or two orders of magnitude

higher. The capacitance of the device is composed of the capacitance of the molecule (C_{mol}) and that of the electrodes ($C_{electrode}$). During the calculation of C_{mol}, we assumed that each atom within the molecule contributes with an average capacitance of single carbon atom capacitance. If we have 100 atom, we have $C_{mol} = 100 \times C_{carbon}$. The capacitance of a carbon atom is calculated as a spherical capacitor. According to real values, the outer radius is $0.77\,\text{Å}$. The inner radius (atomic nucleus) is calculated for any atom as ($r_o \times Z^{1/3}$), where $r_o = 1.25\,\text{fm}$ and Z is the atomic number. Thus

$$C_{carbon} = 4\epsilon_0\,\epsilon\,\frac{r1 \times r2}{r2 - r1} \approx 1.4 \times 10^{-25} F \qquad (0.2)$$

We used the electric permittivity of benzene which is 2.3. Thus, $C_{mol} \approx 1.4 \times 10^{-23}$ F. Therefore, the capacitance due to the electrodes dominates the capacitance of the whole device since

$$C_{electrodes} = \epsilon_0\,\epsilon\,\frac{A}{d}, \qquad (0.3)$$

where A is the cross-section are of the electrode (much greater than the cross-section of the molecule) and d is the distance between them (roughly the length of the molecule). Consequently, we may end up with a $C_{electrodes} > 10^{-19}$ F, whence the frequency ranges from $1\,\text{GHz}$ to $1\,\text{THz}$. This is a very promising operating speed.

Power dissipation and Energy

The power is expected to be dissipated in the contacts or due to phonon. The calculation of power is simply the multiplication of current by voltage. Accordingly, the power dissipation ranges from 10^{-9} watt to 10^{-7} watt. For calculating the energy range:

$$
\begin{aligned}
Energy &= power[10^{-9}, 10^{-7}] \times time[10^{-12}, 10^{-9}] & (0.4)\\
&\approx 10^{-21}\,\text{joule } to\ 10^{-16}\,\text{joule} & (0.5)\\
&\approx 5\,\text{meV } to\ 500\,\text{eV} & (0.6)
\end{aligned}
$$

This is an extremely high amount of energy which opens a question regarding the lifetime and reproducibility of such devices.

Appendix B: Switching Conductance in a Molecular Device

We discuss an explanation for the conductance switching observed in the bipyridyl-dinitro oligophenylene-ethynelene dithiol (BPDN-DT) molecule. Although the explanation may disclose the secret behind the conductance switching phenomenon, we still cannot provide enough atomistic simulation to prove it. Time-dependent DFT method may help in the calculation since it can treat exited states of the device that occur during switching [38, 39]. The proposed explanation may be checked experimentally through an accurate measurement of the input and output charges under the switching bias. However, this requires advanced tools that we currently cannot afford.

We suggest that oxygen atom within a molecule has multi-stable states of charging and bonding. When charges accumulate over oxygen under bias for specific period of time, discrete changes occur in the bond distance and angle between the oxygen and neighboring atoms. The new state would stay stable as long as the forces that act on withdrawing back the charges are negligible, and this is usually the case if negative charges came from an electrode with weakly bounded electrons.

Now, let us hypothesize the operation principle of the BPDN-DT molecule. Comparing the BPDN-DT molecule with a bipyridyl oligophenylene-ethynelene dithiol (BP-DT) molecule, we notice that BP-DT is almost planar but BPDN-DT has an interamolecular angle almost 90° (Figure 1). This non-planar structure of the molecule leads to strong reduction in the molecular conductivity because the conjugated bonds are broken. However, the nitro group is used as a dopant to increase the conductivity of molecules [23, 190]. Because of these two contradicting factors, the conductivity of BP-DT is only 4-6 times that of BPDN-DT.
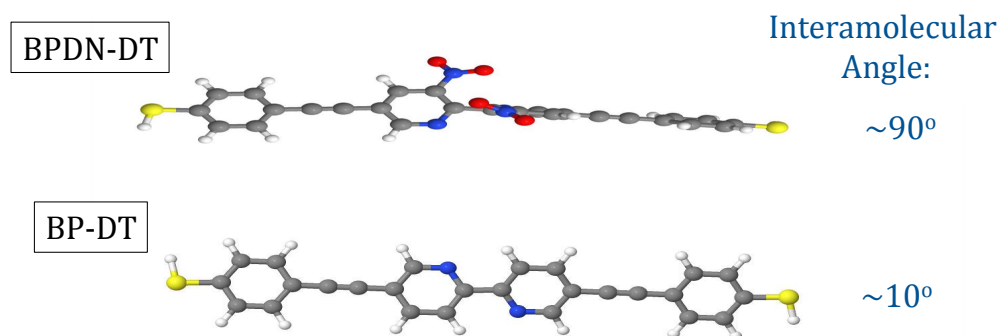
Figure 1: The geometrically optimized structure of BPDN-DT and BP-DT molecules.

Figure 2 illustrates resonance structures[1] of a pyridyl with a nitro group; the one on the right has a broken conjugation within the pyridyl ring. This may be one reason for the interamolecular angle of 90°. Upon applying the bias, the potential drop is mostly in the middle region where the conjugation is broken. This results in a charge accumulation in this region. When a specific amount of negative charge accumulates at one side of the molecule for a particular period of time, the oxygen changes its bonding state. We suggest that the contribution of the resonance structure with broken conjugation is reduced, hence the conductivity increases. Figure 3 illustrates the effect of adding hydrogen atoms (as a source of negative charges) to the nitro groups in the molecule. The hydrogen acts on reducing the interamolecular angle and improve the molecule conductivity.

Experimental measurements show that the off-switching (V_{th-off}) of the molecule occurs at higher bias value than the on-switching (V_{th-on}) [9]. This can be attributed to the fact that conductance of the on-state is high; hence the charge accumulation at the on-state is lower than that at the off-state under the same bias. Consequently, higher V_{th-off} bias is required in order to achieve the initial charging state of oxygen.

---

[1]Molecules with resonance contributors must have an electron Source and an electron Sink that are properly connected.

- The Source: unbounded/unshared electron or π electrons
- The Sink: electronegative atom or a bond connecting an open shell
- Electronic conductivity: planar set of atoms or linear conjugated
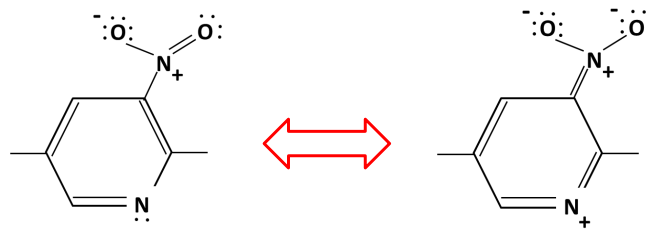
Figure 2: Possible resonance structures of a pyridyl molecule with a nitro group.

The molecule without H

Interamolecular Angle: ~90°

Conductivity at bias = 0.4V: ~ 3x10⁻⁹ S

The molecule with one H

Interamolecular Angle: ~55°

Conductivity at bias = 0.4V: ~ 1x10⁻⁷ S

The molecule with two H

Interamolecular Angle: ~25°

Conductivity at bias = 0.4V: ~ 2x10⁻⁷ S
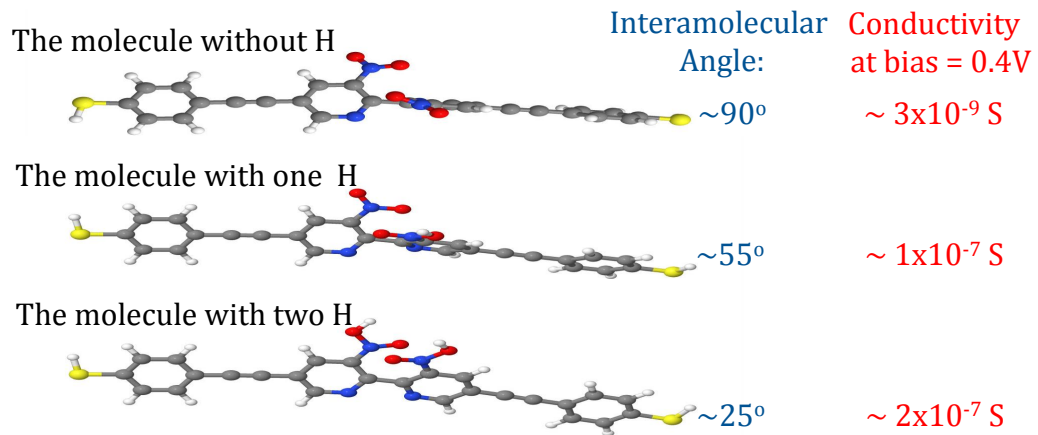
Figure 3: The geometrically optimized structure and conductivity of BPDN-DT molecule without and with reduction of the nitro group with hydrogen atoms.

The same explanation may be applicable to transition metal oxides which exhibit the switching conductance, as well. This contradicts the postulates which claim that the switching is due to movement of oxygen or oxygen vacancies [191]. We believe that these postulates may not be valid because the movement of oxygen or oxygen vacancies implies a complete breaking and creation of bonds. This seems difficult with the few applied voltages to switch the device. Instead, we claim that just the sharing of electron changes within the bonds of oxygen atom and leads to the conductance switching.

Let us discuss for instance the TiO_2-TiO_{2-x} device. TiO wire behaves like n-doped semiconductor, while TiO_2 wire behaves like an insulator. The high oxidation (low share of electrons in the covalent bonds) of Ti in TiO_2 is the reason behind the insulating property. The TiO_2-TiO device switches to high conductance state when a particular threshold bias is applied, and the negative electrode is connected to the TiO_2 region. This can be attributed to accumulation of negative charges in the TiO_2 region which forces some of the oxygen atoms to

release part of the shared electrons with Ti atoms, hence part of the TiO_2 section is converted merely to TiO_{2-x}.

We performed atomistic simulation for the charge density distribution of TiO_2 and TiO crystals at equilibrium. In both crystals, negative charges accumulate over the oxygen atoms. However, a visibly more positive charges accumulate over Ti in TiO_2 crystal than TiO crystal. Thus, We expect that when oxygen atoms in TiO_2 gain negative charges from the contact electrode under bias, the charge distribution of TiO_2 becomes similar to that of TiO.

Bibliography

[1] G. E. Moore, "Cramming more components onto integrated circuits," *Electronics*, vol. 38, no. 8, pp. 114–117, 1965.

[2] J. C. Cuevas and E. Scheer, *Molecular electronics: an introduction to theory and experiment*. World Scientific, 2010, vol. 1.

[3] J. M. Seminario, *Molecular and Nano Electronics: Analysis, Design and Simulation: Analysis, Design and Simulation*. Elsevier, 2006, vol. 17.

[4] A. Aviram and M. Ratner, "Molecular rectifiers," *Chemical Physics Letters*, vol. 29, no. 2, pp. 277–283, 1974.

[5] J. Chen, M. Reed, A. Rawlett, and J. Tour, "Large on-off ratios and negative differential resistance in a molecular electronic device," *Science*, vol. 286, no. 5444, pp. 1550–1552, 1999.

[6] M. Reed, J. Chen, A. Rawlett, D. Price, and J. Tour, "Molecular random access memory cell," *Applied physics letters*, vol. 78, p. 3735, 2001.

[7] Y. Chen, G.-Y. Jung, D. A. Ohlberg, X. Li, D. R. Stewart, J. O. Jeppesen, K. A. Nielsen, J. F. Stoddart, and R. S. Williams, "Nanoscale molecular-switch crossbar circuits," *Nanotechnology*, vol. 14, no. 4, p. 462, 2003.

[8] P. Kornilovitch, A. Bratkovsky, and R. Williams, "Current rectification by molecules with asymmetric tunneling barriers," *Physical Review B*, vol. 66, no. 16, p. 165436, 2002.

[9] E. Lörtscher, J. W. Ciszek, J. Tour, and H. Riel, "Reversible and controllable switching of a single-molecule junction," *Small*, vol. 2, no. 8-9, pp. 973–977, 2006.

[10] E. Lörtscher, B. Gotsmann, Y. Lee, L. Yu, C. Rettner, and H. Riel, "Transport properties of a single-molecule diode," *ACS nano*, vol. 6, no. 6, pp. 4931–4939, 2012.

[11] F. von Wrochem, D. Gao, F. Scholz, H.-G. Nothofer, G. Nelles, and J. M. Wessels, "Efficient electronic coupling and improved stability with dithiocarbamate-based molecular junctions," *Nature nanotechnology*, vol. 5, no. 8, pp. 618–624, 2010.

[12] F. v. Wrochem, F. Scholz, A. Schreiber, H.-G. Nothofer, W. E. Ford, P. Morf, T. Jung, A. Yasuda, and J. M. Wessels, "Structure and conductance of aromatic and aliphatic dithioacetamide monolayers on au (111)," *Langmuir*, vol. 24, no. 13, pp. 6910–6917, 2008.

[13] J. E. Green, J. W. Choi, A. Boukai, Y. Bunimovich, E. Johnston-Halperin, E. DeIonno, Y. Luo, B. A. Sheriff, K. Xu, Y. S. Shin *et al.*, "A 160-kilobit molecular electronic memory patterned at 1011 bits per square centimetre," *Nature*, vol. 445, no. 7126, pp. 414–417, 2007.

[14] S. H. Jo, K.-H. Kim, and W. Lu, "High-density crossbar arrays based on a si memristive system," *Nano letters*, vol. 9, no. 2, pp. 870–874, 2009.

[15] M. M. Ziegler and M. R. Stan, "Cmos/nano co-design for crossbar-based molecular electronic systems," *Nanotechnology, IEEE Transactions on*, vol. 2, no. 4, pp. 217–230, 2003.

[16] P. J. Kuekes, R. S. Williams, and J. R. Heath, "Molecular-wire crossbar interconnect (mwci) for signal routing and communications," Nov. 6 2001, uS Patent 6,314,019.

[17] G. Cerofolini and E. Romano, "Molecular electronics in silico," *Applied Physics A*, vol. 91, no. 2, pp. 181–210, 2008.

[18] G. Csaba and P. Lugli, "Read-out design rules for molecular crossbar architectures," *Nanotechnology, IEEE Transactions on*, vol. 8, no. 3, pp. 369–374, 2009.

[19] G. Cerofolini and D. Mascolo, "A hybrid micro-nano-molecular route for nonvolatile memories," *Semiconductor science and technology*, vol. 21, no. 9, p. 1315, 2006.

[20] A. Mahmoud and P. Lugli, "First-principles study of a novel molecular rectifier," *Nanotechnology, IEEE Transactions on*, vol. 12, no. 5, pp. 719–724, 2013.

[21] ——, "Study on molecular devices with negative differential resistance," *Applied Physics Letters*, vol. 103, no. 3, pp. 033 506–033 506, 2013.

[22] ——, "Transport characterization of a gated molecular device with negative differential resistance," in *Nanotechnology (IEEE-NANO), 2012 12th IEEE Conference on*. IEEE, 2012, pp. 1–5.

[23] ——, "Influence of doping variation on the transport behavior of aviram-ratner molecular diodes," in *Nanotechnology (IEEE-NANO), 2013 13th IEEE Conference on*. IEEE, 2013, pp. 1–4.

[24] ——, "Towards circuit modeling of molecular devices," *Nanotechnology, IEEE Transactions on*, 2014, submitted.

[25] R. H. Petrucci, W. S. Harwood, G. Herring, and J. Madura, *General chemistry: principles and modern applications*. Prentice Hall Upper Saddle River, NJ, 1997.

[26] S. Datta, *Electronic transport in mesoscopic systems*. Cambridge Univ Pr, 1997.

[27] ——, *Quantum transport: atom to transistor*. Cambridge Univ Pr, 2005.

[28] M. Born and R. Oppenheimer, "Zur quantentheorie der molekeln," *Annalen der Physik*, vol. 389, no. 20, pp. 457–484, 1927.

[29] J. E. Lennard-Jones, "The electronic structure of some diatomic molecules," *Transactions of the Faraday Society*, vol. 25, pp. 668–686, 1929.

[30] C. J. Cramer, *Essentials of computational chemistry: theories and models*. Wiley.com, 2005.

[31] J. C. Slater, "A simplification of the hartree-fock method," *Physical Review*, vol. 81, no. 3, p. 385, 1951.

[32] P. Hohenberg and W. Kohn, "Inhomogeneous electron gas," *Physical review*, vol. 136, no. 3B, pp. B864–B871, 1964.

[33] A. D. Becke, "Density-functional exchange-energy approximation with correct asymptotic behavior," *Physical Review A*, vol. 38, no. 6, p. 3098, 1988.

[34] M. Brandbyge, J.-L. Mozos, P. Ordejón, J. Taylor, and K. Stokbro, "Density-functional method for nonequilibrium electron transport," *Physical Review B*, vol. 65, no. 16, p. 165401, 2002.

[35] J. Taylor, H. Guo, and J. Wang, "Ab initio modeling of quantum transport properties of molecular electronic devices," *Physical Review B*, vol. 63, no. 24, p. 245407, 2001.

[36] W. Kohn and L. J. Sham, "Self-consistent equations including exchange and correlation effects," *Physical Review*, vol. 140, no. 4A, p. A1133, 1965.

[37] A. Zupan and M. Causà, "Density functional lcao calculations for solids: Comparison among hartree–fock, dft local density approximation, and dft generalized gradient approximation structural properties," *International Journal of Quantum Chemistry*, vol. 56, no. 4, pp. 337–344, 1995.

[38] E. Gross and W. Kohn, "Time-dependent density functional theory," *Adv. Quantum Chem*, vol. 21, pp. 255–291, 1990.

[39] D. Guillaumont and S. Nakamura, "Calculation of the absorption wavelength of dyes using time-dependent density-functional theory (td-dft)," *Dyes and pigments*, vol. 46, no. 2, pp. 85–92, 2000.

[40] D. Porezag, T. Frauenheim, T. Köhler, G. Seifert, and R. Kaschner, "Construction of tight-binding-like potentials on the basis of density-functional theory: Application to carbon," *Physical Review B*, vol. 51, no. 19, p. 12947, 1995.

[41] P. Koskinen and V. Mäkinen, "Density-functional tight-binding for beginners," *Computational Materials Science*, vol. 47, no. 1, pp. 237–253, 2009.

[42] A. Pecchia and A. Carlo, "Atomistic theory of transport in organic and inorganic nanostructures," *Reports on Progress in Physics*, vol. 67, p. 1497, 2004.

[43] G. C. Solomon, A. Gagliardi, A. Pecchia, T. Frauenheim, A. Di Carlo, J. R. Reimers, and N. S. Hush, "The symmetry of single-molecule conduction," *The Journal of chemical physics*, vol. 125, p. 184702, 2006.

[44] D. Q. Andrews, G. C. Solomon, R. P. Van Duyne, and M. A. Ratner, "Single molecule electronics: increasing dynamic range and switching speed using cross-conjugated species," *J. the American Chemical Society*, vol. 130, no. 51, pp. 17 309–17 319, 2008.

[45] G. Penazzi, J. M. Carlsson, C. Diedrich, G. Olf, A. Pecchia, and T. Frauenheim, "Atomistic modeling of charge transport across a carbon nanotube–polyethylene junction," *The Journal of Physical Chemistry C*, vol. 117, no. 16, pp. 8020–8027, 2013.

[46] A. Pecchia, G. Penazzi, L. Salvucci, and A. Di Carlo, "Non-equilibrium green's functions in density functional tight binding: method and applications," *New Journal of Physics*, vol. 10, no. 6, p. 065022, 2008.

[47] M. Elstner, D. Porezag, G. Jungnickel, J. Elsner, M. Haugk, T. Frauenheim, S. Suhai, and G. Seifert, "Self-consistent-charge density-functional tight-binding method for simulations of complex materials properties," *Physical Review B*, vol. 58, no. 11, p. 7260, 1998.

[48] T. Frauenheim, G. Seifert, M. Elsterner, Z. Hajnal, G. Jungnickel, D. Porezag, S. Suhai, and R. Scholz, "A self-consistent charge density-functional based tight-binding method for predictive materials simulations in physics, chemistry and biology," *physica status solidi(b)*, vol. 217, no. 1, pp. 41–62, 2000.

[49] K. Stokbro, J. Taylor, M. Brandbyge, and P. Ordejón, "Transiesta: a spice for molecular electronics," *Annals of the New York Academy of Sciences*, vol. 1006, no. 1, pp. 212–226, 2003.

[50] J. J. Stewart, "Mopac: a semiempirical molecular orbital program," *Journal of computer-aided molecular design*, vol. 4, no. 1, pp. 1–103, 1990.

[51] M. J. Dewar, J. A. Hashmall, and C. G. Venier, "Ground states of conjugated molecules. ix. hydrocarbon radicals and radical ions," *Journal of the American Chemical Society*, vol. 90, no. 8, pp. 1953–1957, 1968.

[52] W. Thiel and A. A. Voityuk, "Extension of mndo to d orbitals: Parameters and results for the second-row elements and for the zinc group," *The Journal of Physical Chemistry*, vol. 100, no. 2, pp. 616–626, 1996.

[53] M. C. Zerner, "Semiempirical molecular orbital methods," *Reviews in computational chemistry*, vol. 2, pp. 313–365, 1991.

[54] R. Hoffmann, "An extended hückel theory. i. hydrocarbons," *The Journal of Chemical Physics*, vol. 39, p. 1397, 1963.

[55] J. Cerda and F. Soria, "Accurate and transferable extended hückel-type tight-binding parameters," *Physical Review B*, vol. 61, no. 12, pp. 7965–7971, 2000.

[56] M. Magoga and C. Joachim, "Conductance and transparence of long molecular wires," *Physical Review B*, vol. 56, no. 8, p. 4722, 1997.

[57] D. Kienle, K. Bevan, G.-C. Liang, L. Siddiqui, J. Cerda, and A. W. Ghosh, "Extended hückel theory for band structure, chemistry, and transport. ii. silicon," *Journal of applied physics*, vol. 100, no. 4, pp. 043 715–043 715, 2006.

[58] J. C. Slater, "Atomic shielding constants," *Physical Review*, vol. 36, no. 1, p. 57, 1930.

[59] R. Mulliken, C. Rieke, D. Orloff, and H. Orloff, "Formulas and numerical tables for overlap integrals," *The Journal of Chemical Physics*, vol. 17, p. 1248, 1949.

[60] "Atomistix toolkit version 11.2.3, quantumwise a/s (www.quantumwise.com)."

[61] K. Stokbro, D. Petersen, S. Smidstrup, A. Blom, M. Ipsen, and K. Kaasbjerg, "Semiempirical model for nanoscale device simulations," *Physical Review B*, vol. 82, no. 7, p. 075420, 2010.

[62] E. Polizzi, S. Datta, L. Siddiqui, A. Ghosh, M. Paulsson, and F. Zahid, "A self-consistent transport model for molecular conduction based on extended hückel theory with full three-dimensional electrostatics," *The Journal of chemical physics*, vol. 123, no. 6, pp. 064 707–064 707, 2005.

[63] A. Blom and K. Stokbro, "Towards realistic atomic-scale modeling of nanoscale devices," in *Nanotechnology (IEEE-NANO), 2011 11th IEEE Conference on*.   IEEE, 2011, pp. 1487–1492.

[64] Y. Xue, S. Datta, S. Hong, R. Reifenberger, J. I. Henderson, and C. P. Kubiak, "Negative differential resistance in the scanning-tunneling spectroscopy of organic molecules," *Physical Review B*, vol. 59, no. 12, pp. R7852–R7855, 1999.

[65] H. Fang, R.-Z. Wang, S.-Y. Chen, M. Yan, X.-M. Song, and B. Wang, "Strain-induced negative differential resistance in armchair-edge graphene nanoribbons," *Applied Physics Letters*, vol. 98, no. 8, pp. 082 108–082 108, 2011.

[66] M. Paulsson, "Non equilibrium green's functions for dummies: Introduction to the one particle negf equations," *arXiv preprint cond-mat/0210519*, 2002.

[67] F. Zahid, M. Paulsson, and S. Datta, "Electrical conduction through molecules," *Advanced Semiconductors and Organic Nano-Techniques*, 2003.

[68] R. Landauer, "Electrical resistance of disordered one-dimensional lattices," *Philosophical Magazine*, vol. 21, no. 172, pp. 863–867, 1970.

[69] N. Tao, "Electron transport in molecular junctions," *Nature Nanotechnology*, vol. 1, no. 3, pp. 173–181, 2006.

[70] A. Gagliardi, G. Romano, A. Pecchia, and A. Di Carlo, "Simulation of inelastic scattering in molecular junctions: application to inelastic electron tunneling spectroscopy and dissipation effects," *Journal of Computational and Theoretical Nanoscience*, vol. 7, no. 12, pp. 2512–2526, 2010.

[71] R. M. Metzger, "Electrical rectification by a molecule: the advent of unimolecular electronic devices," *Accounts of chemical research*, vol. 32, no. 11, pp. 950–957, 1999.

[72] J. Kushmerick, D. Holt, J. Yang, J. Naciri, M. Moore, and R. Shashidhar, "Metal-molecule contacts and charge transport across monomolecular layers: Measurement and theory," *Physical review letters*, vol. 89, no. 8, p. 086802, 2002.

[73] J. Pan, Z. Zhang, K. Ding, X. Deng, and C. Guo, "Current rectification induced by asymmetrical electrode materials in a molecular device," *Applied Physics Letters*, vol. 98, no. 9, pp. 092 102–092 102, 2011.

[74] J. Chen, W. Wang, M. Reed, A. Rawlett, D. Price, and J. Tour, "Room-temperature negative differential resistance in nanoscale molecular junctions," *Applied physics letters*, vol. 77, no. 8, pp. 1224–1226, 2000.

[75] J. Chen, W. Wang, J. Klemic, M. Reed, B. Axelrod, D. Kaschak, A. Rawlett, D. Price, S. Dirk, J. Tour *et al.*, "Molecular wires, switches, and memories," *Annals of the New York Academy of Sciences*, vol. 960, no. 1, pp. 69–99, 2002.

[76] J. D. Le, Y. He, T. R. Hoye, C. C. Mead, and R. A. Kiehl, "Negative differential resistance in a bilayer molecular junction," *Applied physics letters*, vol. 83, no. 26, pp. 5518–5520, 2003.

[77] P. Liljeroth, J. Repp, and G. Meyer, "Current-induced hydrogen tautomerization and conductance switching of naphthalocyanine molecules," *Science*, vol. 317, no. 5842, pp. 1203–1206, 2007.

[78] J. He, Q. Fu, S. Lindsay, J. W. Ciszek, and J. M. Tour, "Electrochemical origin of voltage-controlled molecular conductance switching," *Journal of the American Chemical Society*, vol. 128, no. 46, pp. 14 828–14 835, 2006.

[79] S. Schmaus, A. Bagrets, Y. Nahas, T. K. Yamada, A. Bork, M. Bowen, E. Beaurepaire, F. Evers, and W. Wulfhekel, "Giant magnetoresistance through a single molecule," *Nature Nanotechnology*, vol. 6, no. 3, pp. 185–189, 2011.

[80] L. Bogani and W. Wernsdorfer, "Molecular spintronics using single-molecule magnets," *Nature materials*, vol. 7, no. 3, pp. 179–186, 2008.

[81] M. Zeng, L. Shen, Y. Cai, Z. Sha, and Y. Feng, "Perfect spin-filter and spin-valve in carbon atomic chains," *Applied Physics Letters*, vol. 96, no. 4, pp. 042 104–042 104, 2010.

[82] V. Mujica, M. Kemp, A. Roitberg, and M. Ratner, "Current-voltage characteristics of molecular wires: Eigenvalue staircase, coulomb blockade, and rectification," *The Journal of chemical physics*, vol. 104, p. 7296, 1996.

[83] J. Park, A. N. Pasupathy, J. I. Goldsmith, C. Chang, Y. Yaish, J. R. Petta, M. Rinkoski, J. P. Sethna, H. D. Abruña, P. L. McEuen *et al.*, "Coulomb blockade and the kondo effect in single-atom transistors," *Nature*, vol. 417, no. 6890, pp. 722–725, 2002.

[84] W. Liang, M. P. Shores, M. Bockrath, J. R. Long, and H. Park, "Kondo resonance in a single-molecule transistor," *Nature*, vol. 417, no. 6890, pp. 725–729, 2002.

[85] P. E. Laibinis, G. M. Whitesides, D. L. Allara, Y. T. Tao, A. N. Parikh, and R. G. Nuzzo, "Comparison of the structures and wetting properties of self-assembled monolayers of n-alkanethiols on the coinage metal surfaces, copper, silver, and gold," *Journal of the American Chemical Society*, vol. 113, no. 19, pp. 7152–7167, 1991.

[86] J. M. Tour, L. Jones, D. L. Pearson, J. J. Lamba, T. P. Burgin, G. M. Whitesides, D. L. Allara, A. N. Parikh, and S. Atre, "Self-assembled monolayers and multilayers of conjugated thiols,. alpha.,. omega.-dithiols, and thioacetyl-containing adsorbates. understanding attachments between potential molecular wires and gold surfaces," *Journal of the American Chemical Society*, vol. 117, no. 37, pp. 9529–9534, 1995.

[87] F. Chen, X. Li, J. Hihath, Z. Huang, and N. Tao, "Effect of anchoring groups on single-molecule conductance: comparative study of thiol-, amine-, and carboxylic-acid-terminated molecules," *Journal of the American Chemical Society*, vol. 128, no. 49, pp. 15 874–15 881, 2006.

[88] M. J. Robertson and R. J. Angelici, "Adsorption of aryl and alkyl isocyanides on powdered gold," *Langmuir*, vol. 10, no. 5, pp. 1488–1492, 1994.

[89] M. Kamenetska, S. Y. Quek, A. Whalley, M. Steigerwald, H. Choi, S. G. Louie, C. Nuckolls, M. Hybertsen, J. Neaton, and L. Venkataraman, "Conductance and geometry of pyridine-linked single-molecule junctions," *Journal of the American Chemical Society*, vol. 132, no. 19, pp. 6817–6821, 2010.

[90] W. Su, J. Jiang, W. Lu, and Y. Luo, "First-principles study of electrochemical gate-controlled conductance in molecular junctions," *Nano letters*, vol. 6, no. 9, pp. 2091–2094, 2006.

[91] S. Hong, R. Reifenberger, W. Tian, S. Datta, J. Henderson, and C. Kubiak, "Molecular conductance spectroscopy of conjugated, phenyl-based molecules on Au(111): the effect of end groups on molecular conduction," *Superlattices and Microstructures*, vol. 28, no. 4, pp. 289–303, Oct. 2000.

[92] E. Lörtscher, C. J. Cho, M. Mayor, M. Tschudy, C. Rettner, and H. Riel, "Influence of the anchor group on charge transport through single-molecule junctions," *ChemPhysChem*, vol. 12, no. 9, pp. 1677–1682, 2011.

[93] A. Ulman, "Formation and structure of self-assembled monolayers," *Chemical reviews*, vol. 96, no. 4, pp. 1533–1554, 1996.

[94] S. Datta, W. Tian, S. Hong, R. Reifenberger, J. I. Henderson, and C. P. Kubiak, "Current-voltage characteristics of self-assembled monolayers by scanning tunneling microscopy," *Physical review letters*, vol. 79, no. 13, p. 2530, 1997.

[95] J. C. Love, L. A. Estroff, J. K. Kriebel, R. G. Nuzzo, and G. M. Whitesides, "Self-assembled monolayers of thiolates on metals as a form of nanotechnology," *Chemical reviews*, vol. 105, no. 4, pp. 1103–1170, 2005.

[96] L.-J. Wan, "Fabricating and controlling molecular self-organization at solid surfaces: Studies by scanning tunneling microscopy," *Accounts of chemical research*, vol. 39, no. 5, pp. 334–342, 2006.

[97] C. M. Guédon, H. Valkenier, T. Markussen, K. S. Thygesen, J. C. Hummelen, and S. J. van der Molen, "Observation of quantum interference in molecular charge transport," *Nature Nanotechnology*, vol. 7, no. 5, pp. 305–309, 2012.

[98] H. Watanabe, C. Manabe, T. Shigematsu, K. Shimotani, and M. Shimizu, "Single molecule dna device measured with triple-probe atomic force microscope," *Applied Physics Letters*, vol. 79, no. 15, pp. 2462–2464, 2001.

[99] M. A. Reed, C. Zhou, C. Muller, T. Burgin, and J. Tour, "Conductance of a molecular junction," *Science*, vol. 278, no. 5336, pp. 252–254, 1997.

[100] A. R. Champagne, A. N. Pasupathy, and D. C. Ralph, "Mechanically adjustable and electrically gated single-molecule transistors," *Nano letters*, vol. 5, no. 2, pp. 305–308, 2005.

[101] D. Xiang, H. Jeong, T. Lee, and D. Mayer, "Mechanically controllable break junctions for molecular electronics," *Advanced Materials*, 2013.

[102] C. Li, A. Bogozi, W. Huang, and N. Tao, "Fabrication of stable metallic nanowires with quantized conductance," *Nanotechnology*, vol. 10, no. 2, p. 221, 1999.

[103] A. Morpurgo, C. Marcus, and D. Robinson, "Controlled fabrication of metallic electrodes with atomic separation," *Applied Physics Letters*, vol. 74, no. 14, pp. 2084–2086, 1999.

[104] T. Li, W. Hu, and D. Zhu, "Nanogap electrodes," *Advanced Materials*, vol. 22, no. 2, pp. 286–300, 2010.

[105] S. Strobel, S. Harrer, G. Penso Blanco, G. Scarpa, G. Abstreiter, P. Lugli, and M. Tornow, "Planar nanogap electrodes by direct nanotransfer printing," *Small*, vol. 5, no. 5, pp. 579–582, 2009.

[106] L. Cai, Y. Yao, J. Yang, D. W. Price, and J. M. Tour, "Chemical and potential-assisted assembly of thiolacetyl-terminated oligo (phenylene ethynylene) s on gold surfaces," *Chemistry of materials*, vol. 14, no. 7, pp. 2905–2909, 2002.

[107] X. Xiao, L. A. Nagahara, A. M. Rawlett, and N. Tao, "Electrochemical gate-controlled conductance of single oligo (phenylene ethynylene) s," *Journal of the American Chemical Society*, vol. 127, no. 25, pp. 9235–9240, 2005.

[108] T. Dadosh, Y. Gordin, R. Krahne, I. Khivrich, D. Mahalu, V. Frydman, J. Sperling, A. Yacoby, and I. Bar-Joseph, "Measurement of the conductance of single conjugated molecules," *Nature*, vol. 436, no. 7051, pp. 677–680, 2005.

[109] L. Zang, Y. Che, and J. Moore, "One-dimensional self-assembly of planar π-conjugated molecules: Adaptable building blocks for organic nanodevices," *Accounts of chemical research*, vol. 41, no. 12, pp. 1596–1608, 2008.

[110] Y. Li, J. Zhao, and G. Yin, "Theoretical investigations of oligo (phenylene ethylene) molecular wire: Effects from substituents and external electric field," *Computational materials science*, vol. 39, no. 4, pp. 775–781, 2007.

[111] J. C. Ellenbogen and J. C. Love, "Architectures for molecular electronic computers. i. logic structures and an adder designed from molecular electronic diodes," *Proceedings of the IEEE*, vol. 88, no. 3, pp. 386–426, 2000.

[112] R. Hentschke, B. L. Schürmann, and J. P. Rabe, "Molecular dynamics simulations of ordered alkane chains physisorbed on graphite," *The Journal of chemical physics*, vol. 96, p. 6213, 1992.

[113] S. Franzen, "Density functional calculation of a potential energy surface for alkane thiols on au (111) as function of alkane chain length," *Chemical physics letters*, vol. 381, no. 3, pp. 315–321, 2003.

[114] Z. Wang, J. A. Carter, A. Lagutchev, Y. K. Koh, N.-H. Seong, D. G. Cahill, and D. D. Dlott, "Ultrafast flash thermal conductance of molecular chains," *Science*, vol. 317, no. 5839, pp. 787–790, 2007.

[115] W. Wang, T. Lee, and M. Reed, "Mechanism of electron conduction in self-assembled alkanethiol monolayer devices," *Physical Review B*, vol. 68, no. 3, p. 035416, 2003.

[116] R. M. Metzger, "Unimolecular electrical rectifiers," *Chemical reviews*, vol. 103, no. 9, pp. 3803–3834, 2003.

[117] Z. Zhang, C. Guo, D. J. Kwong, J. Li, X. Deng, and Z. Fan, "A dramatic odd–even oscillating behavior for the current rectification and negative differential resistance in carbon-chain-modified donor–acceptor molecular devices," *Advanced Functional Materials*, 2013.

[118] J. Pan, Z. Zhang, X. Deng, M. Qiu, and C. Guo, "The transport properties of d-σ-a molecules: A strikingly opposite directional rectification," *Applied Physics Letters*, vol. 98, no. 1, pp. 013 503–013 503, 2011.

[119] J. G. Kushmerick, C. M. Whitaker, S. K. Pollack, T. L. Schull, and R. Shashidhar, "Tuning current rectification across molecular junctions," *Nanotechnology*, vol. 15, no. 7, p. S489, 2004.

[120] X. Wu, J. Xiao, L. Chen, C. Cao, H. Xu, and M. Long, "The effect of asymmetrical electrode on the transport properties of molecular device," *Physica B: Condensed Matter*, 2012.

[121] K. Zhou, Y. Zhang, L. Wang, K. Xie, Y. Xiong, H. Zhang, and C. Wang, "Can azulene-like molecules function as substitution-free molecular rectifiers?" *Phys. Chem. Chem. Phys.*, 2011.

[122] G. M. Morales, P. Jiang, S. Yuan, Y. Lee, A. Sanchez, W. You, and L. Yu, "Inversion of the rectifying effect in diblock molecular diodes by protonation," *Journal of the American Chemical Society*, vol. 127, no. 30, pp. 10 456–10 457, 2005.

[123] R. M. Metzger, "Electrical rectification by a molecule: the advent of unimolecular electronic devices," *Accounts of chemical research*, vol. 32, no. 11, pp. 950–957, 1999.

[124] S. K. Yee, J. Sun, P. Darancet, T. D. Tilley, A. Majumdar, J. B. Neaton, and R. A. Segalman, "Inverse rectification in donor–acceptor molecular heterojunctions," *ACS nano*, vol. 5, no. 11, pp. 9256–9263, 2011.

[125] H. Zhang, J. Zeng, and K.-Q. Chen, "Rectifying and negative differential resistance behaviors induced by asymmetric electrode coupling in pyrene-based molecular device," *Physica E: Low-dimensional Systems and Nanostructures*, vol. 44, no. 7, pp. 1631–1635, 2012.

[126] S. Yuan, S. Wang, Q. Mei, Q. Ling, L. Wang, and W. Huang, "First-principles study of rectification in bis-2-(5-ethynylthienyl) ethyne molecular junctions," *The Journal of Physical Chemistry A*, vol. 115, no. 32, pp. 9033–9042, 2011.

[127] L. Esaki, "New phenomenon in narrow germanium pn junctions," *Physical Review*, vol. 109, no. 2, p. 603, 1958.

[128] C. Todd, "Tunnel diode applications," *Electrical Engineering*, vol. 80, no. 4, pp. 265–271, 1961.

[129] T. Coffey, Z. Bayindir, J. DeCarolis, M. Bennett, G. Esper, and C. Agosta, "Measuring radio frequency properties of materials in pulsed magnetic fields with a tunnel diode oscillator," *Review of Scientific Instruments*, vol. 71, no. 12, pp. 4600–4606, 2000.

[130] Y. Xu, G. Zhang, and B. Li, "Large negative differential resistance in a molecular junction of carbon nanotube and anthracene," *The Journal of Physical Chemistry B*, vol. 112, no. 51, pp. 16 891–16 894, 2008.

[131] J. Fan, N. N. Gathitu, Y. Chang, and J. Zhang, "Effect of length on the position of negative differential resistance and realization of multifunction in fused oligothiophenes based molecular device," *The Journal of chemical physics*, vol. 138, p. 074307, 2013.

[132] H. Geng, Y. Hu, Z. Shuai, K. Xia, H. Gao, and K. Chen, "Molecular design of negative differential resistance device through intermolecular interaction," *The Journal of Physical Chemistry C*, vol. 111, no. 51, pp. 19 098–19 102, 2007.

[133] C.-J. Xia, D.-S. Liu, H.-C. Liu, and X.-J. Zhai, "Large negative differential resistance in a molecular device with asymmetric contact geometries: A first-principles study," *Physica E: Low-dimensional Systems and Nanostructures*, vol. 43, no. 8, pp. 1518–1521, 2011.

[134] A. Migliore and A. Nitzan, "Nonlinear charge transport in redox molecular junctions: a marcus perspective," *Acs Nano*, vol. 5, no. 8, pp. 6669–6685, 2011.

[135] V. Meded, A. Bagrets, A. Arnold, and F. Evers, "Molecular switch controlled by pulsed bias voltages," *Small*, vol. 5, no. 19, pp. 2218–2223, 2009.

[136] S. Kubatkin, A. Danilov, M. Hjort, J. Cornil, J.-L. Brédas, N. Stuhr-Hansen, P. Hedegård, and T. Bjørnholm, "Single-electron transistor of a single organic molecule with access to several redox states," *Nature*, vol. 425, no. 6959, pp. 698–701, 2003.

[137] N. Zhitenev, A. Erbe, H. Meng, and Z. Bao, "Gated molecular devices using self-assembled monolayers," *Nanotechnology*, vol. 14, p. 254, 2003.

[138] H. Song, Y. Kim, Y. Jang, H. Jeong, M. Reed, and T. Lee, "Observation of molecular orbital gating," *Nature*, vol. 462, no. 7276, pp. 1039–1043, 2009.

[139] M. I. Schukfeh, K. Storm, A. Mahmoud, R. R. Søndergaard, A. Szwajca, A. Hansen, P. Hinze, T. Weimann, S. F. Svensson, A. Bora, K. A. Dick, C. Thelander, F. C. Krebs, P. Lugli, L. Samuelson, and M. Tornow, "Conductance enhancement of inas/inp heterostructure nanowires by surface functionalization with oligo(phenylene vinylene)s," *ACS Nano*, vol. 7, no. 5, pp. 4111–4118, 2013.

[140] N. D. Lang and P. M. Solomon, "Gating of a three-leg molecule," *ACS nano*, vol. 3, no. 6, pp. 1437–1440, 2009.

[141] ——, "Charge control in a model biphenyl molecular transistor," *Nano letters*, vol. 5, no. 5, pp. 921–924, 2005.

[142] S. Ami, M. Hliwa, and C. Joachim, "Molecular "or" and "and" logic gates integrated in a single molecule," *Chemical physics letters*, vol. 367, no. 5, pp. 662–668, 2003.

[143] N. Jlidat, M. Hliwa, and C. Joachim, "A semi-classical xor logic gate integrated in a single molecule," *Chemical Physics Letters*, vol. 451, no. 4, pp. 270–275, 2008.

[144] N. Renaud, M. Ito, W. Shangguan, M. Saeys, M. Hliwa, and C. Joachim, "A nor–and quantum running gate molecule," *Chemical Physics Letters*, vol. 472, no. 1, pp. 74–79, 2009.

[145] H. Haug and A. Jauho, *Quantum kinetics in transport and optics of semiconductors*.   Springer Verlag, 2008, vol. 6.

[146] S. Datta, "Nanoscale device modeling: the green's function method," *Superlattices and Microstructures*, vol. 28, no. 4, pp. 253–278, 2000.

[147] A. Di Carlo, M. Gheorghe, P. Lugli, M. Sternberg, G. Seifert, and T. Frauenheim, "Theoretical tools for transport in molecular nanostructures," *Physica B: Condensed Matter*, vol. 314, no. 1-4, pp. 86–90, 2002.

[148] F. Zahid, M. Paulsson, E. Polizzi, A. Ghosh, L. Siddiqui, and S. Datta, "A self-consistent transport model for molecular conduction based on extended hückel theory with full three-dimensional electrostatics," *The Journal of chemical physics*, vol. 123, p. 064707, 2005.

[149] A. Ghosh, F. Zahid, S. Datta, and R. Birge, "Charge transfer in molecular conductors–oxidation or reduction?" *Chemical physics*, vol. 281, no. 2-3, pp. 225–230, 2002.

[150] A. Ghosh, T. Rakshit, and S. Datta, "Gating of a molecular transistor: electrostatic and conformational," *Nano Letters*, vol. 4, no. 4, pp. 565–568, 2004.

[151] R. Metzger, B. Chen, U. Höpfner, M. Lakshmikantham, D. Vuillaume, T. Kawai, X. Wu, H. Tachibana, T. Hughes, H. Sakurai *et al.*, "Unimolecular electrical rectification in hexadecylquinolinium tricyanoquinodimethanide," *Journal of the American Chemical Society*, vol. 119, no. 43, pp. 10 455–10 466, 1997.

[152] M. Ng, D. Lee, and L. Yu, "Molecular diodes based on conjugated diblock co-oligomers," *Journal of the American Chemical Society*, vol. 124, no. 40, pp. 11 862–11 863, 2002.

[153] C. Guo, Z. Zhang, G. Kwong, J. Pan, X. Deng, and J. Zhang, "Enormously enhanced rectifying performances by modification of carbon chains for d-σ–a molecular devices," *The Journal of Physical Chemistry C*, vol. 116, no. 23, pp. 12 900–12 905, 2012.

[154] I. Díez-Pérez, J. Hihath, Y. Lee, L. Yu, L. Adamska, M. Kozhushner, I. Oleynik, and N. Tao, "Rectification and stability of a single molecular diode with controlled orientation," *Nature Chemistry*, vol. 1, no. 8, pp. 635–641, 2009.

[155] "[online]. available: http://www.dftb-plus.info/."

[156] W. Andreoni, A. Curioni, and H. Grönbeck, "Density functional theory approach to thiols and disulfides on gold: Au (111) surface and clusters," *International Journal of Quantum Chemistry*, vol. 80, no. 4-5, pp. 598–608, 2000.

[157] B. Aradi, B. Hourahine, and T. Frauenheim, "Dftb+, a sparse matrix-based implementation of the dftb method," *The Journal of Physical Chemistry A*, vol. 111, no. 26, pp. 5678–5684, 2007.

[158] J. M. Soler, E. Artacho, J. D. Gale, A. García, J. Junquera, P. Ordejón, and D. Sánchez-Portal, "The siesta method for ab initio order-n materials simulation," *Journal of Physics: Condensed Matter*, vol. 14, no. 11, p. 2745, 2002.

[159] I. Díez-Pérez, J. Hihath, Y. Lee, L. Yu, L. Adamska, M. Kozhushner, I. Oleynik, and N. Tao, "Rectification and stability of a single molecular diode with controlled orientation," *Nature Chemistry*, vol. 1, no. 8, pp. 635–641, 2009.

[160] H. Nakamura, Y. Asai, J. Hihath, C. Bruot, and N. Tao, "Switch of conducting orbital by bias-induced electronic contact asymmetry in a bipyrimidinyl-biphenyl diblock molecule: Mechanism to achieve a pn directional molecular diode," *The Journal of Physical Chemistry C*, vol. 115, no. 40, pp. 19 931–19 938, 2011.

[161] G. Zhang, G. Hu, Z. Li, and C. Wang, "Theoretical studies on protonation-induced inversion of the rectifying direction in dipyrimidinyl–diphenyl diblock molecular junctions," *The Journal of Physical Chemistry C*, vol. 116, no. 5, pp. 3773–3778, 2012.

[162] F. Allen, O. Kennard, D. Watson, L. Brammer, A. Orpen, and R. Taylor, "Tables of bond lengths determined by x-ray and neutron diffraction. part 1. bond lengths in organic compounds," *J. Chem. Soc., Perkin Trans. 2*, no. 12, pp. S1–S19, 1987.

[163] J. Trotter, "Bond lengths in benzene derivatives: Hybridization or resonance," *Tetrahedron*, vol. 8, no. 1, pp. 13–22, 1960.

[164] K. Stokbro, J. Taylor, M. Brandbyge, J. Mozos, and P. Ordejon, "Theoretical study of the nonlinear conductance of di-thiol benzene coupled to au (111) surfaces via thiol and thiolate bonds," *Computational Materials Science*, vol. 27, no. 1, pp. 151–160, 2003.

[165] R. Søndergaard, S. Strobel, E. Bundgaard, K. Norrman, A. Hansen, E. Albert, G. Csaba, P. Lugli, M. Tornow, and F. Krebs, "Conjugated 12 nm long oligomers as molecular wires in nanoelectronics," *J. Mater. Chem.*, vol. 19, no. 23, pp. 3899–3908, 2009.

[166] R. Stadler, V. Geskin, and J. Cornil, "A theoretical view of unimolecular rectification," *Journal of Physics: Condensed Matter*, vol. 20, no. 37, p. 374105, 2008.

[167] K. H. Khoo, J. Neaton, Y. W. Son, M. L. Cohen, and S. G. Louie, "Negative differential resistance in carbon atomic wire-carbon nanotube junctions," *Nano letters*, vol. 8, no. 9, pp. 2900–2905, 2008.

[168] T. Yuzvinsky, W. Mickelson, S. Aloni, G. Begtrup, A. Kis, and A. Zettl, "Shrinking a carbon nanotube," *Nano letters*, vol. 6, no. 12, pp. 2718–2722, 2006.

[169] A. Chuvilin, J. C. Meyer, G. Algara-Siller, and U. Kaiser, "From graphene constrictions to single carbon chains," *New Journal of Physics*, vol. 11, no. 8, p. 083019, 2009.

[170] I. Kratochvilova, M. Kocirik, A. Zambova, J. Mbindyo, T. E. Mallouk, and T. S. Mayer, "Room temperature negative differential resistance in molecular nanowires," *Journal of Materials Chemistry*, vol. 12, no. 10, pp. 2927–2930, 2002.

[171] P. Lugli, A. Mahmoud, G. Csaba, M. Algasinger, M. Stutzmann, and U. Rührmair, "Physical unclonable functions based on crossbar arrays for cryptographic applications," *International Journal of Circuit Theory and Applications*, 2012.

[172] D. A. Corley, T. He, and J. M. Tour, "Two-terminal molecular memories from solution-deposited c60 films in vertical silicon nanogaps," *ACS nano*, vol. 4, no. 4, pp. 1879–1888, 2010.

[173] C. Joachim and M. A. Ratner, "Molecular electronics: Some views on transport junctions and beyond," *Proceedings of the National Academy of Sciences of the United States of America*, vol. 102, no. 25, pp. 8801–8808, 2005.

[174] A. Aviram, "Molecular electronics-science and technology," *Advanced Materials*, vol. 1, no. 4, pp. 124–125, 1989.

[175] S. Tsoi, I. Griva, S. Trammell, A. Blum, J. Schnur, and N. Lebedev, "Electrochemically controlled conductance switching in a single molecule: quinone-modified oligo (phenylene vinylene)," *Acs Nano*, vol. 2, no. 6, pp. 1289–1295, 2008.

[176] H. Park, J. Park, A. Lim, E. Anderson, A. Alivisatos, P. McEuen *et al.*, "Nanomechanical oscillations in a single-c60 transistor," *Nature*, vol. 407, no. 6800, pp. 57–60, 2000.

[177] R. Sordan, F. Traversi, and V. Russo, "Logic gates with a single graphene transistor," *Applied Physics Letters*, vol. 94, p. 073305, 2009.

[178] Y. Xu, C. Fang, B. Cui, G. Ji, Y. Zhai, and D. Liu, "Gated electronic currents modulation and designs of logic gates with single molecular field effect transistors," *Applied Physics Letters*, vol. 99, no. 4, pp. 043 304–043 304, 2011.

[179] S. H. Choi, B. Kim, and C. D. Frisbie, "Electrical resistance of long conjugated molecular wires," *Science*, vol. 320, no. 5882, pp. 1482–1486, 2008.

[180] L. Luo and C. D. Frisbie, "Length-dependent conductance of conjugated molecular wires synthesized by stepwise "click" chemistry," *Journal of the American Chemical Society*, vol. 132, no. 26, pp. 8854–8855, 2010.

[181] G. C. Solomon, D. Q. Andrews, T. Hansen, R. H. Goldsmith, M. R. Wasielewski, R. P. Van Duyne, and M. A. Ratner, "Understanding quantum interference in coherent molecular conduction," *The Journal of chemical physics*, vol. 129, p. 054701, 2008.

[182] A. Mahmoud and P. Lugli, "Designing the rectification behavior of molecular diodes," *Journal of Applied Physics*, vol. 112, no. 11, pp. 113 720–113 720, 2012.

[183] I. R. Peterson, D. Vuillaume, and R. M. Metzger, "Analytical model for molecular-scale charge transport," *The Journal of Physical Chemistry A*, vol. 105, no. 19, pp. 4702–4707, 2001.

[184] M. Di Ventra, S. Pantelides, and N. Lang, "First-principles calculation of transport properties of a molecular device," *Physical Review Letters*, vol. 84, no. 5, p. 979, 2000.

[185] A. Pecchiaa, L. Latessaa, A. Gagliardiab, T. Frauenheimb, and A. Di Carloa, "The gdftb tool for molecular electronics," *Molecular and Nano Electronics: Analysis, Design and Simulation: Analysis, Design and Simulation*, vol. 17, p. 205, 2006.

[186] "[online]. available: http://www.linear.com/designtools/software/."

[187] A. Pulimeno, M. Graziano, A. Sanginario, V. Cauda, D. Demarchi, and G. Piccinini, "Bis-ferrocene molecular qca wire: Ab initio simulations of fabrication driven fault tolerance," *IEEE transactions on nanotechnology*, vol. 12, no. 4, pp. 498–507, 2013.

[188] W. M. Haynes, D. R. Lide, and T. J. Bruno, *CRC Handbook of Chemistry and Physics 2012-2013*. CRC press, 2012, section 10, Atomic, Molecular, and Optical Physics; Ionization Potentials of Atoms and Atomic Ions.

[189] Y. Wen, J. Wang, J. Hu, L. Jiang, H. Gao, Y. Song, and D. Zhu, "Reversible nanometer-scale data storage on a self-assembled, organic, crystalline thin film," *Advanced Materials*, vol. 18, no. 15, pp. 1983–1987, 2006.

[190] J. Taylor, M. Brandbyge, and K. Stokbro, "Conductance switching in a molecular device: The role of side groups and intermolecular interactions," *Physical Review B*, vol. 68, no. 12, p. 121101, 2003.

[191] D. B. Strukov, G. S. Snider, D. R. Stewart, and R. S. Williams, "The missing memristor found," *Nature*, vol. 453, no. 7191, pp. 80–83, 2008.

List of Publications

[1] A. Mahmoud and P. Lugli, "First-principles study of a novel molecular rectifier," *Nanotechnology, IEEE Transactions on*, vol. 12, no. 5, pp. 719–724, 2013.

[2] ——, "Study on molecular devices with negative differential resistance," *Applied Physics Letters*, vol. 103, no. 3, pp. 033 506–033 506, 2013.

[3] ——, "Influence of doping variation on the transport behavior of aviram-ratner molecular diodes," in *Nanotechnology (IEEE-NANO), 2013 13th IEEE Conference on*.   IEEE, 2013, pp. 1–4.

[4] ——, "Transport characterization of a gated molecular device with negative differential resistance," in *Nanotechnology (IEEE-NANO), 2012 12th IEEE Conference on*.   IEEE, 2012, pp. 1–5.

[5] ——, "Designing the rectification behavior of molecular diodes," *Journal of Applied Physics*, vol. 112, no. 11, pp. 113 720–113 720, 2012.

[6] M. I. Schukfeh, K. Storm, A. Mahmoud, R. R. Søndergaard, A. Szwajca, A. Hansen, P. Hinze, T. Weimann, S. F. Svensson, A. Bora *et al.*, "Conductance enhancement of inas/inp heterostructure nanowires by surface functionalization with oligo (phenylene vinylene) s," *ACS nano*, 2013.

[7] P. Lugli, A. Mahmoud, G. Csaba, M. Algasinger, M. Stutzmann, and U. Rührmair, "Physical unclonable functions based on crossbar arrays for cryptographic applications," *International Journal of Circuit Theory and Applications*, 2012.

[8] U. Rührmair, J. Sölter, F. Sehnke, X. Xu, A. Mahmoud, V. Stoyanova, G. Dror, J. Schmidhuber, W. Burleson, and S. Devadas, "PUF modeling attacks on simulated and silicon data." *Information Forensics and Security, IEEE Transactions on*, vol. 8, no. 11, pp. 1876–1891, 2013.

[9] A. Mahmoud and P. Lugli, "Towards circuit modeling of molecular devices," *Nanotechnology, IEEE Transactions on*, 2014, accepted.

[10] ——, "Atomistic study on three-leg molecular devices," is being prepared.

[11] ——, "Atomistic study of a gated oligo-phenylenevinylene molecular device," is being prepared.

Acknowledgments

أَنِ ٱشْكُرْ لِى وَلِوَٰلِدَيْكَ إِلَىَّ ٱلْمَصِيرُ

The possibility and success of this work would not have been likely without the trust, patience and support of several individuals and organizations. I hereby thank all those who contributed to this work in any way.

Special thanks goes to:

- Prof.Dr. Paolo Lugli for his cooperation and support for allowing me to conduct this thesis under his supervision. His continuous valuable advices had a great contribution in the success of this work

- Mrs Lucia Weik for her kind cooperation in many administrative issues

- TUM International Graduate School for Science and Engineering and TUM Institute of Advanced Study for their partial financial support

Furthermore, I want to express my gratitude to my friends Farook Mokhtar, Ahmed Saleh, Alaa Abdellah, Ahmed Abdelhalim, Bogdan Popescu, Dan Popescu, Bernhard Fabel, Mohammed Fahmy, Akram Amin, Mohamed Mohsin, Safy-Allh, Shoukry Abdelaziz, Abdelhakim Salami and Anas for their company and emotional support throughout the study period.
Finally, I would like to thank my family and my dear wife Alaa for their continuous support.